SYNTHESIS AND CHARACTERIZATION OF TITANIUM – ALUMINUM INTERMETALLIC HARD COATINGS BY SPUTTERING

Thesis
Submitted in partial fulfillment of the requirements for the degree of
DOCTOR OF PHILOSOPHY
by
SUDHEENDRA P.

DEPARTMENT OF METALLURGICAL & MATERIALS ENGINEERING

NATIONAL INSTITUTE OF TECHNOLOGY KARNATAKA,

SURATHKAL, MANGALORE – 575025

JANUARY, 2017

SYNTHESIS AND CHARACTERIZATION OF TITANIUM – ALUMINUM INTERMETALLIC HARD COATINGS BY SPUTTERING

Thesis
Submitted in partial fulfillment of the requirements for the degree of
DOCTOR OF PHILOSOPHY
by
SUDHEENDRA P.

DEPARTMENT OF METALLURGICAL & MATERIALS ENGINEERING

NATIONAL INSTITUTE OF TECHNOLOGY KARNATAKA,

SURATHKAL, MANGALORE – 575025

JANUARY, 2017

DECLARATION

by the Ph.D. Research Scholar

I hereby declare that the Research Thesis entitled **“Synthesis And Characterization of Titanium – Aluminum Intermetallic Hard Coatings By Sputtering”** which is being submitted to the National Institute of Technology Karnataka, Surathkal in partial fulfillment of the requirements for the award of the degree of **Doctor of Philosophy** in **Metallurgical and Materials Engineering** is a bonafide report of the research work carried out by me. The material contained in this Research Thesis has not been submitted to any University or Institution for the award of any degree.

Sudheendra P.

(Reg. No: MT08F02)
Department of Metallurgical and Materials Engineering
National Institute of Technology Karnataka, Surathkal.

Place: NITK-Surathkal
Date:

CERTIFICATE

This is to certify that the Research Thesis entitled **“Synthesis And Characterization of Titanium – Aluminum Intermetallic Hard Coatings By Sputtering”** submitted by **Sudheendra P**. (Register Number: MT08F02) as the record of the research work carried out by him, is accepted as the **Research Thesis** submission in partial fulfillment of the requirements for the award of degree of **Doctor of Philosophy**.

Prof. A. O. Surendranathan	**Prof. N.K. Udayashankar**
Research Guide	Research Guide

Chairman - DRPC

(Signature with Date and Seal)

Contents **Page Number**

CHAPTER 1

CHAPTER 2

CHAPTER 3

CHAPTER 4

CHAPTER 5

CHAPTER 6

List of Figures **Page Number**

List of Tables **Page Number**

DEDICATED

TO

MY PARENETS,

FAMILY

AND

TEACHERS

ACKNOWLEDGEMENTS

Being a teacher is difficult. A teacher teaches, a good one demonstrates and a great one inspires. Being inspired by my guides, I would like to offer my sincerest gratitude to, Dr. A.O. Surendranathan (Dept. of Metallurgical & Materials Engg.) and Dr. N. K. Udayashankar (Dept. of Physics), for their advice, continuous support and encouragement throughout this research project. I am grateful for the faith they had in me and that they pushed me to my limits during the research process. Their perfect balance between laboratory freedom and supervision, gave me a lot of liberty to pursue my own ideas and to work independently. I am fortunate enough to work under the guidance of very helpful and understanding supervisors. Without their help, I could not have got as much as I have today.

I also would like to thank Dr. Mrs. H. D. Shashikala (Dept. of Physics) and Dr. H. Suresh Hebbar (Dept. of Mechanical Engg.) for serving in my Research Progress Assessment Committee (RPAC) and for their influence and advice during my academic studies.

Sincerest thanks go out to Dr. Rajendra Udupa, Dr. K. Narayana Prabhu, Dr. Jagannatha Nayak and Dr. Udaya Bhat for all their advice and encouragement for this research work. I would also like to acknowledge all the Metallurgical & Materials Engg. Professors and other staff’s for all their hard work and for providing me with a quality education in both my graduate and research studies. I would also like to thank Mrs. Sharmila Dinesh for all her help with graduate forms and sending emails for me. I would also like to acknowledge all the Metallurgical & Materials Engg. non teaching staff for providing me with a quality work whenever necessary.

I would also like to give my sincerest gratitude to Dr. K. Mohan Rao, Dr. Dhananjay Kekuda (Dept. of Physics, MIT – Manipal) for their kind advice and assistance for AFM analysis in this research work.

I would like to acknowledge the following companies that have provided technical support, general knowledge and materials that helped propel this research: V R Technology, Bangalore (Mr. Ravi Babu and Mr. Venkatesh), Sri Durga Labs (Mr. Sunil and Mr. Sudhir), Mangalore.

I would also like to give my sincerest gratitude to all my friends, who have all been very supportive to my research and helped me remember the good times in life. I specifically want to thank my batch mates Mr. Sreekanth Jois and Mrs. Prakrithi, who struggled alongside me to get through my research courses; I am grateful for their companionship and support. To my best friends Shellar Vikas, Hidayath Ulla and Nagaraj K K who are always there with me through all the tough times as well as the fun times, for all their time, help and assistance throughout my research. I want to acknowledge and thank all my lab mates for helping me with any problems I had.

Finally, I would like to thank my parents, P. Chandrashekhar Hebbar and Veena, my brother Ravindra P., my sister Rashmi, and my wife Shobha and to my twin kids Ankith and Akshitha. Through their love, support and encouragement, I had the strength to pursue and complete my Ph. D degree.

ABSTRACT

The titanium – aluminum intermetallics are extensively used in aerospace applications. Such materials systems basically consist of different percentage of titanium and aluminum. The characteristics of a given phase depend on percentages of titanium and aluminum. When titanium – aluminum are coated on the bulk materials in thinfilm forms, oxidation resistance, wear resistance, and surface hardness of the material improve to suit particular applications. Hence the work concentrates on the development of hard intermetallic coatings suitable for aerospace applications by reactive co-deposition of titanium and aluminum using unbalanced dc magnetron sputtering in oblique angle mode. The process parameters were optimized to obtain high quality uniform films. Thin films were deposited on glass, copper, aluminum, alumina and mild steel substrates for different types of characterization. The materials developed by the above-mentioned root were studied in detail with greater emphasis on its phase formation, texture, microstructure evolutions and oxidation resistance. The characterization of deposited films was done using X-Ray diffraction, scanning electron microscopy with energy dispersive spectroscopy, atomic force microscopy microhardness and nanohardness measurements.

The XRD characterization carried out confirmed growth of intermetallic TiAl. The crystal structure of the grown film was found to be orthorhombic. This analysis revealed the crystallite size of 123.7Å with lattice strain of 0.1352. Also it was found to be in gamma region of Ti – Al phase diagram. The scanning electron microscopy study revealed continuous columnar growths of the film on to the substrates. There was a good adherence of the films to the substrates. The heat treatment study carried out in the temperature regions of 400°C to 1200°C showed decrease in crystallite size with increase in the lattice strain due to the formation of TiO_2 and Al_2O_3. The microhardness and nanohardness studies carried out showed a value of 18.34 GPa and 36.3GPa respectively and values are found to be in accordance with the literature.

CHAPTER 1

INTRODUCTION

The surface properties of structural units greatly influence their behavior. In most of the cases the structural units are stressed at the surface region by the combination of mechanical, tribological, corrosive and thermal influences. Under such circumstances protective layer coatings are employed to overcome the above-mentioned influences. These coatings can be developed on steel, light weight materials, ceramics and polymers. The coatings are widely used as thermal barrier coating on turbine blades to insulate thermally loaded airfoils (Brogren et al. 2000 and Tetsui and Miura 2002). Thermal barrier coatings (TBCs) are coatings applied to metal components that are exposed to high temperatures in order to extend the service life of that component. Even though research in this area began over 70 years ago, many researchers are still trying to find ways to improve TBCs for engines operating at higher temperature ranges to achieve higher efficiencies. The current work concentrates to modify sputter system to incorporate reactive sputtering capabilities and to produce titanium – aluminum thin films by reactive magnetron sputtering. Eventually, this process can be used to produce thermal barrier coatings.

Miller consolidated (Miller, 2007) the history of surface coatings. A form of thermal barrier coatings have been around since the 1940s when they were first introduced as frit enamel coatings for turbine blades by W.N. Harrison, D.C. Moore, and J.C. Richmond of the National Bureau of Standards. As early as 1948, one of the first frit coatings was tested on turbine blades in an engine. Bartoo and Clure tested a coating in an engine for 100 hours in 1953. In 1960, the first flame sprayed coating used for rocket applications was the Rokide thermal barrier coatings on the rocket engine nozzles developed by L.N. Hjelm and B.R. Bornhorst. The Rokide had a zirconia top coat and a nickel chrome bond coat. In the 1960s and early 1970s, materials-oriented thermal spray research conducted using alumina, zirconia and hafnia for rocket applications. Since 1970 plasma sprayed TBCs were used in combustors. Stecura et al. played important roles in the development of new thermal spray coatings in the mid-1970s. These coatings, survived for high temperature test, used yttria to stabilize zirconia and MCrAlY. Electron-beam physical vapor deposition (EB-PVD) was introduced for the production of TBCs in 1989 and remains the coating of choice for first-stage turbine blades.

Nowadays it is more common to use sputtering for TBC deposition because it offers superior thermo-mechanical properties and lifetime performance over plasma spray process (Kelly, 2006). A thermal barrier coating system usually consists of three layers: the ceramic top layer, a thermally grown oxide (TGO) layer, and a bond coat layer to the substrate. The most common ceramic material for the top layer is yttria-stabilized zirconia, which has low thermal conductivity, a high coefficient of thermal expansion and is chemically inert to combustion atmospheres (Leyens, 1999). The bond coat, typically made with compositions of aluminides, must provide sufficient bonding between the ceramic top coat and the superalloy substrate and should have corrosion resistance. The aluminides in the bond coat also provide oxidation protection to the metal blades by forming an oxide scale.

TBCs have found application in the automotive industry. They are used to coat components of the exhaust system, such as exhaust manifolds, turbocharger casings, exhaust headers, etc. The most recent research has been on the development of multi-layer TBCs to protect against radiation heat transfer as engine temperatures are rising to increase efficiency. In order to fabricate these structures using reactive sputtering, the process of sputter deposition needs to be studied.

Due to the presence of coatings with low thermal conductivity, a temperature gradient is established across interface between the bulk material and coating. Hence the temperature in bulk material remains low compared to uncoated region of it. The coatings of intermetallics will push the service temperature limit of the material up to about 150 – 175˚C above the normal service temperature (Key to metals 2011). The coatings will reduce the material cost and consumption for making such systems. The other advantages of the coatings are superior tolerance against straining, erosion, corrosion, thermal shock etc. Intermetallic coating is one of such coatings which is widely used for these types of applications (Jones et al. 2006, Pan and Luzzi, 2006, Hu et al. 2006 and Xinhua et al. 2006).

The intermetallics have low ductility at ambient temperatures and there is certain difficulty in manufacturing them into useful forms. The main properties of interest for these materials are high temperature strength and high temperature corrosion resistance (Wei et al. 2005). Also they frequently exhibit very good resistance to high temperature corrosion due to the formation of oxide rich films. These properties have been the driving force behind increasing research activities worldwide. Considerable success has now been achieved and many alloys are now emerging. At the forefront, the titanium aluminides are of intense interest to the gas turbine and aircraft engine industries where their high temperature properties and low density offer prospectus for tremendous weight savings. Also creep deformation was improved due to presence of TiAl compared to lamellar superalloys (Chakraborty and Earthman 1998). However, iron and nickel aluminides have also found momentum rapidly and these alloys are of great interest in corrosive environments. Nickel aluminides have considerable potential for hot corrosive environments containing chlorine, whereas iron aluminides can be utilized in high sulfur environments.

Intermetallic is the short designation for the intermetallic phases and compounds, which result from the combination of various metals. Intermetallics are compounds of metals whose crystal structures are different from those of the constituent metals. Intermetallics form because the strength of bonding between the respective unlike atoms is larger than that between like atoms. Accordingly, intermetallics form particular crystal structures with ordered atom distribution where atoms are preferentially surrounded by unlike atoms. Such intermetallics result from the alloy systems with low melting temperatures, and the applications relied on the outstanding hardness and wear resistance of the intermetallics together with their metallic properties. Intermetallics were not used as structural materials in the beginning because of their brittleness. The attractive physical and mechanical properties of ordered intermetallic alloys have been recognized since early in this century. However, periodic attempts to develop intermetallics for structural application were unsuccessful, due to inadequate low-temperature ductility and toughness, together with poor elevated temperature performance. After the discovery by researchers in Japan in year 1979 that the ternary alloying elements in the intermetallics are able to improve and overcome these problems, the intermetallics are gaining more and more importance in the structural applications. Intermetallics, specifically the titanium aluminides (Ti-Al) are among the most attractive intermetallics to be used in majority of the applications. This is due to the advantage in terms of low density (4.1 g/cm^3), specific modulus (40 – 45 GPa), specific high temperature strength (100 MPa at 700 – 800 ˚C), creep resistance and oxidation resistance (above 700 ˚C). Experimental evidence has shown that titanium aluminides with an aluminum content roughly below 50 at.% essentially form nonprotective mixed TiO_2 + Al_2O_3 scales in air at elevated temperature rather than the protective Al_2O_3 scale.

The first intensive and successful structural intermetallic materials developments were based on the titanium aluminides Ti_3Al and TiAl. Another example of intermetallics that are used in the structural applications is Ni_3Al, which is well known as the strengthening second phase in the superalloys. There are only three classes of the intermetallics that are able to offer an emerging competitive balance of properties in the structural applications.

They are the L_{12} structured nickel aluminides (Ni-Al), B_2 structured iron aluminides (Fe-Al) and the L_{10} structured gamma titanium aluminides. Among these, the gamma titanium aluminides appear to have successfully advanced toward the structural applications. This is due to the low density, high specific strength, high specific stiffness and high temperature strength retention compared to the other two. Titanium aluminide intermetallics are believed to have potential applications as high temperature materials to replace Ni based superalloys due to their low density and excellent high temperature strength. A crucial requirement for the practical applications of the Ti-Al based alloys is sufficient oxidation resistance and hot corrosion resistance to prevent environmental degradation during service. The Ti-Al intermetallics are gaining high usage in the high temperature applications. The main reason for this is the strength which they are able to retain at high temperatures as compared to other materials.

1.1 About Ti – Al

Titanium aluminide intermetallics are finding emergent applications in aerospace because of superior properties. Due to the presence of lamellar nature of TiAl low oxidation and corrosion resistance with enhanced creep deformation were observed compared to super alloys. Among all the combinations dual phase ($\gamma + \alpha_2$) i.e. equiaxed and fully lamellar forms possess attractive high temperature properties. On this basis, it was planned to develop intermetallic titanium (Ti) – aluminum (Al) coatings by reactive magnetron sputtering.

Table 1. Properties of Ti, Al, TiAl, Ti_3Al and $TiAl_3$

	Titanium	**Aluminum**	**TiAl**	**Ti_3Al**	**$TiAl_3$**
Density (g/cc)	4.54	2.7	3.90	4.48	3.43
Modulus of Elasticity (GPa)	115	62	173	206	207
Melting point (°C)	1668	660	1536	1200	960
Crystal Structure	HCP	FCC	$L1_0$ (Face Centered Tetragonal)	DO_{19} (Hexagonal Super Lattice)	FCT (Face Centered Tetragonal)

1.2 Phase Diagram And Microstructure of Ti – Al

Alloys based on Ti-Al have been under development since 1955 and these are generally based on Ti_3Al since 1960. The binary phase diagram includes Ti_3Al (α_2), TiAl (γ), $TiAl_2$, δ and $TiAl_3$ intermediate phases, and α (Ti), β (Ti) and Al (α) terminal solid solutions. There are different crystal structures for different phases. The crystal structures of the alloys are shown in Figure1. However, neither the invariant reaction temperatures nor some phase boundaries, such as the α_2/γ and β/α, have been accurately defined. Further, a Ti – 50 at% Al alloy will solidify as cubic dendrites of β surrounded by γ formed according to the peritectic reaction. Whereas α forms from the β and γ phases by a peritectoid reaction with subsequent decomposition taking place eutectoidally to a lamellar α_2/γ structure. In fact recent results obtained from both ingot metallurgy and rapid solidification routes indicate that α phase (around 50% Al) forms directly from the liquid state according to the peritectic reaction $L + \beta = \alpha$. The TiAl (γ) phase is stable from 48% to 66% Al and is considered to be ordered up to its melting point of about 1450°C. This phase is considered to be the most promising among the other titanium aluminides from the point of view of the ratio of melting point to density. The solidification in this stage can be denoted as L→ (α) + L → (α) + γ → γ.

With the aid of the phase diagram shown in Figure 2, the microstructure obtainable in TiAl - based materials can be divided into three different groups, which are gamma (γ), duplex and lamellar structures. Alloys above 50 at% Al generally lie in the single phase γ field during heat treatment, and are single-phase γ after cooling to room temperature. The grains are equiaxed and about 50µm in diameter. For alloy between 46 to 50 at% heat treatment in the α + γ phase field results in a two phase structure upon cooling. This structure consists of γ grains and grains of a lamellar structure. The lamellar grains contain alternating α_2 and γ plates, which form as a result of transformation from the primary α during cooling to room temperature. The grains are typically 10-35 µm in diameter, and the lamellar plates are 0.1-1 µm thick. This structure is referred to as the duplex structure. Finally, alloys bellow 48 at% Al that are heat-treated in the single-phase α field can form the fully lamellar structure; the grains are typically greater than 500 µm in diameter, which reflects the rapid coarsening rate of the disordered α.

Single phase γ, like most of the intermetallics compounds, is brittle at low temperature. Even in fine-grained materials, less than 1% plastic elongation can be measured before fracture. The brittle behavior appears to be intrinsic in nature, since single crystals of various orientations all have little ductility. The brittleness is likely to be the result of the limited dislocation mobility in the compound. The brittleness behavior was to be improved by alloying modification, but no practical breakthrough was made until binary alloys were systematically studied as a function of Al concentration. Two results from the binary alloy study are critical to alloy design. First, the ductility is sensitive to microstructure. The duplex structure is significantly more ductile than others at room temperature and the ductile duplex structure exists in a narrow range of Al concentration. Only the alloys containing 46 – 52 at.% Al show appreciable plasticity.

The ductility peak occurs at 48 at.% Al, particularly when the alloy is heat-treated near the center of the α+ γ phase field where the two phases have equal volume fractions. Alloys, which are not in this range, tend to have either the single phase γ or the lamellar structure, and they are relatively brittle.

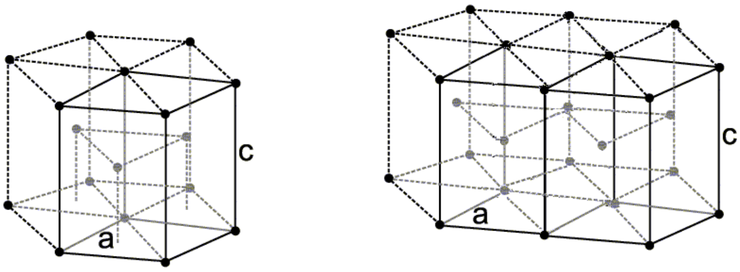

A3 (HCP) Ti (c/a = 1.59) DO$_{19}$ Ti$_3$Al (c/a = 0.80)

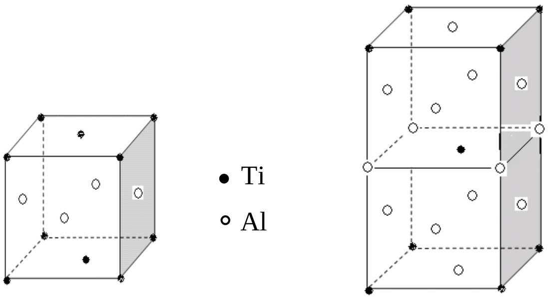

L$_{10}$ TiAl (c/a = 1.02) DO$_{22}$ TiAl$_3$ (c/a = 2.23)

Figure 1. Crystal structures of four different phases in Ti-Al system.

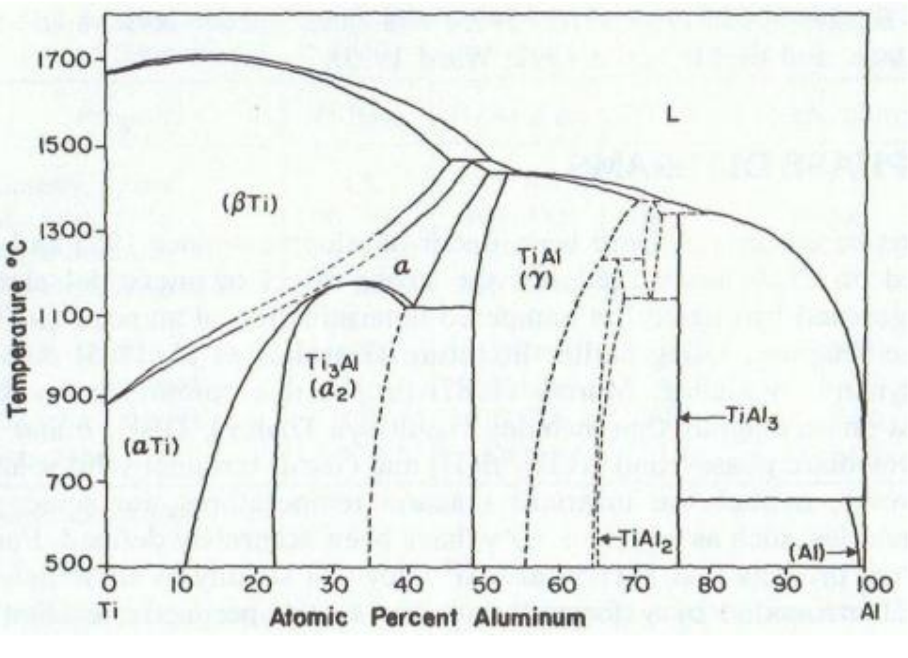

Figure 2. Phase diagram of the Ti-Al system. Rocha et. al (2003).

The characteristic of titanium base material is the reversible transformation of the crystal structure from α (HCP) (Figure 3a.) to β (BCC) (Figure 4a.) when the temperature exceeds 883 °C. This behavior is mainly dependent on the amount of alloy content, which allows variations in the microstructure and strengthening of these alloys compared to non-ferrous alloys. Depending on the alloying elements there are five grades for titanium alloys, i.e. with Grade 1 to Grade 4 and Grade 7. Each grade has its own impurity level; Grade 1 being the most pure. Tensile strength varies from 170 MPa (Grade 1) to 490 MPa (Grade 4).

α- alloys are containing more amount of alpha stabilizers (Figure 3b.) such as aluminum, tin etc. These are not responding for heat treatment but are weldable. Hence they are mainly used in the cryogenic applications, airplane parts and chemical processing equipments.

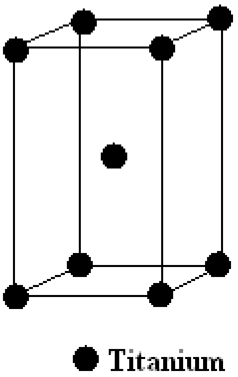

Figure 3a. Crystal structure of Titanium

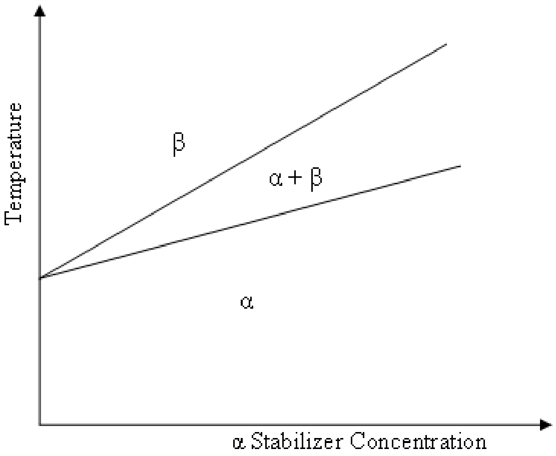

Figure 3b. α - titanium stabilization.

α – β alloys contain 10% to 50% **β**-phase at room temperature. They can be strengthened by heat treatment and aging which is an advantage. The alloys of this group are used in the aircraft turbine parts, marine hardware, and prosthetic devices.

β – alloys (Figure 4b.) form a small group of titanium alloys. The transition elements such as vanadium, niobium, and molybdenum are present in these alloys. They are having good hardenability; cold formability when they are solution treated and gets high strength on aging. Also the densities vary from 4.8 g/cm^3 to 5.1 g/cm^3. These alloys are used in heavy duty parts of aircrafts.

The **γ** – phase (Figure 5.) i.e. TiAl is widely used in aerospace application. The other two important phases are Ti_3Al (Figure 6.), and $TiAl_3$, which are used in limited application areas of aerospace engines. These two phases are having less solubility to the ternary alloying additions such as nitrogen, vanadium and chromium etc., which are easily soluble in the **γ** – phase. Also Ti_3Al and $TiAl_3$ are the hardest phases compared to the **γ** – phase which make them limited application materials.

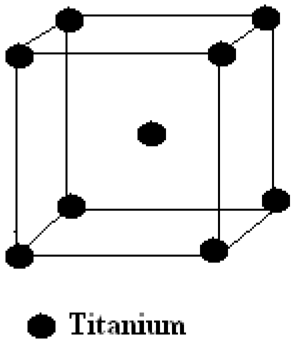

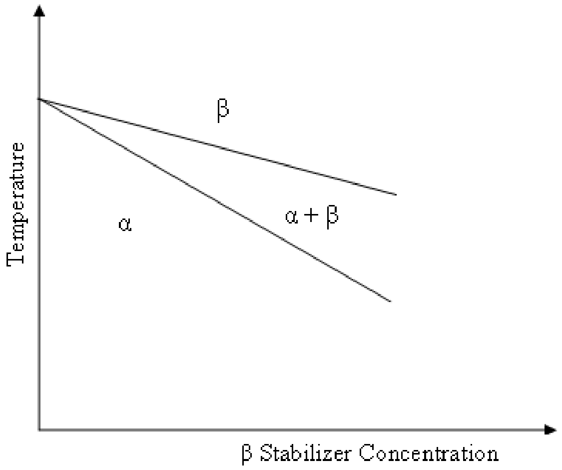

Figure 4a. Crystal structure of β - Titanium Figure 4b. β - Titanium stabilization.

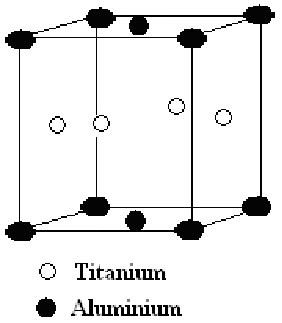

Figure 5. Crystal Structure of γ -TiAl.

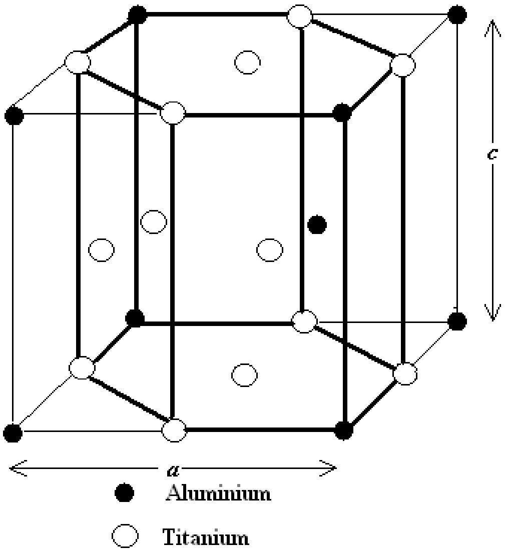

Figure 6. Crystal structure of Ti_3Al.

1.3 Thin film Technology

Modern day technology requires several types of thin films for a variety of applications such as in space research, electronics, medicine etc. The attractive properties of thin films viz. high optical reflection/transmission, hardness, wear resistance and single crystal nature can be exploited in applications. There will be a large difference in properties between thin films and bulk materials. This is mainly due to the variation in the thickness of the thin film and bulk materials. In thin films, the thickness is of the order of mean free path of the electrons or of the order of the wave length of incident visible light. Depending on the applications, films can be of single or multi component or may be multi-layer coatings on different substrates.

The film deposition involves

a. Creation of material to be deposited in an atomic, ionic, molecular or particulate form.
b. Transport of the material to the substrate.
c. Deposition of the material on the substrate.
d. Film growth by nucleation and growth process.

One can get films of desired properties by properly modifying these four steps. The deposition technique can be broadly classified as:

1. Thermal Evaporation (Physical Vapour Deposition)
2. Chemical Methods
3. Cathodic Sputtering

1.3.1 Thermal evaporation (physical vapour deposition - PVD)

In this process, the solid materials are vaporized by heating the material to sufficiently high temperatures and the vapors are made to deposit on the cooler substrate to yield thin solid film. Due to collision with ambient gas atoms a fraction of vapour atoms will be scattered and hence randomized in direction during their transfer to the substrate through the gas. Thus pressure lower than 10^{-5} torr is necessary to ensure a straight line path for the most of the emitted vapor atoms for a substrate to vapour-producing material distance of approximately 10 to 50 cm in vacuum evaporation. A high vacuum has an additional effect of reducing the contamination of the films by the gas molecules. The rate of deposition of the vapour on a substrate depends upon the source geometry, its position relative to the substrate and the condensation coefficient.

Among physical vapor deposition techniques thermal evaporation (TE) is the one with the longest standing tradition. However, during the last 30 years of booming in surface modification industry involving a great deal of thin film technology, deposition techniques like CVD (chemical vapor deposition) or sputtering, which often offer unquestionable advantages, have been developed to perfection and TE has largely been replaced in production lines. On the laboratory scale, due to their simplicity, techniques like PLD (pulsed laser deposition) and sputtering were much more promising to realize fast results.

However, as time went by it became clear that the performance of the various deposition methods strongly depends on material issues as well as economic aspects. With progressive commercialization, cost effective volume production and reproducibility became the driving forces and the intrinsic advantages of TE turned the scales. In this sense, the story of high temperature film deposition can serve as an example how this technique, sometimes regarded as old – fashioned, still bears a high potential for innovation and surprising efficiency. TE is the classical technique applied for metal plating on glass or plastic surfaces, e.g. aluminum coatings widely used for capacitors, plastic wrappings, and as barrier against water diffusion. It is evident that the deposition of multiple metal compounds imposes quite different requirements to the technique and will go far beyond the rudimentary concept of evaporating multiple metals in a vacuum chamber.

The evaporation may be achieved directly or indirectly by a variety of physical methods like

- Resistive heating
- Flash evaporation
- Arc evaporation
- Exploding wire technique
- Pulsed LASER ablation
- RF heating
- Electron bombardment

The resistive heating method consists of heating the material with a resistively heated filament or boat, generally made up of refractory metals such as tungsten, molybdenum, tantalum and niobium with or without ceramic coating. Crucibles of quartz, graphite, alumina, beryllia and zirconia are used in indirect heating. The choice of support material is primarily determined by the evaporation temperature and resistance to alloying and/or chemical reaction with evaporants. To control the film composition the evaporation rates have to be online monitored individually by some kind of sensor heads. The substrate is mounted in or on a heater element and kept at a temperature which promotes epitaxial film growth.

On the other hand the vacuum specifications are mostly relaxed in comparison with deposition processes which often take place under UHV conditions. Due to the low carrier densities in films even tiny impurity levels have significant if not detrimental effects on the properties. The compound films can be prepared by reactive thermal evaporation. Here elemental constituents of the compound are vaporized and codeposited or deposited material reacts with each other to form the compound. For the formation of second phase the surface heating is necessary.

Were as sputtering requires elevated argon gas pressure for the formation of sputter, introduction of argon gas is an essential but tricky task. To avoid flooding of the chamber with argon gas the main chamber is permanently pumped at, while the argon gas has to be introduced close to the substrate. In the early days, a housing as described by Baudenbacher et. al (1990) served to confine the gas around the substrate. Its small opening towards the sources constitutes an enhanced gas flow resistance and allows differential pumping to a certain extent. Since the height of the region with enhanced argon gas pressure is comparable to its extension, i.e. the dimensions of the substrate, this concept can be applied only for small chips. Otherwise, with increasing thickness of this zone the metal vapors start scattering. Since the scattering cross section depends on the molecular weight, as a first consequence the composition gets extremely pressure dependent. If the gas pressure or the length of the path through the argon gas is further increased, the vapor does not penetrate this barrier and cannot reach the substrate any more. In comparison to most other techniques (PLD, CVD, sputtering) operating at fore pump pressure level TE requires a high vacuum ambience, and if a gas flow is introduced, a high pumping speed. These requirements can be met by oil diffusion pumps.

1.3.2 Chemical methods

These are:

a) Chemical vapour deposition by pyrolysis, dissociation and reaction in vapour phases.
b) Chemical deposition from solution including electrodeposition, anodic oxidation, electroless plating, chemical reaction or displacement.

Chemical vapour deposition and electroplating are another two methods of depositing thin films. These techniques enable coating thickness to be varied from a few angstroms to a fraction of a few millimeters in a well-controlled fashion. In this method the impurities and their effects vary with the material to be evaporated. Most refractory metals and several non metals are obtained chemically in a purer form than by conventional metallurgical practices.

1.3.3 Cathodic Sputtering

A brief sputtering history is presented to get background on sputter deposition. Cathodic sputtering is the phenomenon of the cathode electrode disintegration under the bombardment of the ionized gas molecules when an electrical discharge is passed between electrodes at a low gas pressure. Over a century ago, early investigators of electrical discharges in gases observed that the wall of a glow discharge tube became coated with a metallic deposit in the negative electrode region (Mattox, 2003). W.R. Grove (1852) was the first to study the sputter deposition. The film deposition from a glow discharge was also observed by M. Faraday in 1854. Prof. A.W. Wright published a paper in 1877 on the use of an "electrical deposition apparatus" to form mirrors and study their properties. C.J. Overbeck reported the deposition of compounds by sputtering in a reactive gas ("reactive sputter deposition") in 1933 for use as optical coating. Penning (1936) proposed the "crossed field" (electric and magnetic) electron trap to enhance plasmas in sputtering from cylindrical-hollow (inverted) magnetrons and cylindrical-post magnetrons. Sputtering is a very mature technology, as evidenced by the many applications of the process. Some examples given by Parsons of these applications are magneto-optical storage media, compact disks, planarized coatings for multilayer circuits, optical multilayer coatings for mirrors and filters, solar control, low emissivity window coatings, conductors and barrier layers, diamond-like coatings, wear-resistant coatings for cutting tools, and decorative coatings (Parsons, 1991). Parsons also gives some reasons for using sputtering: excellent film uniformity; surface smoothness and thickness control; deposition of films with nearly bulk-like properties; good adhesion; high rates which are comparable to evaporation. For film deposition there are two categories of sputter sources: glow discharge (diode, triode or magnetron) and ion beam.

Sputtering is the ejection of atoms from the surface of a (target) material by bombardment with energetic particles. If the ejection is due to positive ions' bombardment, then it is known as CATHODIC Sputtering. The ejected or sputtered atoms can be condensed on a substrate to form a thin solid film.

The thin film deposition by thermal evaporation or cathodic sputtering is based on the Knudsen cosine rule (Figure 7) as given below.

$$\frac{t_1}{t_0} = \left[1 + \left(\frac{x}{h}\right)^2\right]^{-2}$$

t_1 = thickness at point A

t_0 = thickness at point B

x = horizontal distance between points A & B

h = vertical distance from source O to point A

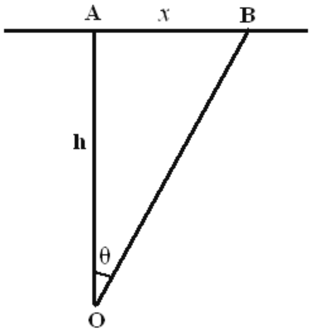

Figure 7. Knudsen rule for thin film deposition.

The basic sputtering process, in which materials are sputtered from the solid state by bombarding their surfaces with energetic ions, has been known for many years. Many materials were successfully deposited by this process, which was limited by low deposition rates, low ionisation efficiency in the plasma, and high substrate heating effects. Also other limitation of sputtering techniques was, the inability to deposit at useful rates, dense defect-free insulation coatings of oxides.

These limitations were overcome by the magnetron sputtering and unbalanced magnetron sputtering. The difference between conventional and unbalanced magnetrons is the degree of plasma confinement. In a conventional magnetron the plasma is strongly confined to the target region, with a region of dense plasma extending to a few centimeters in front of the target. During film growth, substrates positioned within this region are subjected to ion bombardment and this strongly modifies the structure and properties of the resulting film. But substrates positioned outside this region experiences insufficient bombardment to modify the microstructure of the growing film. Therefore, it is difficult to produce fully dense, high quality coatings on large, complex components using conventional magnetrons. This problem was overcome by the developments in unbalanced magnetron, and incorporation of multiple target-magnetron systems.

1.4 Unbalanced Magnetrons

The concept of the unbalanced magnetron was first developed by Window and Savvides who investigated the effect of varying the magnetic configuration of a conventional magnetron (Mattox, 1998). By strengthening rings of magnets, electrons in the plasma were confined to the target region and able to follow the magnetic field lines and flow towards the substrates. As a result, ion bombardment at the substrate was increased with a improvement in coating structure. The use of unbalanced magnetron allows high ion currents to the substrate so that coatings of excellent quality can be deposited. However, it is still difficult to deposit uniform coatings onto complex components using a single magnetron source. Therefore, in order to exploit this, multiple-magnetron system was introduced. The use of this system has led to great improvements in the structure and properties of sputtered coatings.

In the closed-field configuration, the magnetic field lines between the magnetrons form a closed trap for electrons in the plasma. A few electrons are lost to the chamber walls and a dense plasma is maintained in the substrate region leading to denser film. The magnetic fields in a conventional magnetron, and unbalanced magnetron system (UBMS) are compared schematically in Figure 8. In addition to pure metal and alloy films, UBMS has been successfully used to deposit a range of reactively sputtered coatings onto various components. The reactive sputtering process can be controlled by plasma emission or control of partial pressure of the reactive gas, both processes offering control of the coating composition and properties. The multiple-magnetron systems are ideally suited to the deposition of alloy, as each of the magnetron targets can, in principle, be of a different material, and by sputtering the targets at different rates, any desired alloy composition can be attained. Use of the UBMS allows coatings with graded properties to be produced. Thus, both the coating/substrate interface and the coating surface properties can be optimised, so that very high performance coatings can be produced with excellent coating-to-substrate adhesion.

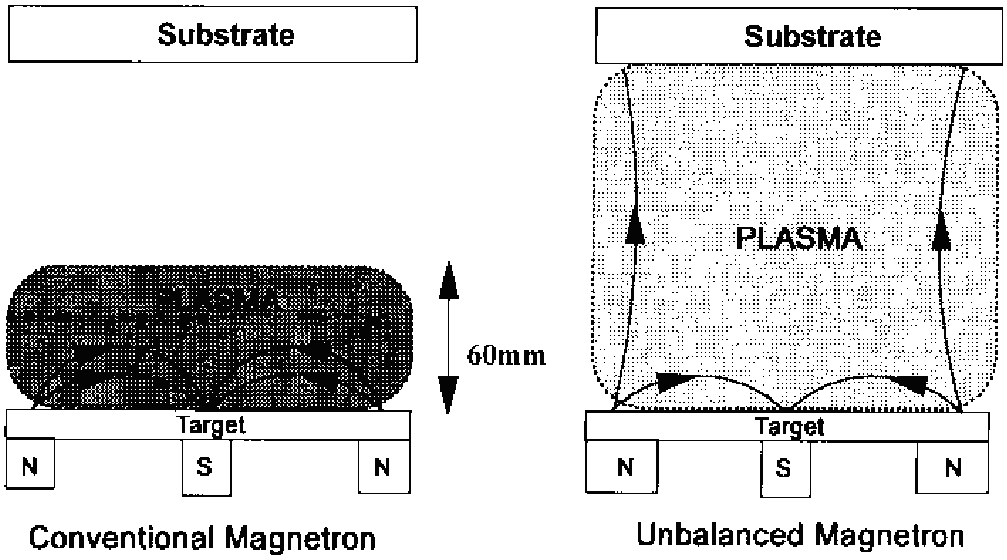

Figure 8. Comparison of the magnetic configuration and plasma confinement in conventional and unbalanced magnetron systems.

Although the two unbalanced magnetrons facing each other, is not the useful arrangement, highly supersaturated alloys and amorphous alloys can be deposited using two magnetrons arranged at oblique angles. Many alloy systems have been studied using this technique, and in particular this can be applied in the deposition of aluminum- titanium coatings. This allows the deposition of alloy films of uniform thicknesses and compositions onto numerous small components. A schematic representation of dual magnetron target along with substrate position are shown in Figure 9.

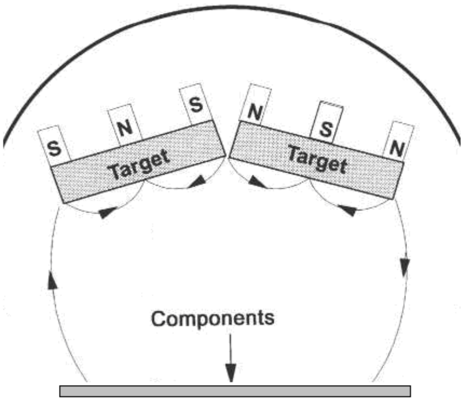

Figure 9. Multiple magnetron arrangements developed to suit specific applications: oblique incident dual magnetron.

1.5 Thin film Nucleation And Growth

Properties of polycrystalline thin films are strongly dependent on their (micro) structure. The deposition parameters have a very strong influence on the structure. Therefore, it is essential to understand the effect of deposition parameters during the formation of a thin film to control the properties of thin films and in turn of the devices based on polycrystalline thin films. The best understood process is the film formation from the vapor phase.

Thin films on a substrate can exhibit mainly two kinds of growth modes (Figure 10) depending on the surface and interfacial energies of the substrate and the condensate. They are as follows:

1. Island growth or Volmer – Weber growth will occur when the condensing particles does not wet the substrate properly and results in the formation of three dimensional islands. In this mode film atoms are more strongly bound to each other than to substrate and / or there will be slow diffusion between the islands. The resulting films are amorphous in nature.
2. Layer-by-Layer growth or Frank – van der Merwe growth will occur when the condensing particles wets the substrate properly and results in the formation of three dimensional continuous networks. In this mode film atoms are more strongly bound to substrate than to each other and / or there is a fast diffusion between the layers. Also the resulting film is crystalline in nature with highest film quality.
3. Mixed growth or Stranski – Krastanov growth will occur when the condensing particles wet the substrate on selected regions. Initially layer by layer growth

occurs and then there is formation of three dimensional islands and the energetics change. The resulting film quality will be crystalline and amorphous in nature.

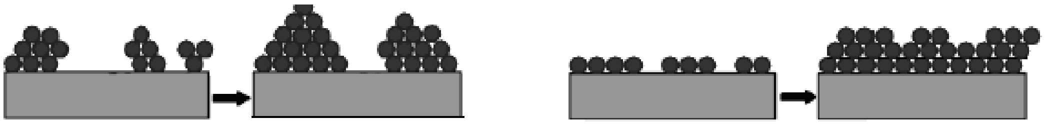

Island Growth (Volmer-Weber Mode) Layer by layer growth (Frank - van der Merwe)

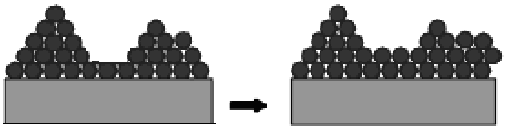

Mixed growth (Stranski - Krastanov)

Figure 10. Growth processes in thin films.

In the case of island mode, it takes considerable time after starting the deposition before a continuous film is formed and a number of steps or growth sequences are involved. The kinetics of each of these stages varies with deposition conditions. The various sequences involved in the formation of a continuous thin film from the vapour phase can be summarized as follows:

1. Vapor atoms arrive at the substrate surface and get adsorbed.
2. The adsorbed atoms or adatoms migrate on the substrate surface during their mean stay time and the nucleation takes place by the combination of adatoms (Figure 11). Gibbs free energy $\Delta G(r)$ for the formation of stable nucleus of radius r and with interfacial angle θ between the nucleus and the substrate having inter facial energy γ_{sv} between solid - vapour interface, and γ_{fs} between film - solid interface is as given below:

$$\Delta G(r) = \frac{\pi}{3}\left(2-3\cos\theta+\cos^3\theta\right) r^3\, \Delta G_v + 2\pi\left(1-\cos\theta\right) r^2\, \gamma_{FV} + \pi \sin^2\theta\, r^2\left(\gamma_{FS}-\gamma_{SV}\right) \quad (1)$$

3.The nuclei grow larger by the combination of adatoms and other nuclei when they come in contact with each other due to growth or mobility with a net reduction in the surface area or the surface coverage. This is known as coalescence stage I. The driving force for this liquid like coalescence is the reduction in surface energy (μ_i).

$$\mu_i = \frac{dG}{dn_i} = \frac{d\left(4\pi r_i^2\, \gamma\right)}{d\left(4\pi r_i^3 / 3\Omega\right)} = \frac{\left(8\pi r_i\, \gamma\right) dr_i}{\left(4\pi r_i^3 / 3\Omega\right) dr_i} = \frac{2\,\Omega\,\gamma}{r_i} \quad (2)$$

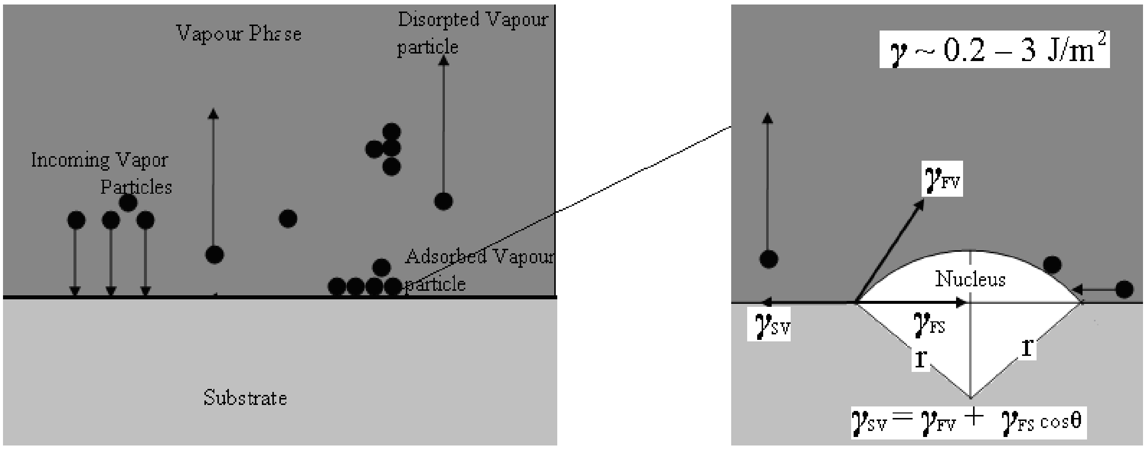

Figure 11. Nucleation process in thin films.

As the deposition progresses, the surface coverage increases, the island size distribution shifts to larger mean radii, it becomes broader and the island shape becomes more and more irregular. The process is as shown in the figure below.

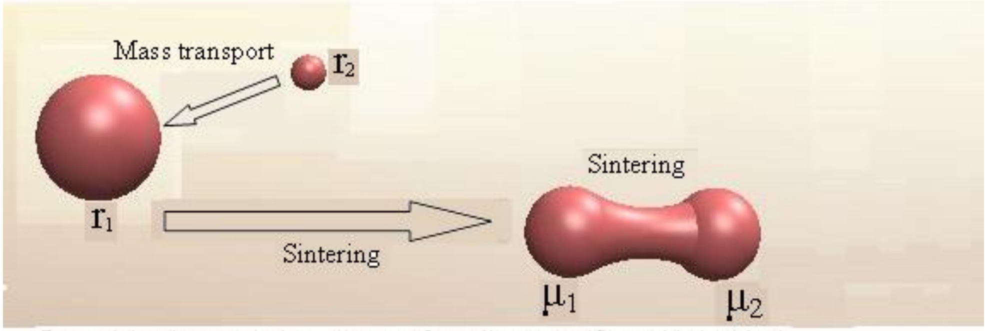

Large island grow at the expense of smaller once (Ostwald ripening)

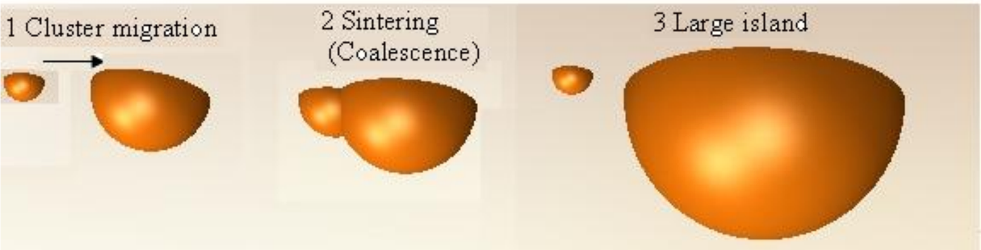

Figure 12. Cluster coalescence process in thin-film growth.

4. At a particular surface coverage large scale coalescence (LSC) takes place with the formation of a connected network-like structure leaving channels and holes in between. It is also referred to as the formation of an infinite cluster. This stage is known as coalescence stage two (CS II, Figure12).
5. Secondary nucleation takes place at these holes and channels with further deposition and a continuous film is formed by the incorporation of these secondary nuclei into the network structure.

The effect of deposition parameters on the structure can be understood by means of two terms via Agglomeration and Mobility. Agglomeration is a tendency to form larger islands and it is due to the mobility of adatoms and clusters. One can talk of increased or decreased agglomeration. An increased agglomeration leads to:

i) Film continuity at a higher average thickness
ii) Large grain size of the film formed
iii) Reduced structural defects.

Higher the mobility, higher would be the agglomeration. The degree of agglomeration can be studied from the thickness at which the film becomes continuous, through electron microscopy to measure the grain size or through aging experiments. The effects of deposition parameters on the nucleation density and mobility need to be considered. Lower nucleation density and higher mobility lead to increased agglomeration and higher nucleation density and lower mobility give rise to a reduced agglomeration.

Important deposition parameters like deposition rate and substrate temperature have a very strong influence on the agglomeration. Apart from these, adsorbed gases, a lateral electric field or a magnetic field applied to the substrate, ultrasonic vibration of the substrate during deposition, substrate smoothness also affect the thin film structure.

1.5.1 Effect of deposition rate

Deposition rates affect the nucleation density significantly according to any of the nucleation theories. Therefore, it contribute to the agglomeration through its effect on the nucleation density significantly.

In the case of vapor deposition, an increased rate also results in higher kinetic energy of the vapor atoms. Higher kinetic energy gives rise to higher mobility leading to increased agglomeration. It is known that sputtered atoms have higher kinetic energy compared to evaporated atoms. Therefore, always sputtered films have larger grain sizes as compared to evaporated films under the same deposition conditions. Thus total effect of deposition rate on agglomeration is significant. Considerable change in the morphology can be realized with very small change in deposition rate, particularly at very low thicknesses. A very high deposition rate results in non-equilibrium conditions with the clusters being formed before the adatoms can migrate to equilibrium positions. This results in a reduced agglomeration and a smaller grain size.

1.5.2 Effect of substrate temperature

Nucleation density has an exponential dependence on the substrate temperature and is very sensitive to this deposition parameter. A higher substrate temperature results in reduced nucleation density with a consequent increased agglomeration. Similarly, lower substrate temperature gives rise to a reduced agglomeration. Substrate temperature affects significantly the mobility also. Higher substrate temperature gives rise to higher mobility and increased agglomeration. Thus, substrate temperature affects both nucleation density and mobility in increasing or decreasing the agglomeration and hence has a very strong influence on the structure of the resultant film.

A higher substrate temperature and higher deposition rate gives rise to mobility of the adatoms and clusters resulting in a film with smooth surface and large grain size respectively. Apart from these two major deposition parameters, adsorbed gases can affect the agglomeration through an increase or decrease in the nucleation density and an increased or reduced mobility, depending on the species adsorbed. Studies suggest that the adsorbed water vapor reduces the nucleation density and consequently an increased grain size. Charges and defects on the substrate surface give rise to increased nucleation density and reduced agglomeration. An electric field will induce LSC at a lower average thickness due to flattening of the islands. This is attributed to the interaction of the field with the charged islands, charges being derived from the ionized vapor atoms. Studies on the effect of magnetic field also suggest a similar flattening. Ultrasonic agitation of the substrate during deposition can result in a film with large grains and better packing density, due to the increased mobility of the adatoms and clusters. All these effects can be suitably used to tailor the structure and properties of thin films to have the desired characteristics of the thin film devices.

CHAPTER 2

LITERATURE REVIEW

Liu and Wang (2005), in their work on γ-TiAl and $TiAl_2$, coatings with the thickness of about 20 μm were made on γ -TiAl substrates by using a close-field magnetron sputter deposition (CFMSD) technique. The developed coatings showed good quality with no micro-cracks being observed in the as-deposited $TiAl_2$ coating cross-sections. Oxidation exposure tests at 800 and 900^0 C in air were carried out to assess the oxidation resistance of the coatings and the cast γ -TiAl. The γ -coating and cast TiAl showed similar oxidation performance. Both of them had suffered great oxide losses with the formation of Al_2O_3 + TiO_2 mixtures and no Al_2O_3-rich layer was found in either case. By contrast, only external Al_2O_3 layers with a θ-phase structure was formed on the $TiAl_2$ coatings at 800 and 900^0C, and the θ -Al_2O_3 scales showed high protective ability with low mass-gains and good scale adherence. After the oxidation exposures, the $TiAl_2$ coating remained to be almost free of micro-cracks, and an inter-diffusion region of about 5 μm was observed between the $TiAl_2$ coating and the γ-substrate, which could act as a metallurgical bonding between the coating and substrate.

Ramos et al. (2006), in their paper on multilayer thin films with periods (periods Λ) ranging from 4 to 1000 nm were studied in order to determine the maximum period leading to the γ-TiAl phase formation. The production of high period multilayers (Λ > 20 nm) requires the use of Ti and Al targets one by one. The influence of silver on the thin films transformation Ti/Al multilayer to γ-TiAl was also analyzed. The introduction of a few percent of silver was performed by superimposing small Ag foils on the targets. The kinetics of the phase transformation were studied by differential scanning calorimetry (DSC) and X-ray diffraction (XRD). Up to Λ =200 nm, heat treating at 600 °C during 1 h leads to γ -TiAl, with or without small amounts of α_2-Ti_3Al, while for Λ =500 and 1000 nm the presence of extra Al-rich phases was detected. For high periods (200, 500 and 1000 nm) an Al_3Ti

intermediate phase is formed. In the presence of silver the peak temperatures are shifted to lower values and the activation energy values slightly decrease.

Liu et al. (2007) utilized three Ti-Al series intermetallic compounds, $TiAl_3$, TiAl, and Ti_3Al to prepare cored wires, which were then used to form coatings on low carbon steel substrates by a supersonic arc spraying process. High temperature erosion (HTE) properties of the coatings were determined in a laboratory elevated temperature erosion tester. The results show that the HTE resistance of the coatings prepared using the cored wires decreased in the order of (from best to worst) $TiAl_3$, TiAl and Ti_3Al. The arc-sprayed coatings prepared using cored wire containing $TiAl_3$ and TiAl powders exhibited better or comparable HTE resistance than that containing a commercial Cr_3C_2-based composite powder, although the hardness of the former two coatings was relatively lower. The laminated structure, which was characteristic of the arc spraying coatings, was found on all the prepared coatings. Oxides resulted from oxidation of both the cored alloy powders and the mild steel sheaths were also identified between the laminated layers. Under the present testing conditions, material loss of the coatings can be contributed to brittle breaking, fatigue spalling, cutting and ploughing mechanisms.

Yamazaki et al. (2009) attempted to apply a TiAl laminate to a sputtering target for the formation of TiAlN films. The structure and the properties of the films formed using this target were investigated and compared with those of films formed using a sintered target and a compound target. The films formed using the laminate target were found to include less oxygen than the films formed using the sintered and compound targets. It is probably due to the lower oxygen concentration in the laminate target than in the other two targets. No substantial difference in the hardness of the film was observed between the laminate target and the other two targets. The laminate target was equally as effective as either the sintered or the compound target.

Illekova et al. (2008) worked on the kinetics of the synthesis of elemental nanoscaled multilayers of Ti and Al in the regime of continuous heating from 300 K up to 973 K was investigated. A series of sputter deposited Ti/Al multilayer thin films with individual layer thickness (d) from 4 nm up to 1000 nm have been used. DSC, classical and time resolved XRD and scanning electron microscopy (SEM) have been applied for analysis. In the Ti/Al multilayers the sequence of reactions leading to the final product TiAl (and Ti_3Al) was determined. The final products as well as the kinetics of their formation depend on the individual layer thickness. Three different kinetic regimes depending on the layer thicknesses have been found.

Moskalewicz et al. (2008) coated γ-TiAl intermetallic alloy with Si and Ag admixtures by magnetron sputtering to improve oxidation resistance of TIMETAL834 (near α – Titanium alloy - Ti-5.8Al-4Sn-3.5Zr-0.7Nb-0.5Mo-0.35Si-0.06C). Analytical scanning and transmission electron microscopy (STEM) were used for detailed analyses of a microstructure and chemical composition of the coating. They found that the coating contains two sublayers with different microstructure and morphology. Energy-dispersive synchrotron radiation diffraction was applied for stress analysis. The results show that there are tensile residual stresses present within the TIMETAL834 substrate and compressive residual stresses within the γ-TiAl sublayer. It was established that the surface treatment applied in this work essentially improved the alloy oxidation resistance.

Chen et al. (2011), who deposited Ti–Al–N coatings, have proven that these coatings were effective protective coating for machining applications. They reported a difference of cubic TiAlN coatings with a similar Ti/Al atomic ratio deposited by magnetron sputtering and cathodic arc evaporation. During annealing, both the coatings exhibited structural transformation into stable phases cubic TiN and hexagonal AlN via an intermediate step of spinodal decomposition with the precipitation of cubic AlN. Compared to sputter coating an increase of tool life-time by 42 % was reported by evaporation coating. A post-deposition vacuum annealing of both coatings in the temperature range of spinodal decomposition improves their cutting performance due to an increase in hardness arising from precipitation of coherent cubic-phase nanometer-size cubic AlN domains. The behaviors can be understood by considering the difference in microstructure and morphology of as-deposited coatings originating from adatom mobility of deposited particles, where arc evaporation technique with higher ion to neutral ratio shows higher adatom mobility.

Shetty et al. (2011) reports the comparison of structure and properties of titanium aluminum nitride (TiAlN) films deposited onto Si(100) substrates under normal and oblique angle depositions using pulsed-DC magnetron sputtering. The substrate temperature was set at room temperature, 400 °C and 650 °C, and the bias voltage was kept at 0, −25, −50, and −80 V for both deposition angles. The surface and cross-section of the films were observed by SEM. It was found that as the deposition temperature increases, films deposited under normal incidence exhibit distinct faceted crystallites, whereas oblique angle deposited (OAD) films develop a kind of "tiles of a roof" or "stepwise structure", with no facetted crystallites. The OAD films showed an inclined columnar structure, with columns tilting in the direction of the incident flux. As the substrate temperature was increased, the tilting of columns nearly approached the substrate normal. Also there were voids formed due to the shadowing effect. Films deposited at $\alpha=0°$ showed a mixed (111) and (200) out-of-plane orientation with random in-plane alignment whereas films deposited at $\alpha=45°$ revealed an inclined texture with (111) orientation moving towards the incident flux direction and the (200) orientation approaching the substrate normal, showing substantial in-plane alignment.

Iriatee et.al. (2011) worked on the influence of the processing pressure and the substrate to target distance on the synthesis by reactive sputtering of c-axis oriented poly-crystalline aluminum nitride thin films. The films exhibited a very high degree of c-axis orientation especially when a low process pressure was used. After growth, residual stress measurements obtained indirectly from radius of curvature measurements of the wafer prior and after deposition. There was a transition from compressive to tensile stress at a processing pressure around 2 mTorr. The transition occurs at different pressures for thin films of different thicknesses. The degree of c-axis orientation was not affected by the target–substrate distance as it was varied between 30 and 70 mm.

Zhao et al. (2012), in their work, deposited TiN/(Ti,Al)N multilayer films on stainless steel substrates with Ti and TiAl alloy targets sources by pulse biased arc ion plating. The crystallographic structures and cross-sectional structures of TiN/(Ti,Al)N multilayer films were evaluated along with hardness. The film/substrate adhesion was determined by nanoindentation and scratch test, respectively. A complex set of microstructures was found between TiN and (Ti,Al)N layers, at the interface. This layered interfacial region consists of extremely fine sub-layers, resulted from the rotation of the substrates at the time of deposition. The hardness values of the multilayers exhibit higher hardness compared with that of monolithic (Ti,Al)N film.

Paksunchai et al. (2012) deposited thin films of $(Ti_{1-x}Cr_x)N$ with varying currents on Si (100) wafers and glass slides by reactive unbalanced magnetron co-sputtering technique without heating and voltage-biasing the substrates. The effects of sputtering current on the structure and morphology of films were studied. The films were grown on the substrates using titanium and chromium targets in a mixed Ar and N_2 atmosphere. The structure of the films was investigated by XRD. The surface and cross-sectional morphologies of the films were examined by atomic force microscopy (AFM) and SEM. Furthermore, the chemical composition of the films was analyzed using energy dispersive x-ray spectroscopy (EDS). The results revealed that the thin films formed solid solutions with the fcc NaCl phase and relative Cr content (x) was figured out in the range from 0.46 to 0.81. The crystal sizes of the films calculated from Scherrer formula were about 12-13 nm. AFM results indicated increasing of the roughness from 3 to 7 nm corresponding to the increased thickness from 400 to 900 nm when Cr was increased and the cross-sectional morphology revealed dense and compact columns.

Zhang et al. (2012) worked on β-TiAl coating fabricated on γ-TiAl through a two-step process: electrophoretic deposition (EPD) of particles of Ti and Al and then hot pressing (HP). The β-TiAl coating was insignificantly degraded by interdiffusion with the γ-TiAl substrate and formed an adherent alumina scale by adding a small amount of Y_2O_3 particles during oxidation at 900 °C.

Ipaz et al. (2012) improved mechanical and tribological properties of AISI D3 steel surfaces by coating (Ti–Al/Ti–Al–N) multilayer systems deposited in various bilayer periods via magnetron co-sputtering pulsed d.c. method, from a metallic binary target. The multilayer coatings were characterized in terms of structural, chemical, morphological, mechanical and tribological properties. The failure mode mechanisms were studied by optical microscopy. Results from XRD analysis revealed that the crystal structure of TiAl/TiAlN multilayer coatings has a tetragonal and FCC NaCl-type lattice structures for Ti–Al and Ti–Al–N, respectively, i.e., it was found to be non-isostructural multilayers. An enhancement of hardness and elastic modulus up to 29GPa and 260GPa, respectively, was observed as the bilayer periods in the coatings were decreased. The sample with a bilayer period of 25 nm and bilayer number n= 100 showed the lowest friction coefficient and the highest critical load (45N), corresponding to 2.7 and 1.5 times better than those values for the coating deposited with n=1, respectively. The results indicated that there was an enhancement of mechanical, tribological and adhesion properties comparing to the (Ti–Al/Ti–Al–N) multilayer systems with 1 bilayer at 26 %, 63 % and 33 % respectively. The enhancement in hardness and toughness for multilayer coatings was endorsed to the different mechanisms for layer formation with nanometric thickness such as the novel Ti-Al/Ti-Al-N and the number of interfaces that act as obstacles for the crack deflection.

Cheng et al. (2012) studied mechanical properties of TiAlN thin films with different residual stress, which were fabricated with magnetic filtered vacuum arc evaporation deposition method on silicon substrate. The mechanical properties of TiAlN thin films vary with the residual stress existed in thin film. For a lower residual stress, the nanoindentation hardness (H) and modulus (E_r) of thin film were 18.96 and 210.16 GPa respectively. With the increasing the residual stress, the H and Er of thin film declined from 18.96 and 210.16 GPa to 16.9 and 185.9 GPa respectively. High residual stress induces the decreasing of the H and Er of thin film.

Yankov et al. (2012) undertook experiments to explore the possibility of creating an oxygen barrier coating, which was effective in preventing oxidation and oxygen embrittlement of Ti and several low-Al content Ti-base alloys during exposure to oxidizing environments at elevated temperatures. The fabrication process has involved three steps, namely co-deposition of Ti and Al by magnetron sputtering onto a substrate material to be protected, followed by vacuum annealing and plasma immersion ion implantation of fluorine. The first two steps produce an overlay of γ-TiAl while the last step provides the necessary conditions for bringing about the halogen effect upon subsequent high-temperature oxidation. Following oxidation in air at 600 °C for 100 h, specimens have been prepared for metallographic analysis, and their cross sections have been characterized by SEM in combination with EDX, and electron probe microanalysis (EPMA). The results obtained show that during oxidation exposure the coating was capable of forming a protective alumina-containing scale which serves as an oxygen barrier, thereby preventing oxygen embrittlement. In addition, since the only constituents of the coating are Ti and Al, it exhibits excellent chemical substrate compatibility.

Chen et al. (2012) studied the thermal stability and oxidation resistance of Ti–Al–N coatings, which are widely used for wear resistant applications due to their excellent mechanical and thermal properties, which depend to a great extent on the Al content. Here, they concentrate on a comparative study of the effect of Al content on crystal structure, thermal stability and oxidation resistance of $Ti_{1-x}Al_xN$ coatings. In agreement to earlier studies, thermal annealing of the individual cubic and wurtzite structured metastable coatings induces decomposition into their stable phases c-TiN and w-AlN. The decomposition process involves an intermediate formation of cubic Al rich and Ti rich domains, which results in a hardness increase to 34.7 and 34.4 GPa for $x = 0.52$ and 0.62 when annealed at 950 and 900 °C, respectively. In general, coatings with an Al content closer to the solubility limit exhibit an earlier decomposition process, and hence an earlier peak-hardness. During exposure of the coatings to ambient air at elevated temperatures Al_2O_3, TiO_2 and Al_2TiO_5 are formed. The oxidation resistance of as-deposited single-phase $Ti_{1-x}Al_xN$ coatings, cubic or wurtzite structured, increases with increasing Al content. However, coatings containing Al contents at the metastable solubility limit, which result in a mixed cubic–wurtzite structure, have the worst oxidation resistance of the Al-containing coatings investigated.

Han et al. (2012) described a combinatorial method for identifying alloy compositions of potential interest as structural materials. To investigate this idea, compositionally graded Ti–Al thin films have been sputter-deposited onto Si substrates, and the mechanical properties of the library of compositions are then probed using nanoindentation. Nanoindentation experiments were used to extract the properties of the film so that the bulk properties of the material may be estimated. A new method for extracting the hardness of films on substrates from nanoindentation experiments has been developed and was applied to the compositionally graded Ti–Al thin films. Together with the nanoindentation data and a compositional analysis, they are able to establish a relationship between the hardness of the film and the composition.

The above literature helped to decide the experimental procedure to be followed in the current work. On this basis the goal was set to produce a thin film of Ti Al on the various substrates using magnetron sputter deposition technique. A deposition of Ti Al with varying currents on various substrates by reactive unbalanced magnetron co-sputtering technique with heating the substrates was to be done. The effects of sputtering current on the structure and morphology of films were studied. The films were grown on the various substrates using titanium and aluminum targets in a varying Ar flow and working pressure. The structure of the films was investigated by XRD. The surface and cross-sectional morphologies of the films were examined by atomic force microscopy (AFM) and SEM. Furthermore, the chemical composition of the films was analyzed using energy dispersive x-ray spectroscopy (EDS).

It was planned that how the surface treatment applied in this work to can improve the coating properties. The structure and the properties of the films formed using individual targets were investigated and compared with various substrates. Coatings with the required thickness of γ -TiAl on various substrates were to be subjected to oxidation resistance measurement tests at 600 and 1100^0 C in oxidizing atmosphere. The micro and nano hardness of the film was to be measured. How the substrate temperature, the target voltage, deposition angles etc. are going to effect the coating. The surface and cross-section of the films were to be observed by SEM. The texture to be observed by XRD. The crystallite sizes of the films calculated from Scherrer formula. The effect of target–substrate distance was to be varied to check its effect.

Work was planned on the synthesis of nanoscaled coatings of Ti Al on the alumina on aluminum substrate developed by anodization. A series of sputter deposited Ti Al coatings with required layer thickness have to be applied for XRD and scanning electron microscopy (SEM) analysis. To check the residual stresses present with the substrate on coating Ti Al layers. The mechanical properties of Ti Al thin films with different residual stress, which were fabricated with magnetic sputtering deposition method on various substrates.

CHAPTER 3

SCOPE AND OBJECTIVES

As an important material in surface application, titanium aluminide has attracted many researchers due to its unique properties (semiconducting, piezoelectric, magnetic etc.). One of the key requirements for many of these applications is the variation of properties with alloying of Ti – Al. The aim of the present work is to grow gamma Ti – Al thin films and to probe the material properties of grown thin film. The following objectives had been set:

1. To optimize various process parameters for the growth of TiAl thin films.
2. To develop intermetallic TiAl thin films of various thicknesses by DC Magnetron Sputtering on different substrates using optimized conditions.
3. To study the effect of process parameters on the growth of TiAl thin films.
4. To study the composition of as deposited and heat treated TiAl thin films.
5. The analyze the growth mechanism involved in the process.
6. To study the effect of annealing on the properties of coated films.
7. To study the microhardness and nanohardness of coating.

CHAPTER 4

EXPERIMENTAL WORKS

In this chapter the pretreatments for the substrates and targets, coating process and characterization carried out on the coated Ti – Al are explained. High purity titanium (99.97 %) and aluminum (99.99 %) were used as the sputtering targets. The targets were pretreated prior to sputtering. It was noted that the pretreatment procedure has significant effects on the sputtering target. The pretreatment process included cleaning of the substrates and surface roughness minimization using electropolishing. Then the substrates were subjected to the sputtering process in the magnetron sputtering system. In this work intermetallic titanium aluminide (TiAl) thin films were prepared by DC magnetron sputtering of titanium (Ti) and aluminum (Al) from two different sputtering targets. A systematic study of the effects of process parameters such as argon (Ar) gas pressure, time of sputtering, target to substrate distance, substrate material were carried out. Studies on the compositional properties of the thin films were performed using XRD (JEOL Model- DX-GE-2P) for composition and phase analysis. The thin films were also studied using EDS and SEM (Model - JEOL / JSM - 6380LA). The focus was given for the composition, strength and hardness of the coated thin film related to their growth process. The structural property of thin films during recrystallization was studied by performing annealing at various temperature regimes. The experimental work was expected to improve the understanding of the compositional, structural and thermal properties of intermetallic TiAl thin films.

4.1 Substrate And Target Preparation

The preparation of the substrate and the target is very important in the thin film deposition. Their pre-preparation will affect the property of the thin film preparation. The preparations are discussed in 4.1.1 to 4.1.3 sections of this chapter.

4.1.1 Sputtering sources – (target material)

For industrial scale deposition sputtering and e-guns are the most common evaporation sources. Sputtering and e-gun can hold a rather large volume of deposition material which usually renders them a good choice for long term deposition. However, with respect to reactive sputtering of films there are limitations. Due to the gas flow into the chamber in the long run metal-oxide skins build up on the surface. Since the deposition rate is mainly controlled by the temperature of the target the oxide formation reduces the vapor flow rate – in the extreme case to zero if the skin cannot be penetrated any more. However, due to their short time constants they also put higher requirements to the speed of the rate control. Multi-component material cannot be sputtered from a single source due to cracking and they will not sputter stoichiometrically. Only a moderate source to substrate distance can compensate for this disadvantage, which in turn reduces the material efficiency. Typically, sputtering employs pure metals which are available in disc forms (termed as sputter targets). They are usually stable and quite cheap compared or their complex metal-organic counterparts used for CVD. Sources provide a rather high degree of flexibility. The film composition can be tuned over a wide range to optimize the desired properties. In turn, the multi-source deposition requires a very accurate and stable control of the deposition rates. However, this technique is restricted to some fine tuning.

Only the analysis of the materials in front of the substrate offers a chance for a reliable online rate control. Due to the emission characteristics of the targets and temperature dependent sticking coefficients on the substrate surface this method cannot provide absolute values but calibrated empirically. However, it allowed a quite accurate relative control to keep the rates and film composition constant over the deposition time.

The common, commercially available rate monitoring is based on frequency shifts of oscillating quartz plates due to the deposited material. These quartz crystal monitors are quite robust and easy to handle. Even for rates of a few Å/s the accuracy is in the range of a few percent and stability as well as reproducibility is excellent. Their only shortcoming becomes evident when used for long term processes. When a certain material thickness has been deposited onto the quartz, the frequency shift is so large that the quartz fails oscillating. Multiple, exchangeable quartz heads may relax but not solve this problem.

4.1.2 Purity of the target materials

The deposited thin films will be contaminated if the target itself is impure. Usually high purity materials are used. A high purity aluminum (99.99 %) and titanium (99.97 %) sheet (3 mm thickness, 50.8 mm width supplied by Alfa Aesar-Chemicals) were cleaned initially using soap solution and then deionized water in an ultrasonic bath followed by degreasing in acetone solution for 10 minutes. The aluminum target was then soaked for 30 minutes in 1M NaOH to remove the natural oxide layer that would have been formed on the aluminum target. Then the substrates were thoroughly cleaned using double distilled water to remove the traces of NaOH. Electropolishing was carried out for this target to reduce the surface roughness. More electropolishing occurs at the surface ridges compared to the valleys due to increased electric fields, resulting in the dissolution of the ridges faster than valleys. Electropolishing was carried out in a mixture solution containing perchloric acid and absolute ethanol (10ml + 40ml) at 25 V and at $15^{o}C$ for 10 minutes, whereas the titanium target was immersed in Kroll's (10ml HF + 20ml HCl) solution for 15 minutes to remove the oxide layer that would have been formed on it in the atmosphere. This target is then thoroughly cleaned in double-distilled water and then dried. After these steps both the targets were mounted on the magnetron target holders for sputtering.

4.1.3 Effect of substrate surface

The quality of the surface is the most important property of a substrate; since it is here that the film-substrate interaction occurs. The nature of the condensed film depends on the structure of the substrate, its temperature and cleanliness. Condensing atoms align according to the structure of the underlying surface, forming amorphous or polycrystalline layers on amorphous substrate and a single crystal substrate respectively. The adhesion of a film to the substrate is strongly dependent on the cleanliness and microscopic topography of the substrate surface. Presence of contaminants on the substrate surface may increase or decrease the adhesion depending on whether absorption energy is increased or decreased.

The glass substrates were well-cleaned using soap solution, and perchloric acid (50˚C) and degreasing was done by acetone followed by drying at 80˚C. Other substrates aluminum, copper and steel were mirror-polished using the emery papers and electropolishing. The surface finished batch of metal substrates were coated with thin layer of vacuum gelly to protect them from environmental degradations. Before loading these substrates into vacuum chamber for coating they were thoroughly cleaned using proper cleaning procedure.

4.2 Sputtering

The sputtering experiments were performed in a stainless steel box coater (0.36 m height D – shape) using unbalanced magnetron sputtering unit. This unit was equipped with 50.8 mm titanium (Ti – 99.97 %) and aluminum (Al – 99.99 %) sputtering targets (Figure 13). The stainless steel deposition chamber was evacuated to a base pressure of (4 – 8) × 10^{-4} Pa using diffusion pump. Sputtering relies on a plasma (usually a noble gas, such as Argon 99.999 % (5N)) to knock material from a target a few atoms at a time. After evacuation, Argon of 5N purity was introduced into the chamber using gas mass flow controller (Make – Aalborg) attached to the system. The base pressure in the system during sputtering was maintained constant using throttle valve. The targets were kept at a relatively low temperature. The films were deposited onto well-polished and ultrasonically precleaned substrates of rectangular plate of width 10 mm x length 15 mm and 2 mm thick and circular disc of 20 mm diameter and 2 mm thick.

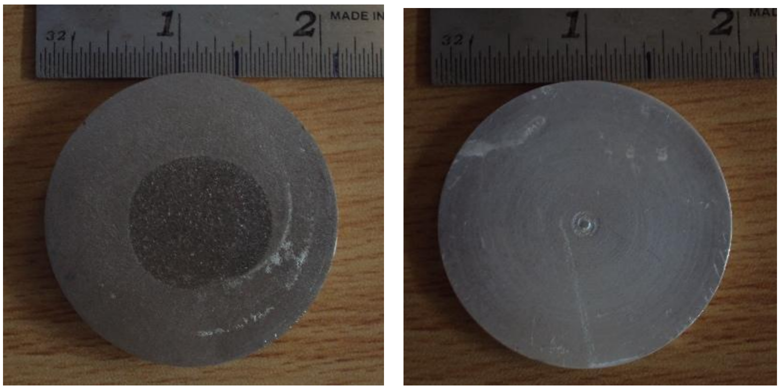

Figure 13. Image of titanium (99.97%) and aluminum (99.99%) sputtering targets.

4.2.1 Substrate holder

The most critical component of the deposition system is the substrate holder. Epitaxial growth of films requires high substrate temperature. Consequently, the substrate holder comprises heating elements to obtain a homogeneous temperature distribution across the entire substrate area. Optimum temperature uniformity is realized by radiation from heated walls surrounding the sample. The lower substrate temperature may turn out as a crucial point in view of coating since diffusion and unwanted substrate reactions are temperature activated processes, which are slowed down if not halted at lower temperature. The probable reason for the lower film growth temperature lies in the higher surface mobility of metal atoms which are already present in the gas phase for those depositing plasma. The substrates were fixed to a rotatable and heatable circular (7.62×10^{-2} m i.e. 3 inch) substrate holder, which was electrically isolated from the grounded deposition chamber. A shutter placed between the magnetron and the substrate holder makes it possible to clean the magnetron cathode surface before the film deposition. The substrate temperature (T) ranged from room temperature (RT) to 550°C. The films were deposited under the following conditions as in the Table 2.

To increase the ionization rate, the emitted secondary electrons were made to travel in magnetic field created by a magnet which was kept right below the target in the magnetron sputtering. The electrons were trapped in magnetic field path and circulated around the target surfaces. By the longer dwell time in the gas they cause a higher ionization probability and hence form a plasma emission at these pressures, which can be up to one hundred times smaller than that for conventional sputtering. Within the sputtering process gas ions out of plasma are accelerated towards a target consisting of the material to be deposited. Material is sputtered from the target and afterwards deposited on a substrate in the vicinity. To enable the blast-off of plasma usually argon is fed into the chamber up to a pressure of 0.5 mbar. In the dc-sputtering a negative potential up to some hundred volts is applied to the targets. As a result, the Ar-ions accelerate towards the targets and set the target material free; on the other hand they produce secondary electrons. These electrons cause a further ionization of the gas. For a sufficient ionization rate a stable plasma results, where sufficient amount of ions are available for sputtering of the material. The two-target magnetron system allows magnetron co-sputtering of two separate magnetrons operating independently from each other. This technique provides control of individual magnetron currents and hence, material yield from each magnetron. However, the technique of deposition used to develop superior coatings, a greater knowledge of the process of film formation, microstructure and their resulting mechanical properties is required, which is determined by the influence of process parameters, like target voltage, magnetron geometry, working pressure etc. on the composition, surface morphology, and mechanical properties of the films. Usually substrate and target surface are parallel to each other. A variation of the deposition angle i.e. sputtering under oblique incidence can be achieved by tilting the target or substrate. Thereby a new preferential direction for the film growth and potentially anisotropic films can be produced. The magnetrons in this work were set at 38° with respect to box coaters' top surface geometry (Figure 14). The targets were sputter cleaned for 10 min. with argon while the substrate was shielded by the shutter over the magnetrons.

The electron density and hence the number of generated ions are highest, where the magnetic field (B) is parallel to the target surface. The highest sputter yield is observed on the target area right below this region (Figure 15b). On the other hand fewer collisions occur for the sputtered material on the way to the substrate because of the trapping in the magnetic field and hence the kinetic energy of the sputtered particle at impact on the substrate is higher.

The sputtering target current I_{sp} for Ti and Al (Table 2) determines mainly the rate of the deposition process and hence the time which remains for the arriving particles during the growth process for either surface diffusion and agglomeration on existing growth centers or nucleation with other adatoms. The applied voltage determines the maximum energy, with which sputtered particles can escape from the target. Energies of the sputtered particles show a broad distribution with a maximum of the distribution between 1 eV and 10 eV. Also, the applied voltage determines sputtering yield, which is the number of sputtered particles per incoming ion. The deposition rate of each target was controlled separately at sputter ratio 3:1 of Al/Ti and was kept constant throughout the process which produced homogeneous Ti – Al coating on the substrates. The targets were maintained at a normal temperature during deposition by using cooled water circulation at a rate of 3 l/min. The pressure (P) in the sputter chamber determines the mean free path for the sputtered material, which is inversely proportional to pressure.

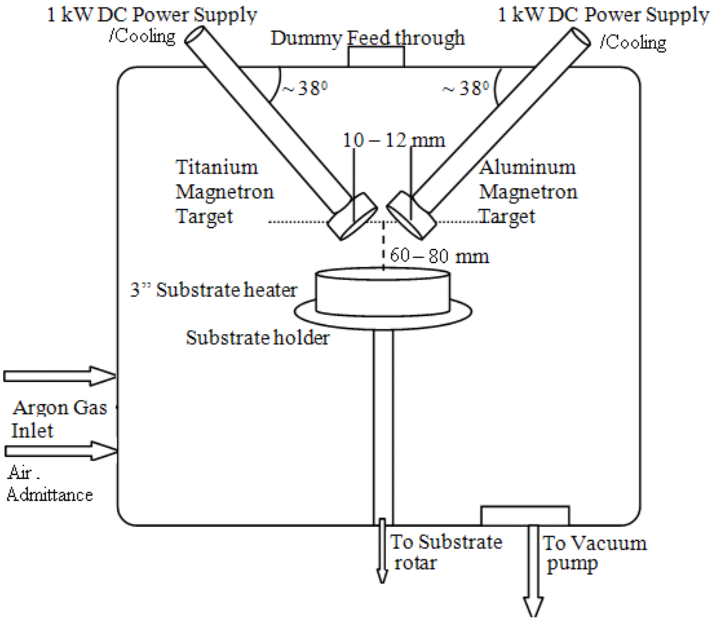

Figure 14. Schematic representation of the sputtering area chamber.

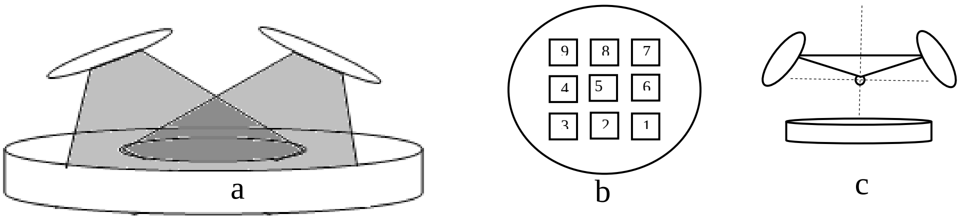

a

b

c

Figure 15. Schematic representation of the (a) sputtering area (b) sample positions and (c) angled argon gas inlet with respect to targets and substrates.

4.2.2 Distance between sources and substrate

The source to substrate distance was varied from 30 mm to 80 mm in such a way that very large region results in a high uniformity of the deposited films. There was a inherent uniformity at a particular distance. A large area can be coated simultaneously in this region. A second important consequence is the high volume deposition rate resulting in uniformity of the film thickness, composition, and the physical properties. Also inhomogeneities of the target are directly mapped onto the substrate. Obviously, there is a tradeoff between uniformity and material exploitation which drops quadratically with increasing distance. To achieve acceptable homogeneity for fixed substrate-target distance and a deposition area the target material must be efficient.

A lot of metal was deposited over the chamber bearing contamination and flaking. All components directly exposed to the vapor will be coated and since the material is hygroscopic, flakes start to peel off when the system is opened giving rise to problems. Capturing material, which propagates in wrong directions and thus confining the vapor in a deposition path, can be realized by metal screens.

Together with the target to substrate distance which was varied from 40 mm to 80 mm the working pressure kept at $5x10^{-3}$ torr (0.666 Pa) in the chamber controls how many collisions occur for the particles on their way from the target to the substrate. This influences the porosity of the films. The crystallinity and texture got affected via the gas input flow which was altered in steps of 5 ml/min from 15 ml/min to 30 ml/min by using gas mass flow controllers (Alborag). Also the angle at which the gas inlet positioned were bombarding the target surface varied from 40° to 55° by adjusting the designed flexible gas flow tube inside the vacuum chamber to serve this purpose, which affects the crystallinity and texture. A good stoichiometry in the growing film was observed when this angle was kept at 50° with sputtering metallic targets.

4.2.3 Substrate heater

During long sputtering times for the deposition of thick films, the substrate temperature raised to 350˚C without external heating. This substrate temperature as measured using thermocouple. This was having a strong impact on the growth behavior with respect to crystallinity or density of the samples. Hence a substrate heater controlled via PID was attached to this system to maintain a constant working temperature. The process parameters which were varied to obtain a good quality coating are as given in the Table 2.

Table 2. Deposition parameters used in this work (The numbers in bold font indicate the parameters which gave good results).

Sl. No.	**Deposition parameters**	**Details**
1	Target	Titanium (99. 97%), Aluminum (99.99%)
2	Base pressure (mbar)	4.0×10^{-5}
3	Total pressure (mbar)	$(4 – 8) \times 10^{-3}$
4	Substrates	Glass, Aluminum, Alumina, Copper, Mild Steel (MS)
5	Argon gas purity	99.999 %
6	Argon flow rate (ml/min)	15, 20, 25, **30**
7	Argon gas in put (I/P) angle (degree)	40, 45, **50**, 55
8	Distance between Ar I/P & Target (mm)	**15**, 20, 25
9	Target current I_{sp} (mA)	Titanium – 600, 700, **800, 900** Aluminum – **300, 400**, 500, 600
10	Deposition time (min)	5 , 10, 20, 30, 40, 50, **60**, 75, 90
11	Target to substrate distance (mm)	40, 50, **60**, 70, 80
12	Substrate rotation (rpm)	3, **5**, 10, 20
13	Substrate temperature (°C)	250, **350**, 450, 550
14	Target cooling temperature (°C)	10, **12**, 15, 20
15	Target coolant flow (l/min)	**3,** 5, 8

4.3 X – Ray Diffraction Analysis

X-ray scattering techniques are a family of non-destructive analytical techniques which reveal information about the crystal structure, chemical composition, and physical properties of materials in bulk and thin films. These techniques are based on observing the scattered intensity of an X-ray beam hitting a sample as a function of incident and scattered angle, polarization, and wavelength or energy. X-Ray Diffraction (XRD) is one of the primary techniques used to examine the physico-chemical make-up of unknown solids. In XRD, diffraction of X-rays takes place due to scattering from atoms configured in regular arrays. Here the atoms of a crystal, by virtue of their uniform spacing, cause interference pattern of the waves in an incident beam of X-rays. The crystal's atomic planes act on the X-rays in the same way a uniformly ruled grating acts on a beam of light. The interference pattern is specific to each substance and gives information on the structure of the atoms or molecules in the crystal. The spacing between atoms and planes of atoms is of the order of the wavelength of the X-rays. Bragg's law equation forms the foundation for X-ray diffraction i.e. constructive interference only occurs for certain θ's correlating to a (hkl) plane, specifically when the path difference is equal to wavelengths. The spacing between planes of atoms essentially functions as a 3-D diffraction grating. The Bragg's diffraction peaks shows that crystalline solid have long range periodic structure.

This data is represented in a collection of X-ray powder diffraction patterns for the three most intense d values in the form of tables of interplanar spacings and relative intensities (I/I_o). In XRD the coated sample of the material to be analyzed is placed in a sample holder, then the sample is illuminated with X-rays of copper K_α (30 kV, 20 mA) wave-length ($\lambda_\alpha = 1.5406$ Å) with a K_β filter and the intensity of the reflected radiation is recorded using goniometer. The diffracting angles will be set to 20° to 80° with a low scanning speed (1 °/min) and in continuous mode. The output data is then analyzed for the reflection angle to calculate the inter-atomic spacing. The intensity (I) is measured to discriminate (using I ratios) the various d spacing and the results are used to identify possible matches. The output data is analyzed using X-pert Highscore$^+$ software.

4.3.1 Texture and strain of the coated films

Texture of the thin films is dependent on the processing parameters as well as the substrates on which they are grown. It is important in most applications that films preferentially oriented rather than randomly oriented. The crystallographic texture of films grown on various substrates has shown interface between the film and substrate determines the final orientation of the film. The experiments showed that films achieved preferred orientations due to secondary grain growth wherein certain grains grow at the expense of the others exhibiting preferred orientations. The factors determining the final orientation of a thin film grown either on various substrates, or polycrystalline and amorphous substrates are now in existence (Krishna et.al 1998).

XRD data were used to determine texture coefficient and strain associated in the lattice. The scanning angle range was set in 20° to 80° at a step size of 0.02°. The texture coefficients of films were determined from the expression $T = \frac{I_{hkl}}{\sum I_{hkl}}$, where I_{hkl} is the intensities corresponding to (hkl) values.

4.4 Scanning Electron Microscopy (SEM) – Energy Dispersive Spectroscopy (EDS)

The scanning electron microscope uses a focused beam of high energy electrons instead of light to generate a variety of signals from solid specimens. The signal is obtained from the electron – sample interactions that reveal information about the external morphology (texture), chemical composition and crystalline structure and orientation of materials making up the sample. In SEM data are collected over a selected area of the surface of the sample, and a 2-D image is generated that displays spatial variations in these properties. The SEM has a large depth of field, which allows observation of an actual surface without any preparation. The SEM has much higher resolution and hence closely spaced specimens can be magnified at much higher levels. Because the SEM uses electromagnets rather than lenses, the researcher has much more control in the degree of magnification. Areas of approximately 1cm to 5 microns in width can be imaged by SEM techniques.

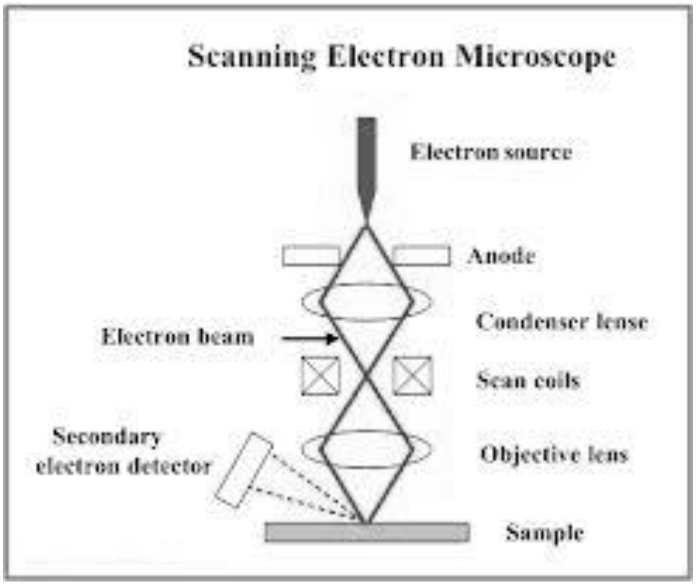

Figure 16. Schematic representation of SEM.

The Figure 16 shows the working diagram of SEM. In SEM, an accelerated beam of electrons is produced at the top of the microscope by an electron gun. The electron beam follows a vertical path through the microscope, which is held within a vacuum. The beam travels through electromagnetic fields and lenses, which focus the beam down toward the sample. Once the beam hits the sample, and its energy is dissipated as a variety of signals produced by electron-sample interactions when the incident electrons are decelerated in the solid sample. These signals include secondary electrons (that produce SEM images), backscattered electrons (BSE), diffracted backscattered electrons (EBSD) that are used to determine crystal structures and orientations of minerals), photons (characteristic X-rays that are used for elemental analysis and continuum X-rays), visible light (cathodoluminescence - CL), and heat. Secondary electrons and backscattered electrons are commonly used for imaging samples.

The scanning electron microscope is capable of producing high-resolution images of a sample surface (Reimer 1998) SEM images have a characteristic three-dimensional appearance and are useful for judging the surface structure of the coated surface. The EDS is a chemical microanalysis technique used in conjunction with SEM. The EDS technique detects x-rays emitted from the sample during bombardment by an electron beam to characterize the elemental composition of the analyzed volume. Phases as small as 1 µm or less can be analyzed. When the coating is bombarded by the SEM's electron beam, electrons are ejected from the atoms comprising the sample's surface and an x-ray is emitted. The x-ray energy is characteristic of the element from which it was emitted. The EDS x-ray detector measures the relative abundance of emitted x-rays versus their energy. The spectrum of x-ray energy versus counts is evaluated to determine the elemental composition of the sample. In this work we used SEM make JEOL JSM-6380LA.

4.5 Atomic Force Microscopy

AFM is one of many scanning probe microscopic techniques and is used to characterize the surface topography of samples. The working principle is that a sharp tip is scanned across the surface in a raster pattern while the vertical position of the tip is monitored as the tip follows the surface profile to build up a height map of the surface. The tip is located at the end of a thin cantilever mounted on a piezoelectric scanner able to scan the tip laterally and vertically. AFM has three main modes of operation - contact mode, tapping mode and non-contact mode. In contact mode the tip is put into contact with the surface and dragged across the surface while the deflection of the cantilever is monitored and kept constant. Contact mode AFM can result in damage of the tip and/or the surface resulting in erroneous measurements of the surface topography. Tapping mode AFM, also known as intermittent contact mode AFM, is gentler on the tip and sample than the contact mode. Here the cantilever is made to oscillate at or near its resonance frequency with constant amplitude. Height information is gained using the oscillation amplitude as a regulation parameter. The tip is lowered towards the surface until the oscillation amplitude decreases because the tip comes into contact with the surface; the height of the cantilever above the surface is then kept constant by the regulator as the tip is scanned across the surface. Non-contact AFM also utilizes an oscillating cantilever and amplitude regulator; here, however, the tip oscillates close to but not touching the surface. At these distances the tip interacts with the sample through attractive Van-der Waals forces causing amplitude shifts when cantilever height above the surface changes. In contact mode and tapping mode the tip penetrates the thin layer present on surfaces exposed to atmosphere allowing for higher resolution imaging of surfaces than non-contact mode under ambient conditions. Tip effects need to be taken into account when interpreting AFM micrographs as they can interfere in image feature. AFM has been used for surface imaging and characterization of the surface morphology and surface roughness in this work.

4.6 Heat Treatment

Heat treatment involves heating the samples normally to extreme temperatures, to achieve a desired result such as hardening or softening of a material. Heat treatment applies only to processes where the heating and cooling are done for the specific purpose of altering properties intentionally; heating and cooling often occur as incidental phases of other manufacturing processes such as hot forming or welding. The oxidation behavior and the structural evolution of the coatings are studied by carrying out soaking at elevated temperatures of 400 – 1100 ˚C. Coated samples are heated in steps of 100˚C for 1 hr. Above 900 °C the films started to crack in regular patterns. This may be due to release of the stresses present inside the coatings. Also it was accompanied by formation of TiO_2 and Al_2O_3 in the film. The formation of TiO_2 and Al_2O_3 above 900˚C was confirmed by XRD analysis. On heat treatment there was a decrease in the crystallite size of the coating TiAl along with the increase of microstrain of the coatings. This was clearly observed in the patterns where the peaks correspond to different orientation planes present. Also intensity of some peaks grew stronger along with the other peaks clearly indicating the decrease of crystallite size. This was due to growth of TiO_2 and Al_2O_3 at the time of heat treatment.

4.6.1 Oxidation measurement

In the present work Ti-Al films were deposited on steel (304) substrates kept at a temperature of 400˚ C by unbalanced oblique incidence magnetron sputtering. Steel (304) specimens of dimensions 10 x 10 x 2 mm were prepared for oxidation testing. These specimens were polished with various grades of SiC paper, up to 2000 grade and wet polished to 0.1 µm grit with diamond paste and degreased in ultrasonic cleaner just prior to coating of Ti-Al. On these well-prepared substrate specimens, ~ 1 µm thick Ti-Al coating was given by sputtering under calibrated conditions. Sputtered Ti-Al coatings were used for oxidation measurement. Oxidation measurements (Meier et al. 1993 and Menzel et al. 2000) were carried out in a resistance-heating furnace, in which the specimens were kept with indexing, and exposed to air at 600, 700, 800, 900, 1000 and 1100˚C respectively, for durations of 1 to 5 hours in an interval of 1 hour each. The weight of each specimen (in g) was measured at regular intervals of time using a micro balance. The nine specimens were weighed after exposure durations of 5, 10, 15, 20, 25, 30, 40, 50 and 60 min. respectively. A few specimens were weighed after exposure durations of 2, 3, 4 and 5 hours respectively. The specimens were not recycled once it was exposed to heat for the specified duration and weighed. To avoid the effects of experimental error three identical specimens of uniform dimensions were tested and the average weight gains were used for plotting the graphs.

CHAPETER 5

RESULTS AND DISCUSSION

The sputtering was carried to get the thin film of Ti Al with the optimised parameters. These parameters are as listed in the Table 3. were used for further characterization and analysis that were carried in this chapter. The SEM, XRD, AFM and heat treatments were done for the thin films obtained by using these optimized parameters.

Table 3. Optimized parameters used in coating thin film of Ti Al for Result and Discussions.

Sl. No.	Deposition parameters	Details
1	Target	Titanium 99. 97%, Aluminum 99.99%
2	Base pressure (mbar)	4.0 x 10^{-5}
3	Total pressure (mbar)	Low Pressure ~ 4 x 10^{-3} High Pressure ~ 8 x 10^{-3}
4	Substrates	Glass, Aluminum, Alumina, Copper, Mild Steel (MS)
5	Argon gas purity	99.999 %
6	Argon flow rate (ml/min)	30
7	Argon gas in put (I/P) angle (degree)	50
8	Distance between Ar I/P & Target (mm)	15
9	Target current I_{sp} (mA)	Titanium – 800, 900 Aluminum – 300, 400
10	Deposition time (min)	60
11	Target to substrate distance (mm)	60
12	Substrate rotation (rpm)	5
13	Substrate temperature (°C)	350
14	Target cooling temperature (°C)	12
15	Target coolant flow (l/min)	3

As the sputtering was carried to get the thin film, there was an erosion zone formed on the target, which follows the form of the magnetic field present at the target surface (Figure 17). The erosion region is found to be 5 mm width in both the targets. Major sputtering occurs from this erosion region of the target where the magnetic field strength is more compared to other regions. The sputtering will continue from this region until the targets get ruptured. If the target thickness is less than 3 mm then there will be buckling of the target after 2 to 5 cycles of sputtering. This may be due to increase in the magnetic field strength of the target holder. Other than the eroded region, there was presence of contaminated region (~ 15 mm) which was developed at the time of sputtering. This region was observed inside and out of the eroded region. The contaminated regions must be cleaned before each sputtering. If not, the properties such as composition, thickness, and yield will get affected at the time of deposition.

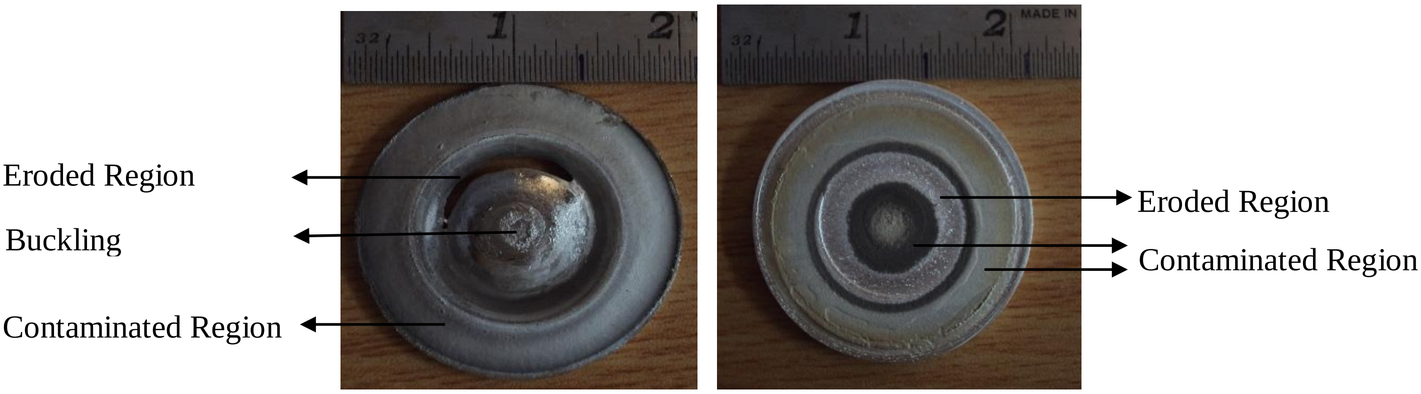

Figure 17. Images of sputtering targets after few cycles of sputtering showing different region on titanium and aluminum sputter targets.

The plasma area (Figure 15a) which was observed at the time of deposition was a truncated cone of approximately 60 – 90 mm in length with top and bottom diameters of ~23 mm and ~37 mm respectively. Approximately in 40 mm region of this truncated cone the coating developed will be that of Ti – Al combination and on other regions the coating is having more amount of either Ti or Al.

Sputtering of target resulted in crater formation (Figure 18) on the surface of targets (Figure 19). The rate at which etching of sample takes place is called sputtering rate (R) and is defined as an amount of materials removed (h) per sputtering time (t). The units for sputtering rate are depth/time (nm/s, or Å/s) (Vincent and Smentkowski 2000).

$$\text{Sputtering rate } R = h/t \tag{3}$$

In order to measure the sputtering rate of a target material accurately we must know the amount of material removed (h) and the sputtering time (t). Sputtering rate measurements were performed on samples of known thickness. Figure 20 shows the depth of the crater (h) measured using a microscope. Thin film of Ti Al of ~ 1.2 µm thickness was coated on a Si substrate during argon ion bombardment and sputtering rate was calculated to be ~ 205.5 Å/min. Sputtering rate depends on number of parameters, such as the incident ion flux, working pressure, background pressure of the sputtering species, gas phase composition and the raster regions. Even when these variables are kept constant there will be sputtering rate change due to target degradation with respect to time. The sputtering phenomenon is accurately described by sputtering yield (Y) (Vincent S. and Smentkowski 2000). This is defined as the quantity of material removed per incident ion.

$$\text{Sputtering yield Y (atoms ejected/ unit area)} = V\rho e / I t \tag{4}$$

Where V is the crater volume, ρ is the density of the sputtered material, I is the ion current, t is the sputtering time and e is the charge of electron.

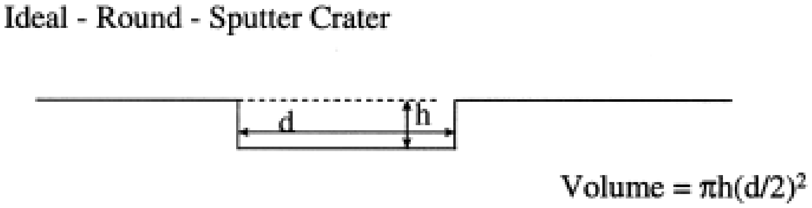

Figure 18. Ideal sputter crater formed at the time of sputtering.

Figure 19. Real sputter crater formed at the time of sputtering of titanium target.

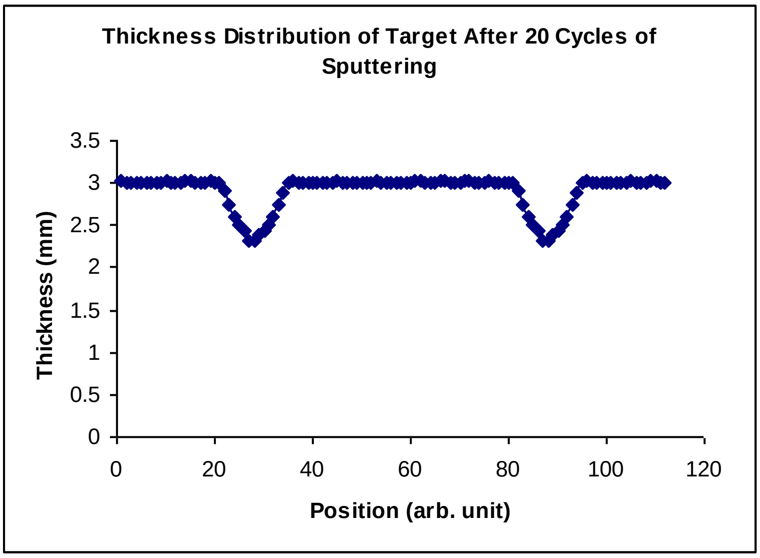

Figure 20. Plot of real sputter crater depth profile of titanium target sputtered for 60 min using travelling microscope.

The temperature of substrate during sputtering strongly influences the deposition rate and film properties of the compound being deposited. The temperature of the substrate was controlled by using substrate heater attached with the PID controller. Since the sputtered atoms are carrying the thermal energy generated from bombardment of sputtering ions the temperature of the substrate gradually increases from RT to ~450˚C (Figure 21) at the time of sputtering. Due to this, there was a thermal mismatch between the depositing film and the substrate which inturn induced cracks in the film. If substrates were not preheated to 350˚C at the time of sputtering, there was composition variation along the film thickness with cracking. Hence the substrates were preheated to above 350˚C at the time of deposition which resulted in uniform film properties.

5.1 Effect of Process Parameters

Flow control of the gas was the simplest method to control the gas flow into the sputtering chamber. The sputter gas flow was maintained at 30ml/min using mass flow controller (Make; Aalborg). Initially the flow of the argon gas to the chamber shoots up to 32ml/min and gets saturated to 30ml/min within a few minutes (~5min) of time (Figure 23). After saturation same flow was maintained throughout the experiment.

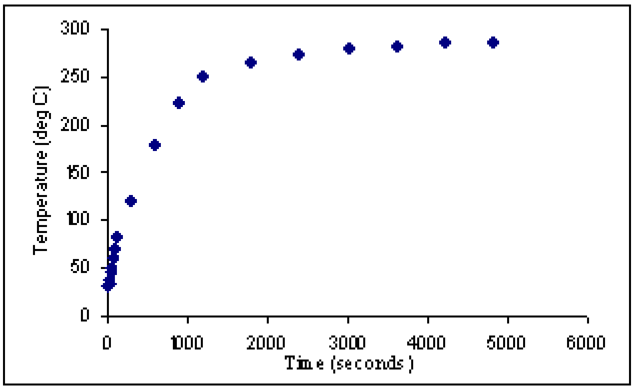

Figure 21. Graphical representation of substrate temperature vs deposition time for substrate to target distance of 60 mm.

This flow rate gave a working pressure of 4 – 5 mbar (0.533 – 0.666 Pa) in the sputtering chamber which was required for sputtering of titanium and aluminum to occur in the present system. Sputtering was done in the elemental mode of the target; the deposition rate was good compared to the rate from the compound target. In addition, the film properties produced by flow control reactive sputtering are optimal. The substrates were placed on the substrate holder as shown in figure 5b. The composition (figure 22) of the coated films was almost constant in position number 5 (figure 15b) on the substrate holder. In other positions, a variation in the composition of the film was observed due to inhomogeneous mixing (figure 15b) of vapour phase of titanium and aluminum when they were inclined with respect to the substrates.

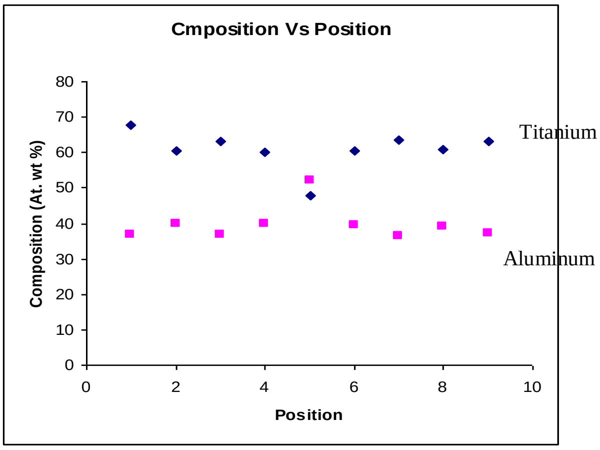

Figure 22. Variation in composition vs substrate position.

5.1.1 Effects of argon (Ar) gas pressure

The sputtering gas flow was maintained at 30 ml/min using mass flow controller (Aalborg). Initially the flow of the argon gas to the chamber shoots up to 32 ml/min and then got saturated to 30 ml/min within a few minutes (~5 min) of time (figure 23). This flow rate gave a working pressure of 4 – 5 mbar (0.533 – 0.666 Pa) in the sputtering chamber which was required for sputtering of titanium and aluminum to occur in the present system. The other flow rates resulted in the unstable sputtering for the required time of deposition.

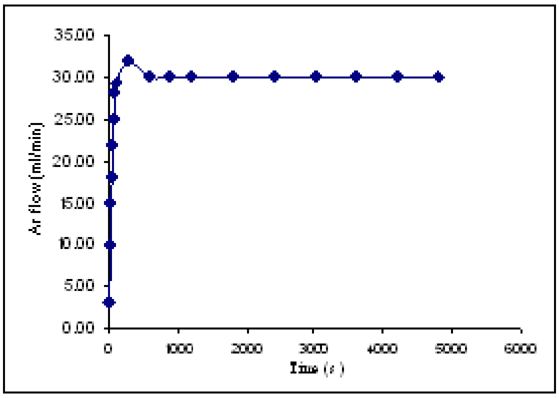

Figure 23. Variation of argon flow vs Time.

It was observed that the deposition pressure had an important effect on crystal orientation, where high and low pressure depositions resulted in a different crystal texturing in thin films. XRD of different argon flow thin film is shown in Figure 24. Thin films deposited at low pressure were textured along (200) orientations. On the other hand, thin films deposited at low pressure (~ 4 x 10^{-3} mbar) were textured along the (202) orientation. Different texture evolved for different argon pressure levels due to the increased shadowing effect. At lower pressures different surface mobility of adatoms comes in to picture resulted in different crystal orientations. At the early stages of deposition, low surface mobility islands grow vertically as compared to higher surface mobility islands which prefer to grow laterally. Due to their height, the shadowing effect enhances vertical growth of adatom making them the grains of dominant crystal orientation. In almost the same way, increasing argon pressure enhances the shadowing effect and the crystal growth on low mobility crystal orientation. During deposition, compressive residual stress was developed in the thin films deposited at a high argon pressure (~ 8 x 10^{-3} mbar). These films could not be grown thicker due to peel off from the substrate.

In contrast, it was possible to deposit almost 1.2 µm thick single layer film at high argon pressure with minimum tensile residual stress. During deposition, a highly compressive residual stress developed in the thin films deposited at a low argon pressure. These films could not be grown thicker due to peel off from the substrate. SEM images (Figure 25) show that these films exhibit a columnar microstructure as predicted by the structure zone model.

It is well known that residual (also called intrinsic) stress naturally evolves during growth of sputter deposited thin films. The control of this stress is essential for high mechanical quality coatings without cracking, buckling, or delamination. Dependence of residual stress on process parameters and microstructure showed strong correlation between residual stress and Thornton's structure zone model for sputtered thin films. Deposition at high argon pressure reduces the directionality of the incoming flux to the substrate and enhances the shadowing effect during film deposition which is responsible for the formation of a columnar structure. Thin films deposited by changing argon pressure successively between high and low pressure are relatively dense and shown low residual stress (439 MPa) values. Also, it was observed that crystal orientation (texture) of thin film was strongly affected by argon pressure level. Low density thin films deposited at high argon pressure and low temperature (regime Zone I) have almost zero residual stress (Karabacak et al. 2004). Decreasing argon pressure develops tensile stress and further decrease in pressure results in change from tensile to compressive stress finally forming a dense thin film (regime Zone T). In order to deposit low stress thin films, working pressure must be kept between tensile to compressive stress transition region which is difficult since the working pressure becomes low and the deposition is unstable. Overall thin film stress was reduced by changing sputtering conditions leading to thin film composed of low and high density regions.

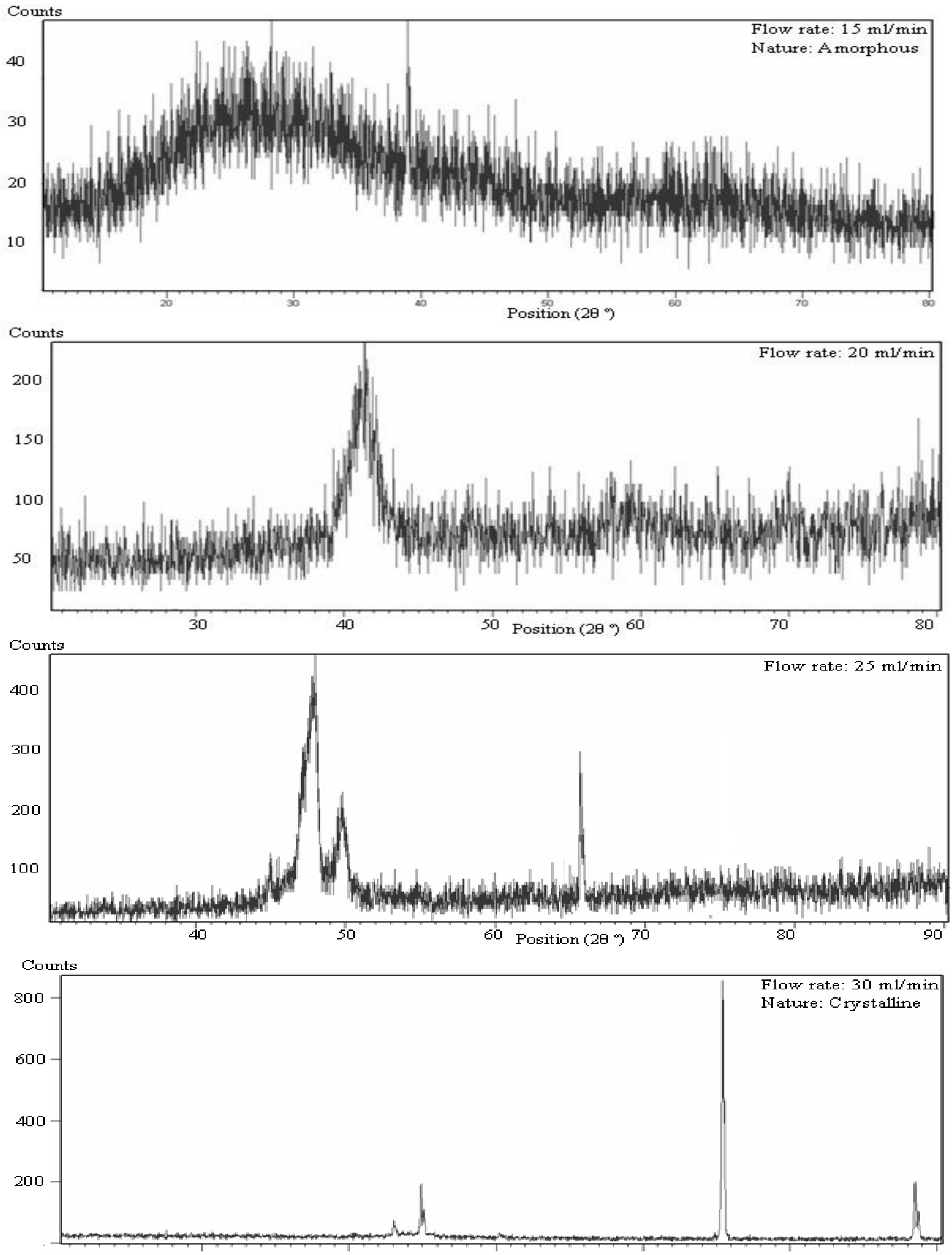

Figure 24. XRD of thin film grown at different argon flow as indicated in figures.

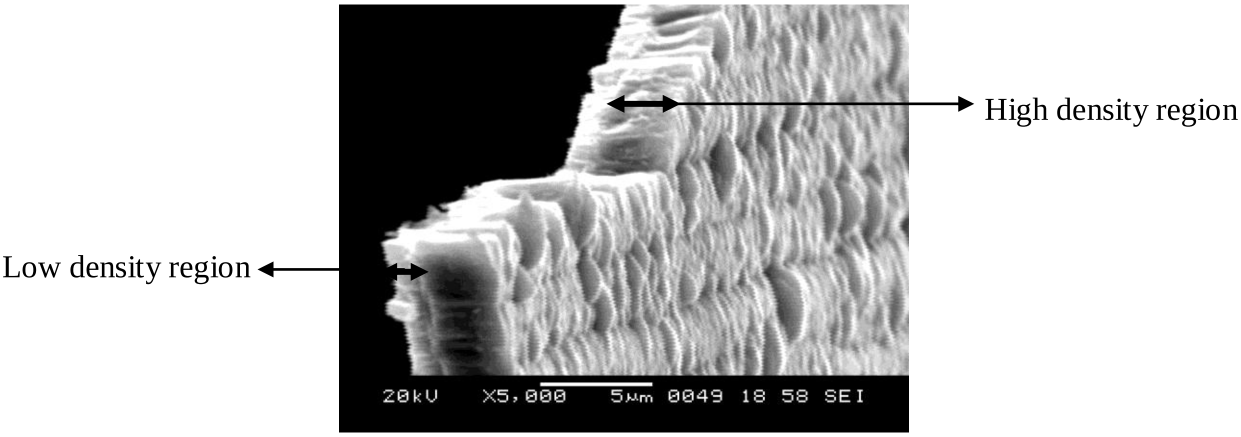

Figure 25. SEM image of the free standing thin film showing layered growth.

5.1.2 Effect of time of sputtering

The sputtering was carried out in times of 5, 10, 20, 30, 40, 50, 60, 75, and 90 minutes. It was observed that a discontinuous film was developed in the time intervals of 5 and 10 minutes. As the deposition time increased to above 10 minutes the film developing was continuous but a peel out of the film from the substrate was observed above 75 minutes. This may be due to accumulation of intrinsic stress. The stress of film increases slowly as the total thickness increases. This can be explained by thermal stress evolution during long deposition times due to the thermal expansion coefficient mismatch between substrate and depositing film. Thermal stress stabilizes at selected thickness regions for a thin film and substrate combination. The variation of the film thickness with time is as shown in the figure 26. Thickness got almost saturated around 1.2 µm in a time of 60 minute. Above this time the sputtering process slowed down due to target contamination in this experiment. This can be overcome by alternating the working pressure to 7 – 8 mbar (0.933 – 1.066 Pa). Thickness and XRD measurement were carried out for the film deposited at 10, 20, and 30 minutes samples. It was observed that the thickness was ~0.5 µm, ~ 0.8 µm and ~1.0 µm. These samples gave an XRD pattern as given in the Figure 27. For the sample coated for 10 minutes, the film was almost amorphous in nature and was observed to be discontinuous in selective regions. As the time of deposition increased the crystallinity started to improve along with the film continuity.

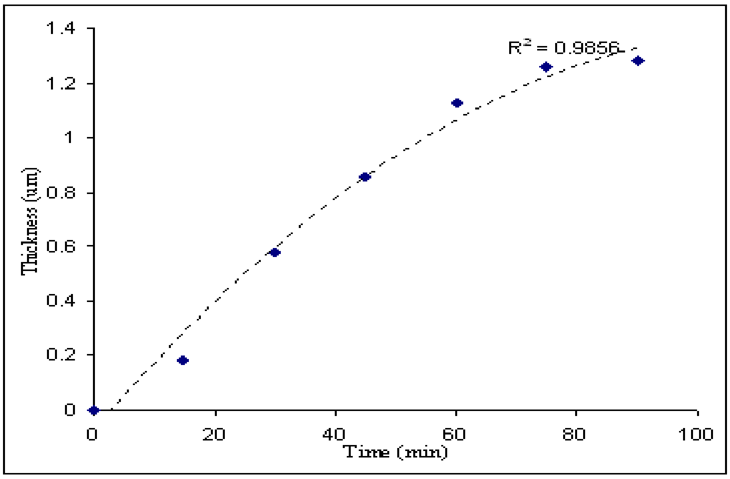

Figure 26. Variation of film thickness vs sputtering time.

5.1.3 Effect of target to substrate distance

The target to substrate distance was varied as 40, 50, 60, 70, and 80 mm. When the target was placed below 60 mm, it was observed that thickness of the coating was low (~0.65 µm) for a time of 60 minutes. Also the sputtering yield got affected by this position due to contamination of the targets by back deposition of the sputtered particles on them. As the working distance was increased above 60 mm, the thickness of the coating was ~0.83 µm for a time of 60 minutes.

But there was a triangular shaped particle observed in films (Figure 28). The film densification was not observed in these regions. Also there was buckling in some of the regions in thin film; this was due to poor adhesion of the film to the substrate. When the working distance was set to 60 mm a good quality film developed with a thickness of 1.2 µm. The adhesion of the film was good compared to other working distances. The film was having uniformity with a granular structure on the surface (Figure 29). The XRD measurements revealed a good texture coefficient of 0.92 for this working distance.

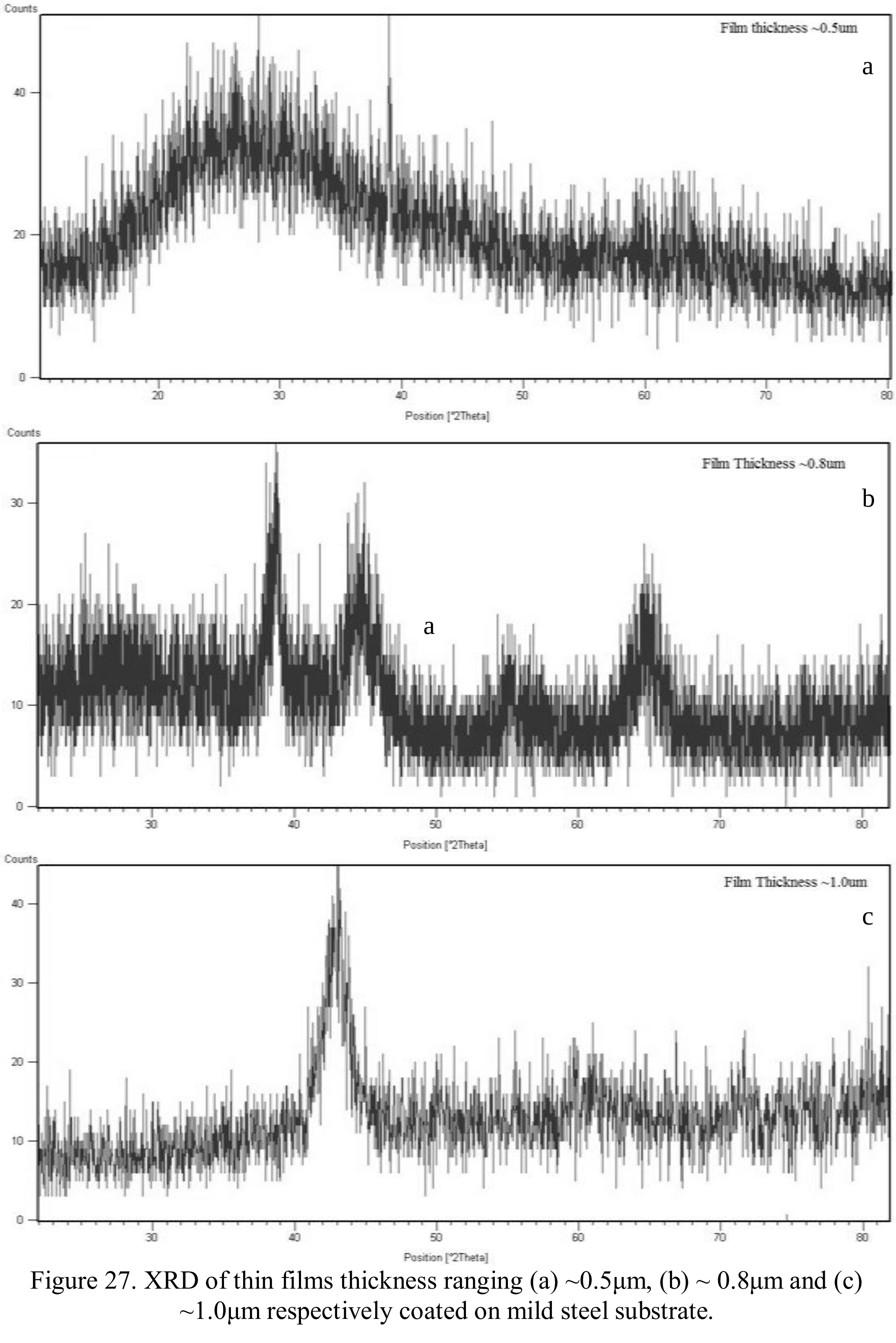

Figure 27. XRD of thin films thickness ranging (a) ~0.5µm, (b) ~ 0.8µm and (c) ~1.0µm respectively coated on mild steel substrate.

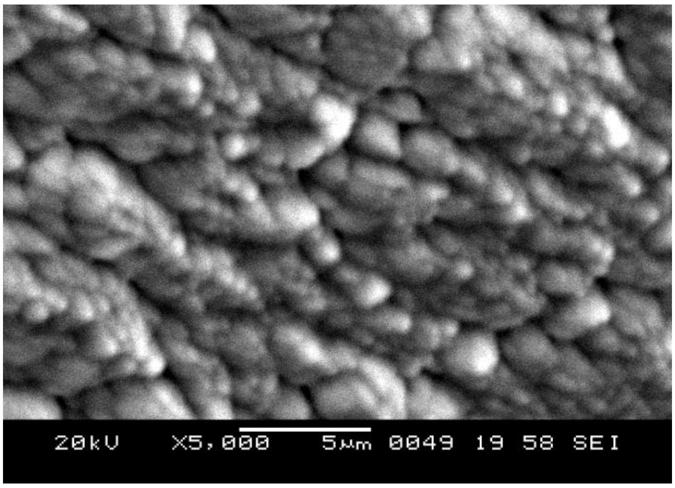

Figure 28. SEM image of coated film developed above 60 mm target to substrate distance.

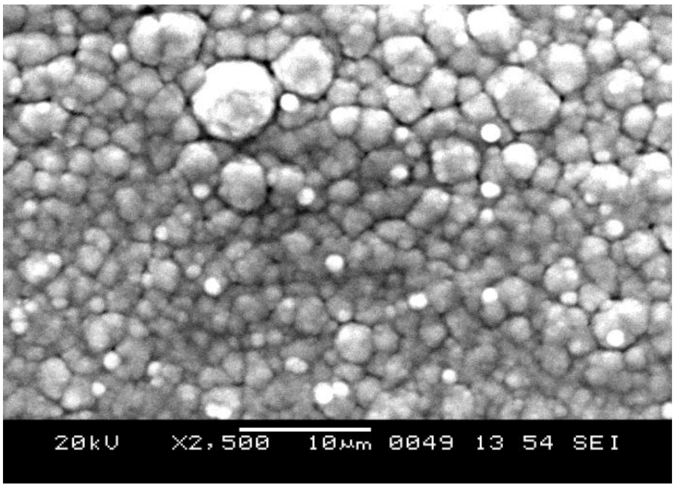

Figure 29. SEM image of coated film developed at 60 mm target to substrate distance.

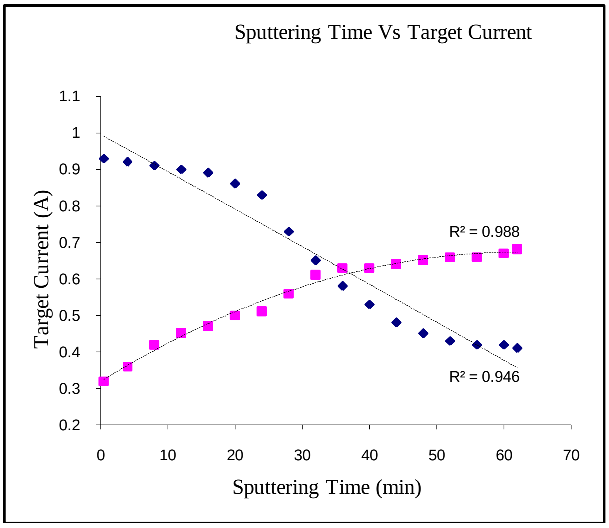

Figure 30. Variation of target current vs sputtering time.

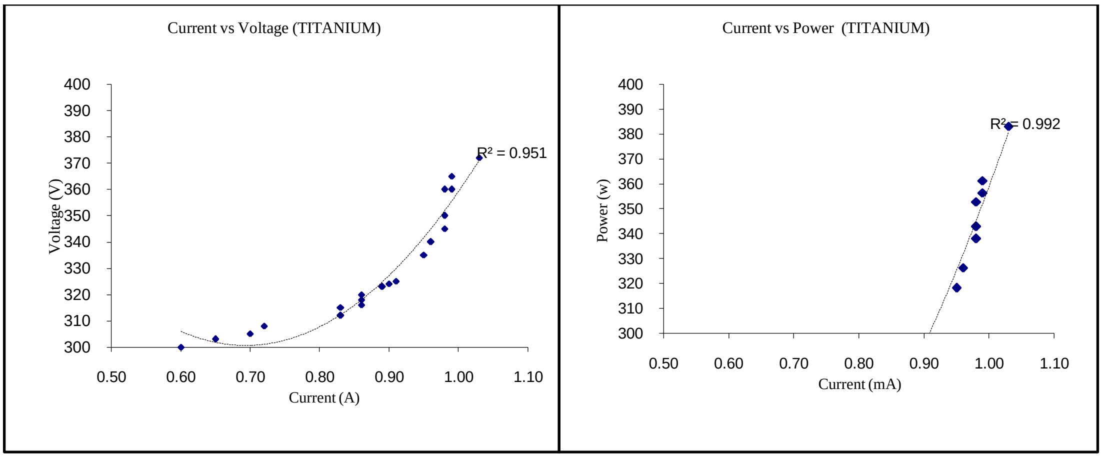

Figure 31. Variation of target current vs sputtering voltage and target current vs power for titanium target.

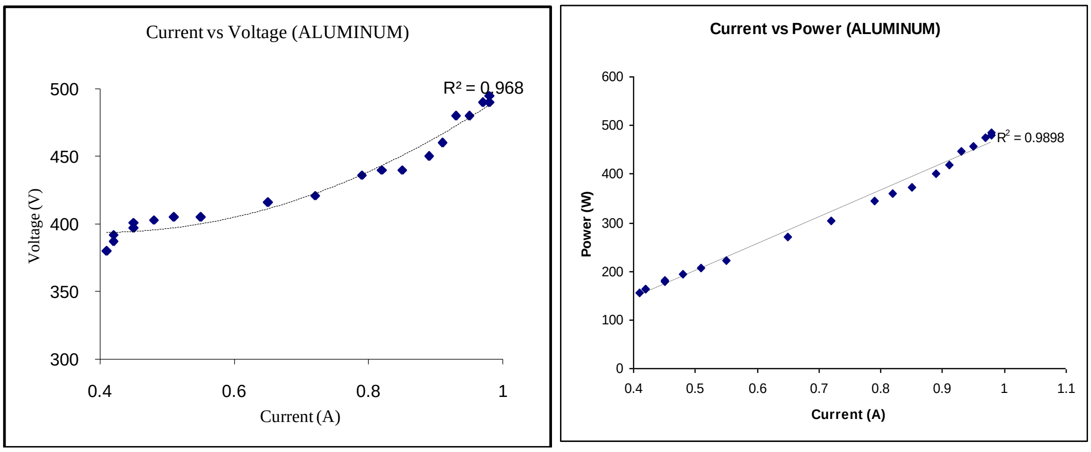

Figure 32. Variation of target current vs sputtering voltage and target current vs power for aluminum target.

The sputtering for films requires the use of the right type of power to prevent arcing on the target, which is detrimental to the quality of the deposited films. Constant dc power prevented arcing during the reactive sputtering of targets. The currents and voltages of the two targets were controlled individually. It was observed that current of the titanium target increases with time and that of the aluminum target decays with time (Figure 30). This may be due to decreased oxide layer thickness formation in titanium and increased oxide layer thickness formation in aluminum targets respectively. But the ratio of the currents can be kept constant in the system which is a necessary condition for sputtering of titanium and aluminum in the desired composition. The variation of depositing power was as represented in the figure 31 and figure 32 for titanium and aluminum targets respectively. Depending on this the arcing was prevented to minimize droplet ejection from the target and allowing the deposition to occur without large fluctuations in the gas pressure. The arc generated at the time of the sputtering induced cracks in the targets of aluminum and through holes in targets of titanium (Figure 33). As long as powers provided for ionization of the sputtering species regulated properly the arc formation was minimized.

Figure 33. Images showing the of crack developed in aluminum target and a through hole in titanium target due to arcing.

The thickness uniformity of films deposited by magnetron sputtering system with rotation and position was studied. Under the conditions of movement of a substrate underneath a magnetron sputter cathode, thickness of thin film and the parameters, such as rotation speed and the distance from target to substrate were obtained. The curve of film thickness versus the time parameter revealed saturation in the film thickness (Figure 26).

From the curves, the optimum parameters of the system can be easily obtained for preparing uniform films. It was found that the relative deviation of film thickness distribution was less than 5% within a diameter of 40 mm when the rotation speed was 5 rpm and target to substrate distance was 60 mm and the results show good agreement during experiments performed repetitively. Generally, for different sputtering systems and different sputtering conditions, the characteristics of the thickness distribution are different.

5.2 X – Ray Diffraction Analysis

The prepared coatings were amorphous and crystalline in nature depending on thickness of the film. The obtained X-Ray Diffraction (XRD) patterns of the coatings on different substrates are shown in figure 34 – figure 36. The diffraction patterns of the coatings were superposed with their respective substrates for confirmations. The diffraction peaks, corresponding to that of the Titanium (Ti) – Aluminum (Al) match with the JCPDS data (47-1137) of $Al_{1+x}Ti_{1-x}$ (Orthorhombic). The amorphous nature of the coating was observed in the 2θ range of 20 to 32 degrees. It can be observed that the diffraction peaks at positions 44.99, 65.56 and 78.89 correspond to (200) (202) and (113) planes of Ti – Al respectively (Table 4., Figure 37.). This characterization revealed the growth of (Ti, Al) intermetallic thin film with a characteristic crystallite size of 123.9 Å and a lattice strain of 0.1352 %.

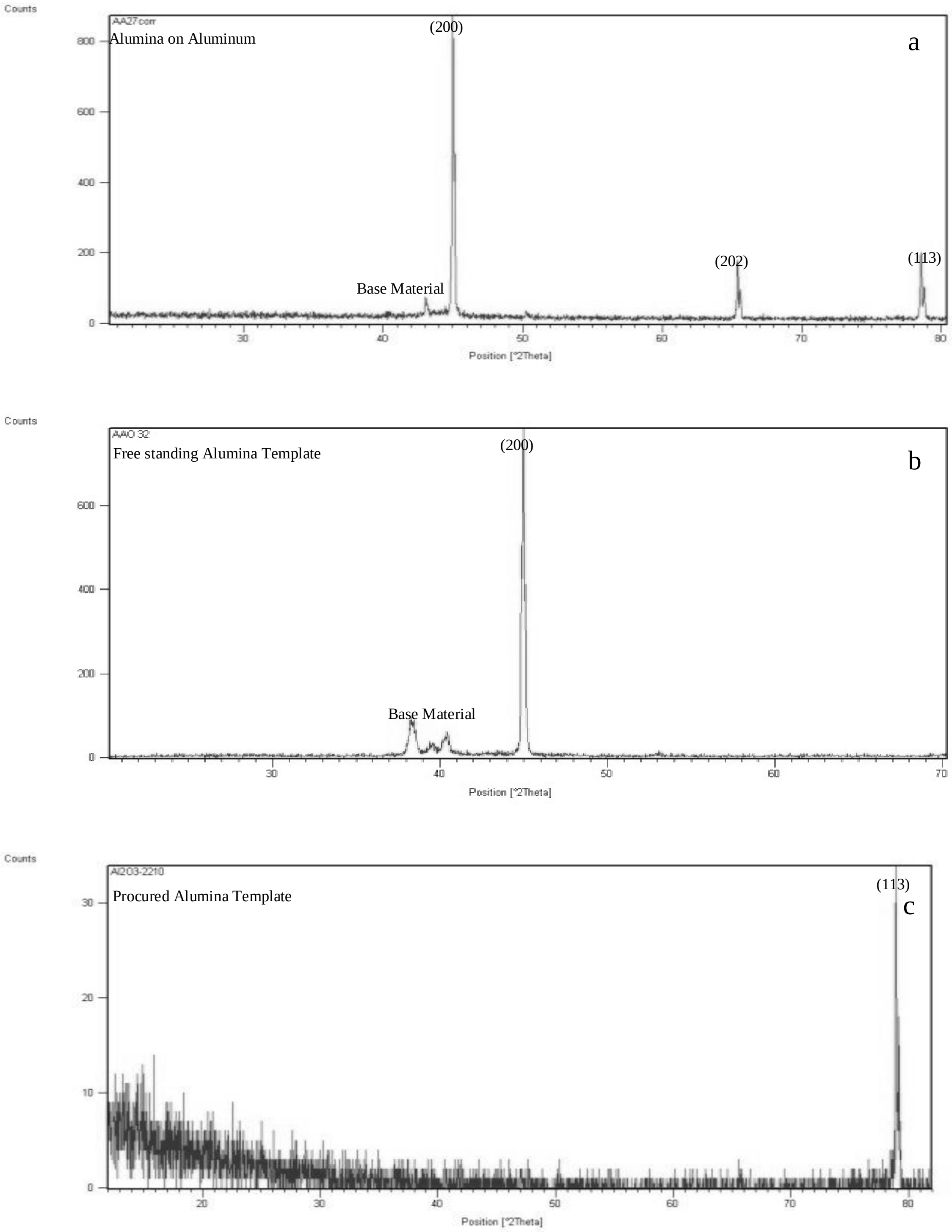

Figure 34. XRD patterns of deposited Ti Al film on prepared (a) alumina on aluminium, (b) free standing alumina template and (c) procured alumina template respectively.

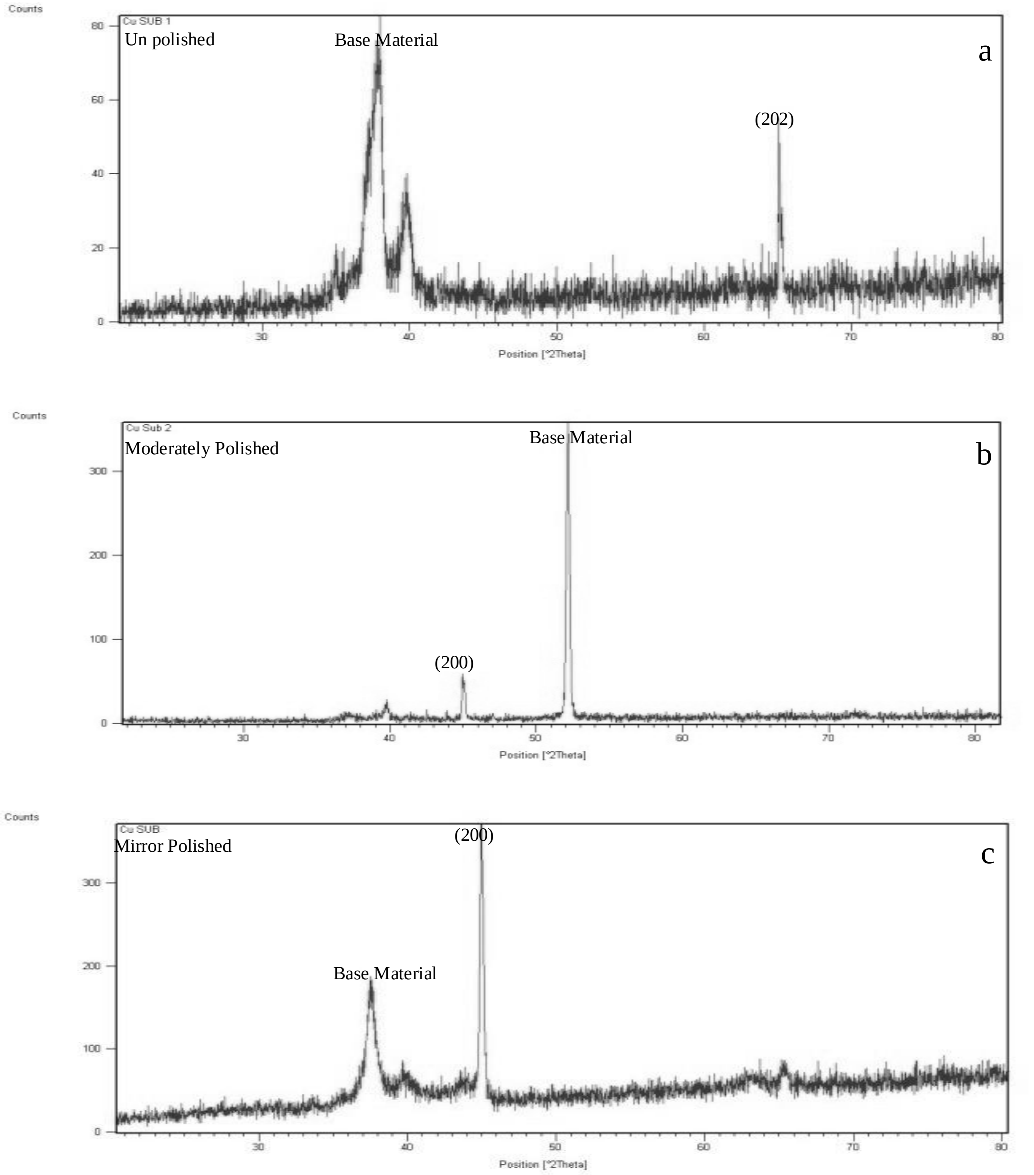

Figure 35. XRD pattern of deposited film on (a) unpolished, (b) polished and (c) mirror finished copper substrates respectively.

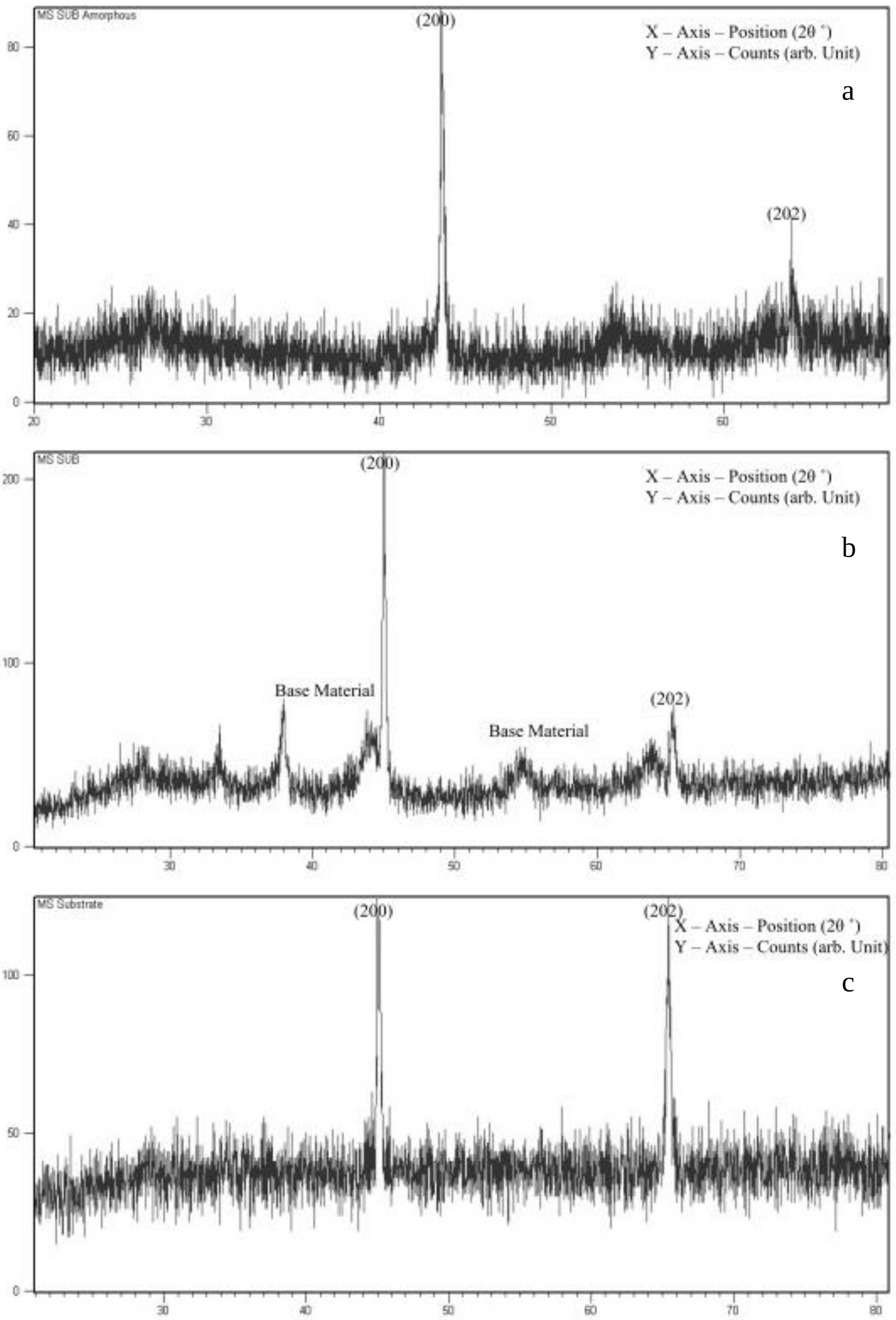

Figure 36. XRD pattern of deposited film on (a) unpolished, (b) roughly polished and (c) mirror finished mild steel substrates respectively.

The chemical composition of the deposited films showed Al to Ti ratio of 1.03 for an average film thickness of 1.2 µm. Films showed a fine crystallite size and they showed columnar growth. The film surface was under low compressive stress up to

679.0 MPa. For Ti – Al, the oxidation behaviour up to 1100˚C (high temperature range) was studied. Therefore, samples were annealed or heated in atmospheric condition using the box furnace. The results show decomposition of the Ti-Al structure to the TiO_2 and the Al_2O_3 phases at temperature values above 900 ˚C. Heating in air causes growing of a thin aluminum oxide layer at the film surface, which is a barrier for further oxygen diffusion to the film boundary. Additionally, at temperatures above 1100˚C oxidation of the substrate surface was obtained in regions of opened cracks and film delamination.

Table 4. The calculated values of d and standard values for Titanium Aluminide film of ~ 1µm thickness deposited at 450°C substrate temperature.

2θ	**I/I_0**	**Inter planar Spacing**		**I/I_0**	**hkl**
		Calculated (nm)	**Standard (nm)**		
44.99	100	2.014	2.118	100	200
65.56	10	1.424	1.461	18	202
78.89	11	1.216	1.286	22	113

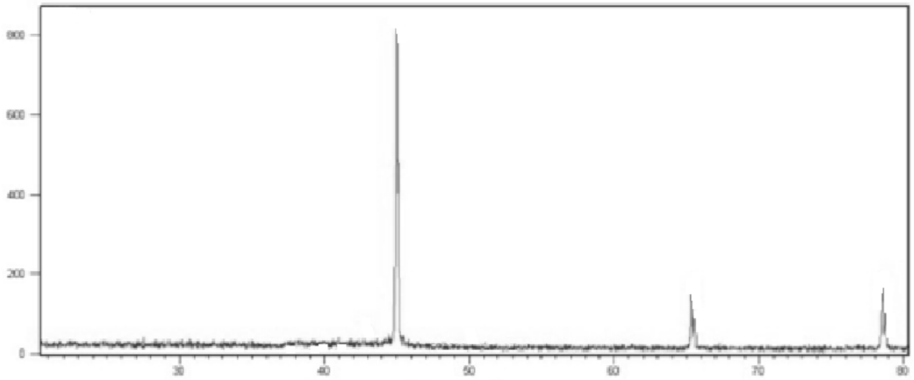

Figure 37. XRD pattern of Ti Al film deposited at 450°C substrate temperature on mild steel substrates.

5.2.1 Texture and strain of the coated films

Texture coefficients (T) for coated Ti – Al films having diffraction peak positions at 44.99°, 65.56° and 78.89° correspond to (200) (202) and (113) planes which were determined from the intensities of Ti – Al peaks using the expression

$T = \frac{I_{hkl}}{\sum I_{hkl}}$, where I_{hkl} is the intensities corresponding to (hkl) values (200), (202) and (113). The values are tabulated in the following Table 5. Assuming no significant micro-strain, the average grain size was estimated by the Debye-Scherrer formula B = kλ / s cosΘ, where s is the crystallite size, λ is the wavelength of the X-ray radiation, k is a constant taken as 0.94, θ is the diffraction angle and B is the line width at half maximum height. The stress was obtained from the micro-strain value of the coatings after deposition, using XRD, which was mainly due to crystal lattice distortion developed in the thin films. The strain in the film could be expressed by the expression $\varepsilon = \frac{d - d_0}{d_0}$, where d and d_0 are strained and unstrained lattice coefficients, which could be calculated according to the Braggs equation. Hence the stress in the film was calculated and found to be 679 MPa, based on biaxial strain model and the equation used was $\sigma = \frac{d - d_0}{d_0}.C$, where C is the elastic constant of single crystal. Also it was noted that the coherent domain size of the thin film crystallite was 1243Å, as estimated by the Scherrer formula $L = \frac{0.9\lambda}{\beta_{eff}.\cos\theta}$, where L is structural coherence length, λ is wavelength of X – Ray, θ is Bragg diffraction angle and $\beta_{eff.}$ is effective FWHM of the diffraction peak.

5.3 Scanning Electron Microscopy - Energy Dispersive Spectroscopy (EDS)

The SEM images were taken in two different directions i.e. planar and cross-sectional view. The planar view showed the formation of spherical shapes in the coating which are evenly spread throughout the coatings (Figure 38 – Figure 42). These spheres are having approximate size of 2 μm in diameter. It was observed that the substrate surface and internal properties were strongly influencing the growth kinetics of the coatings. There are some cracks in the films grown without substrate heating. This may be due to the increased stress in the film. But when the substrate was heated to a temperature of 350 °C – 400 °C there were minimum cracks in the film. The EDS (Figure 43a, Figure 43b) carried over these regions showed that they were comprised of Ti – Al in them throughout. The vertical view (Figure 43c) revealed an almost uniform columnar growth perpendicular to the substrate surface in the coatings.

Table 5. List of texture coefficients and microstrains in the coated films

Substrate	**2θ**	**d-spacing, (Å)**	**Intensity, (%)**	**FWHM**	**h k l**	**Texture Coeff. (T)**
Copper	44.9971	2.01458	100	0.24	2 0 0	0.9398
	65.3722	1.4275	6.4	0.576	2 0 2	0.0601
Alumina	44.9971	2.01458	100	0.072	2 0 0	0.8324
	65.5549	1.42396	9.5	0.12	2 0 2	0.0790
	78.7439	1.21526	10.63	0.096	1 1 3	0.0884
Glass	38.2516	2.3179	100	0.672	1 1 1	0.6849
	44.946	2.2168	23	0.92	2 0 0	0.1575
	48.486	1.8773	23	1.092	2 0 2	0.1575
Steel (304)	38.2608	2.37202	21.94	0.384	1 1 1	0.1593
	45.0108	2.014	100	0.192	2 0 0	0.7262
	65.5011	1.42888	15.75	0.48	2 0 2	0.1144
Aluminum	44.9571	2.01628	100	0.072	2 0 0	0.8324
	65.5149	1.42473	9.5	0.12	2 0 2	0.0790
	78.7039	1.21577	10.63	0.096	1 1 3	0.0884

The columns are of average 1.12 µm diameters in size and were repeatedly observed in working condition as mentioned in Table 3 along with the growth of Ti-Al intermetallic thin film (Figure 44 – Figure 46). Also the columns were continuous with increasing diameter from substrate to top of the coated film and varied as the substrate temperature varied (Table 6). The EDS carried on this cross-sections revealed the presence of TiAl. Also there was combination of substrate materials atoms up to some thickness due to diffusion from the substrates at the coating temperature. When the substrates were heated to 450 °C there was no substrate atoms observed in the coatings in the selected regions for the analysis.

Table 6. The approximate column size of titanium aluminide film deposited at various substrate temperature on mild steel.

Substrate Temperature T_s (°C)	**Approximate Column size (µm)**
250	0.21
300	0.32
350	0.51
400	0.81
450	1.12

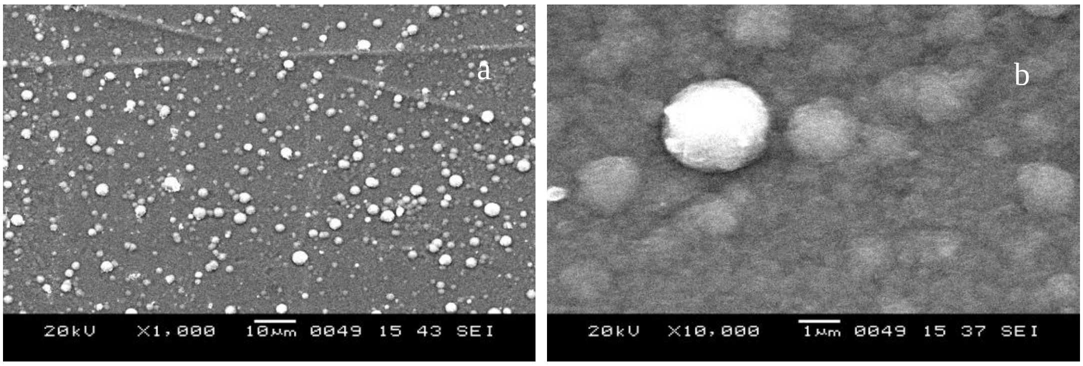

Figure 38. SEM image of as deposited film – Top view (a, b)

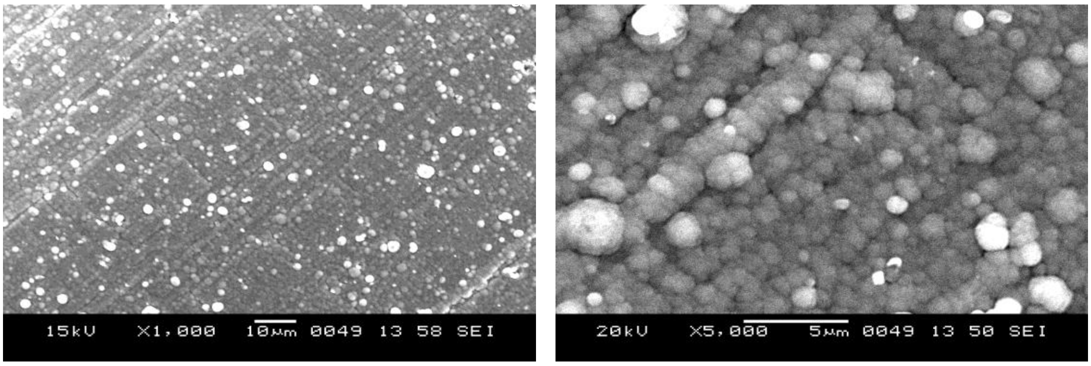

Figure 39. SEM image of film deposited on alumina substrate – Top view (a, b).

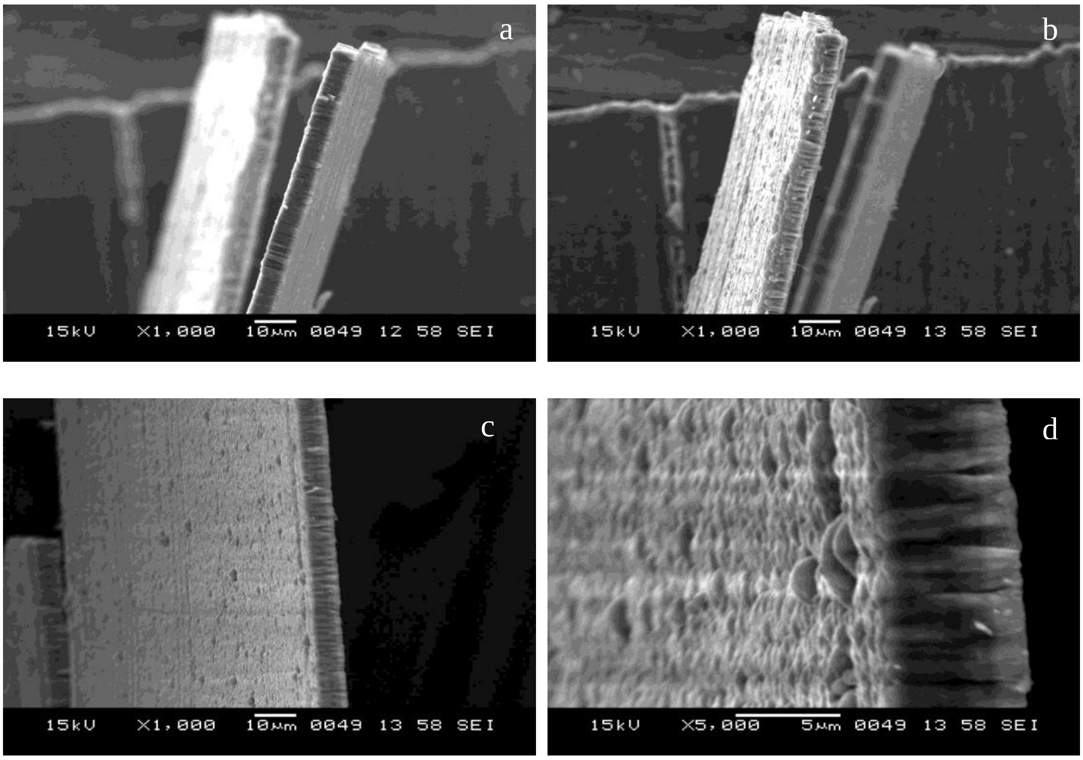

Figure 40. SEM image of free standing film – isometric view (a, b, c, d).

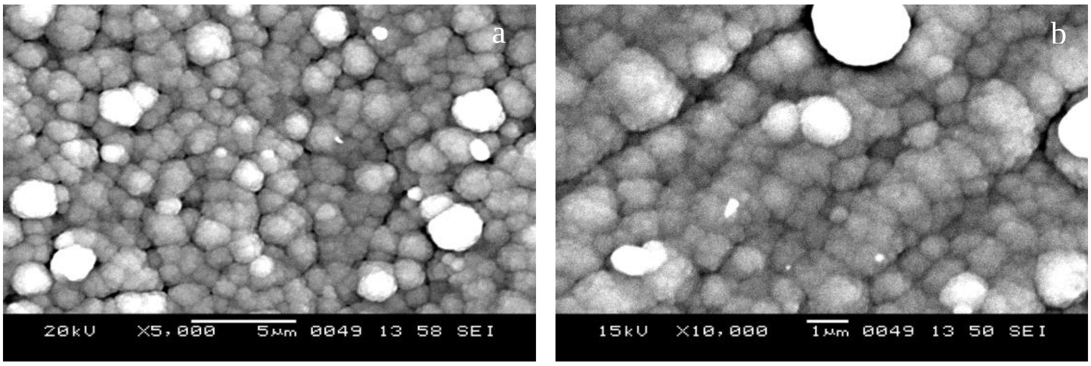

Figure 41. SEM image of film deposited on copper substrate – Top view (a, b).

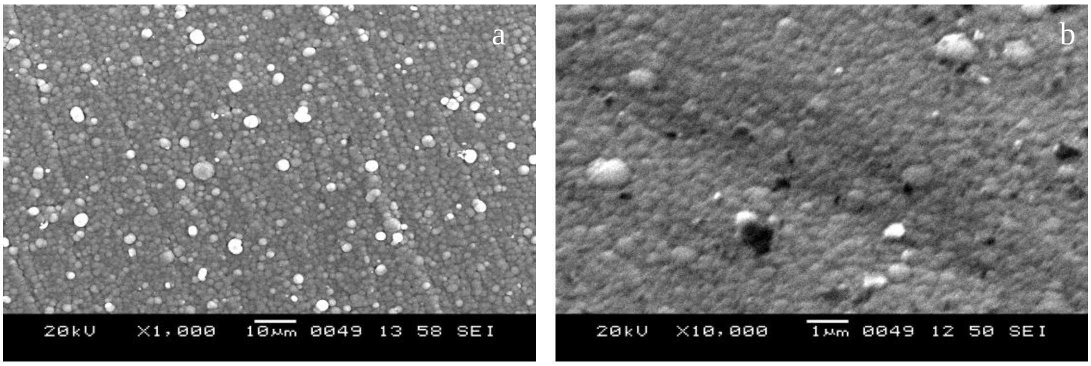

Figure 42. SEM image of as-deposited film on MS substrate – Top view (a, b).

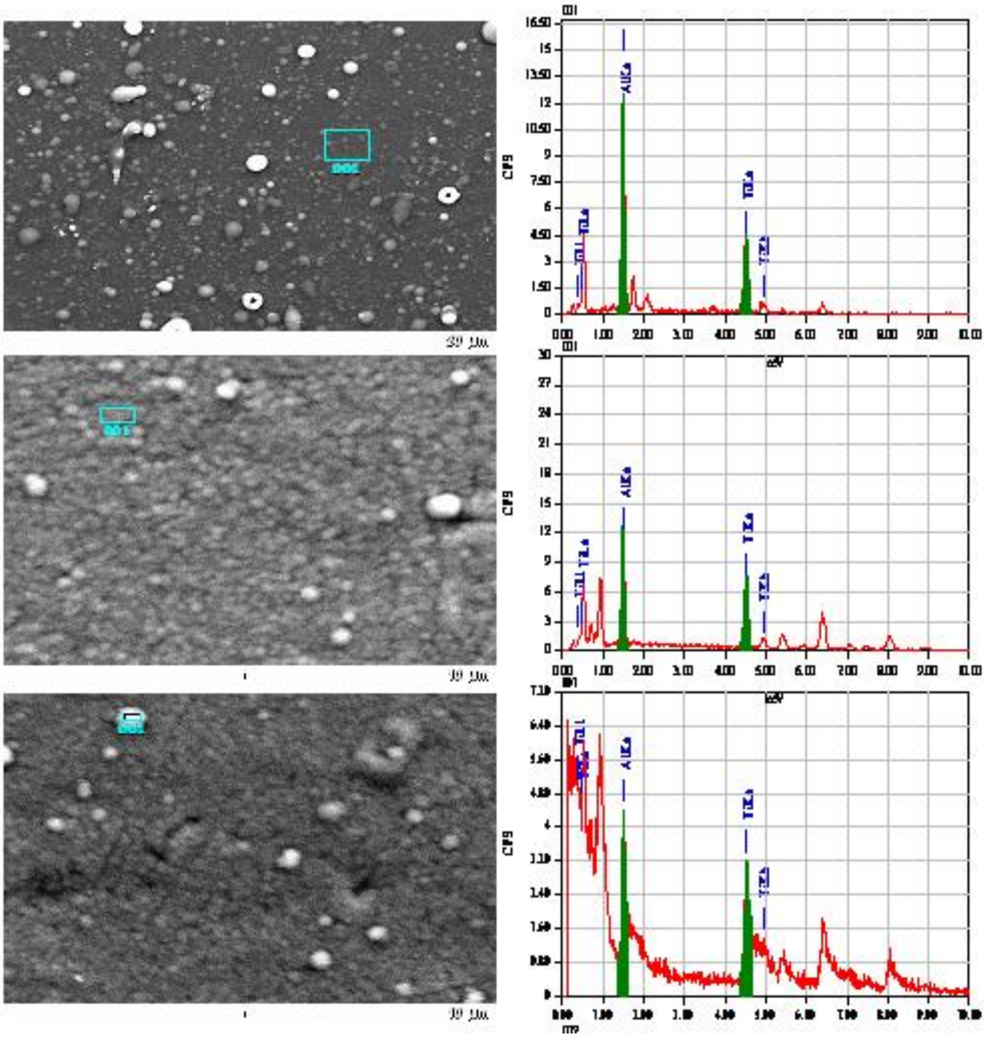

Figure 43a. EDS of films developed on aluminum, copper and mild steel substrates.

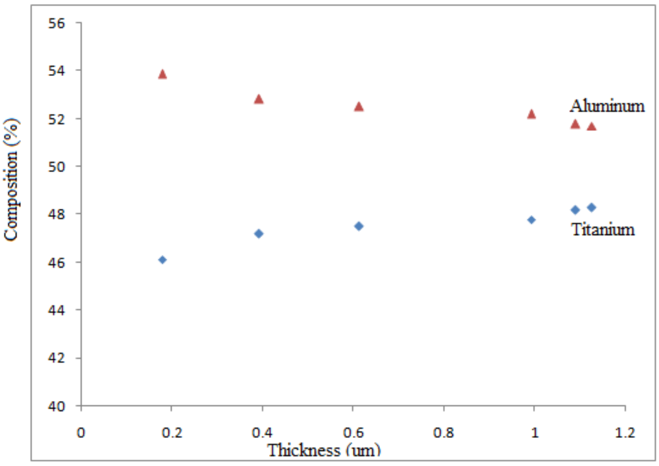

Figure 43b. Variation in composition of Ti – Al along the film thickness.

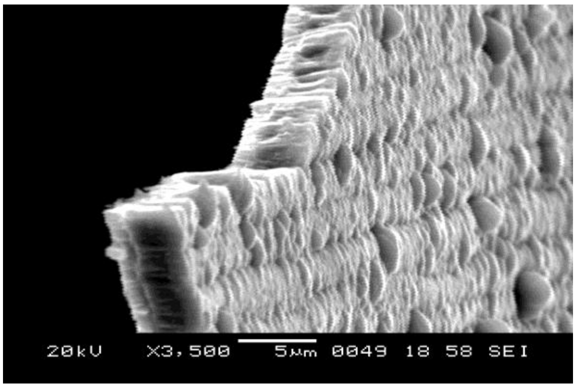

Figure 43c. The cross-sectional SEM image of film developed without substrate heating – showing discontinuous columns of TiAl intermetallic film.

5.4 Structure Formation in Thin film

The relationship between process parameters and coating properties known as zone model was displayed on the structure of the coated film. Zone models (Figure 44 – Figure 45 a, b, c, d) were developed to describe the structure of coatings deposited by sputtering processes (Arnell and Kelly 1999). In all cases, homologous temperature was used to describe the thermally induced mobility of coating atoms. The other variable which influences the model is the bombardment of the energetic particles which is going to be deposited. But this is in turn dependent on parameters such as coating pressure, substrate bias voltage, substrate temperature and the average energy per depositing atom. However, the available models are not enough to describe the unbalanced magnetron sputtering (UBMS) process. In the titanium – aluminum system selected for coating was deposited by UBMS, under systematically varying conditions, and characterised in terms of their structures and properties. These metals were chosen for their wide range of physical properties and their different crystal structures, the deposition variables being target current, coating pressure and substrate-to-target separation. The ratios of the fluxes of ions and condensing atoms at the substrate were estimated from ion current density and deposition rate measurements. The structures of the coatings were distinct from each other, and there were only modest variations in structure from one coating to another. The coatings, which were deposited at homologous temperatures, had dense columnar structures, which necked down completely. SEM investigations showed that all had clearly visible polygonal grain-like regions (Figure 45a and 45b), and that they were similar in size to the width of the columns. It is postulated that the grain-like regions are actually sections through these columns. Thus, the structure appears to consist of a series of columns, separated by regions of high dislocation, in accordance with the Thornton classifications (Thornton 1974, Howson et.al 1989) i.e. zone 3-type structures.

The formation of zone structures, illustrated in Figure 44, which compares, in terms of homologous temperature, the positions of the zonal boundaries for zone models. UBMS process has promoted the formation of "high temperature" structures at relatively low homologous temperatures, and suppressed the formation of "low temperature" zone 1 and zone 2 structures. Additional experiments were carried out for investigation of the influence of deposition parameters on deposition rate and substrate ion current density. Both were found to be directly proportional to target current, but to decrease with increasing substrate to target separation, whereas the bias voltage and pressure had no significant influence on deposition rate.

Deposition rate falls more rapidly with increasing separation than substrate ion current, because the UBMS maintains dense plasma in the substrate region. The ion to atom ratio at the substrate increases with increasing separation. These results mean that the ion to atom ratio can be varied only over a limited range, the only variable which significantly affects this ratio being the substrate to target separation. To increase the ratio for given conditions, it is necessary to increase separation, which in turn lowers the deposition rates. However, the ion-to-atom ratio remains virtually constant with increasing target current. This indicates that the deposition rate can be maximised at each set of conditions. The ion to atom ratio does not decrease with increasing deposition rate, and this is an important practical consideration in coating processes. Based on these results, a structure zone model has been developed, in which the structures of coatings deposited by UBMS are described in terms of parameters, namely homologous temperature and ion to atom ratio. Ion energy and the incident ion to atom ratio must be considered separately when modelling the effects of concurrent ion bombardment on coating microstructure (Adibi et.al 1993).

The formed structural zone model is shown in Figure 45, with the zone 3 boundary as cylindrical surfaces. The UBMS system conditions suppressed the formation of porous columnar zone 1-type structures. Clearly, assumptions were made in the development of this model. In particular, in the estimation of ion to atom ratio, and the plasma potential as assumed to be constant. However, the model accurately reflects the parameters which determine coating structure in the system.

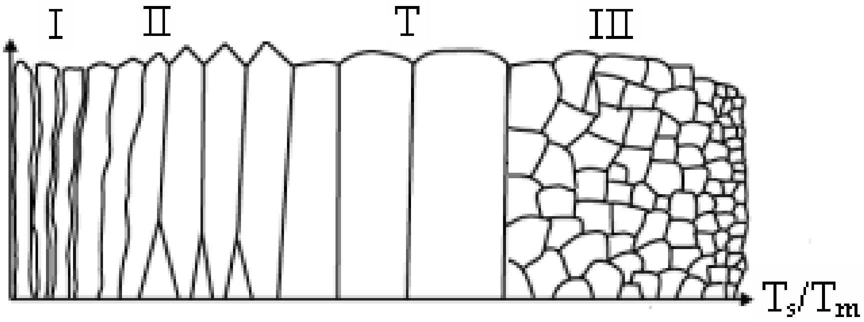

Figure 44. Ideal zone model for sputter deposited films 2D view.

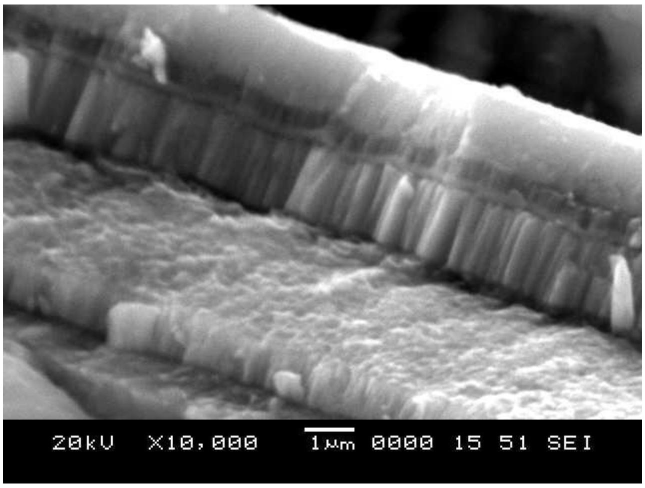

Figure 45a. Real zone for sputter deposited Ti-Al thin films.

5.5 Atomic Force Microscopy (AFM)

AFM topographical images of sputter deposited thin films are shown in Figure 46 - Figure 48. The following figure shows AFM images of the Ti – Al coatings on copper and aluminum substrates of coating thickness 1.2µm. This was recorded in tapping mode of AFM. The deposited film surface topography shows a dense distribution of surface mounds with a total roughness R_q, of 1.13 ± 0.02 nm. Tabulated values of thin film surface morphology parameters determined using AFM is presented in Table 7. It can be proposed that the localized islands seen are responsible for increased R_q values. Topographic profile images along a diagonal line in the middle of scan were constructed from AFM data. The distribution of surface mounds and localized islands were quantified in terms of porosity. The mean value of porosity was determined to be 0.73 fraction for sputtered films. This shows that sputtered surfaces have better separated islands with a larger connecting area. Also, height distribution and bearing ratio of sputtered thin films were calculated and the bearing ratio went to zero beyond 1.3 nm, indicating that surface mounds and islands were connected to each other at these heights above the surface. A non-continuous surface feature height distribution of thin film was obtained due to the high degree of porosity. Additionally, the presence of surface contaminants or oxide layers might considerably alter the behaviour of the surfaces. Therefore, XRD studies were performed to explore possible differences between the surface chemistry and crystalline structure of the thin films deposited using sputtering.

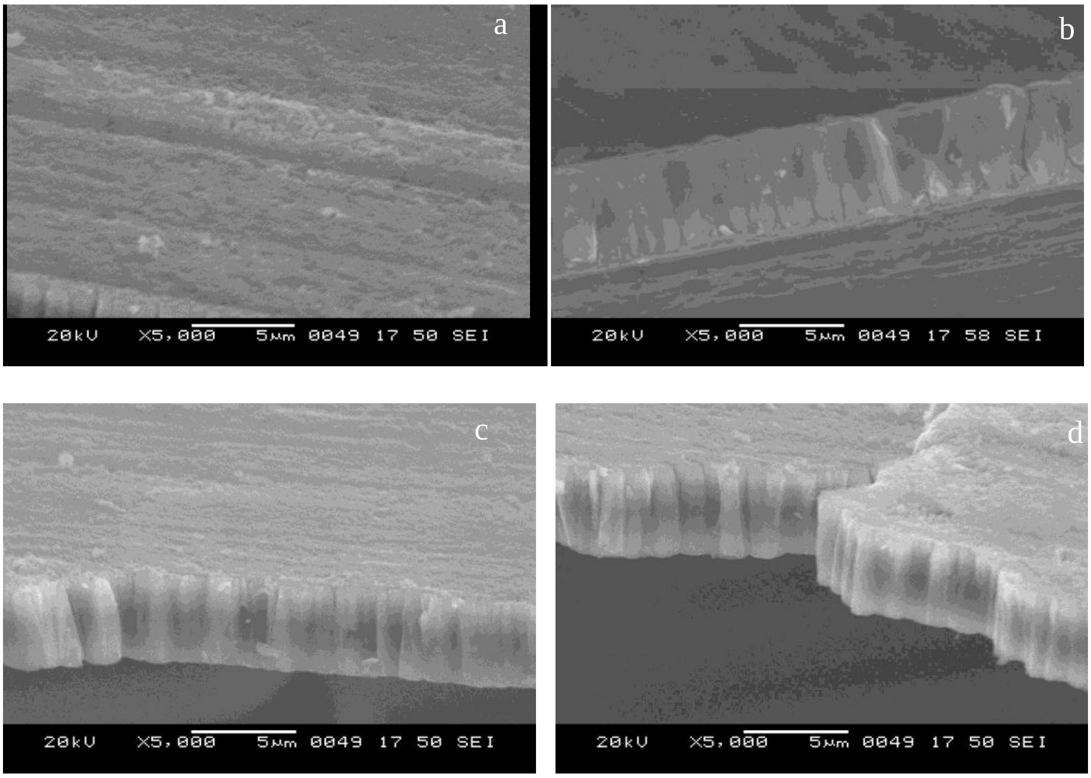

Figure 45b. SEM images showing the angular view of film developed under controlled condition – a, b, c & d – showing continuous columns of TiAl intermetallic film.

The hardness of the coatings was determined by nanoindenter (Make: CSM-NHT) with a Berkovich diamond tip. In this nano hardness tester, an indenter tip with known geometry is driven into a specific site of the material to be tested by applying an increased normal load. The sapphire reference ring was used at the time of indentation. The load is increased and decreased in a linear fashion during the experiment. The diamond Berkovich indenter was forced into thin film being tested under constant load conditions. The loading profile during indentation testing followed linearly increasing with a hold time of 20 s at the peak load. The maximum load used was 5mN at different loading rate. The indentation depth was 100 nm, around one tenth of the coating thickness to minimize the substrate effect. The load – displacement curve obtained during the nanoindentation F testing of the Ti – Al thin film in loading rates of (25 mN/min) is shown in figure 49. Five consecutive measurements (Figure 50) were performed at different loading rates (2 mN/min., 5 mN/min.) and the average value was reported. The hardness of 1.2 µm thick Ti – Al thin film was 36 GPa.

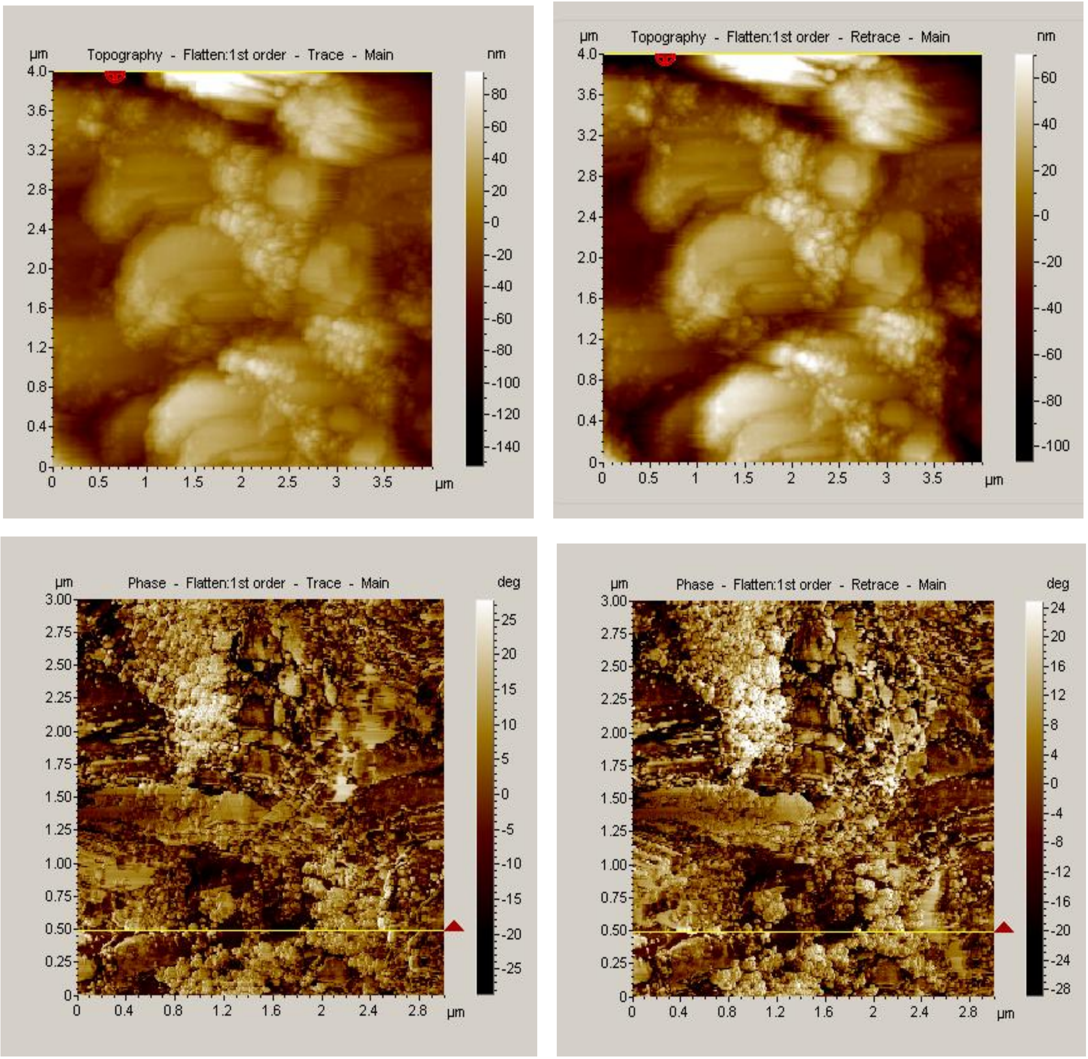

Figure 46. AFM images of Ti – Al along the film surface revealing surface roughness.

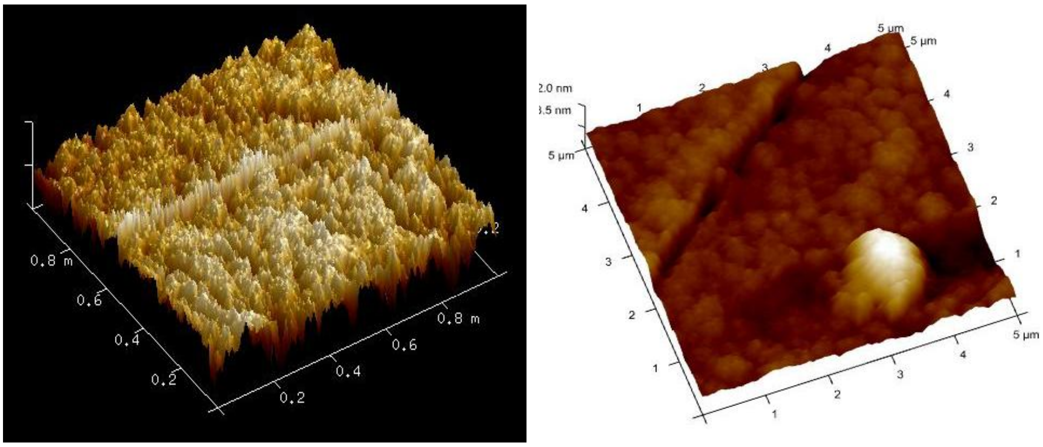

Figure 47. AFM topographical images (3D) of sputter-deposited thin films.

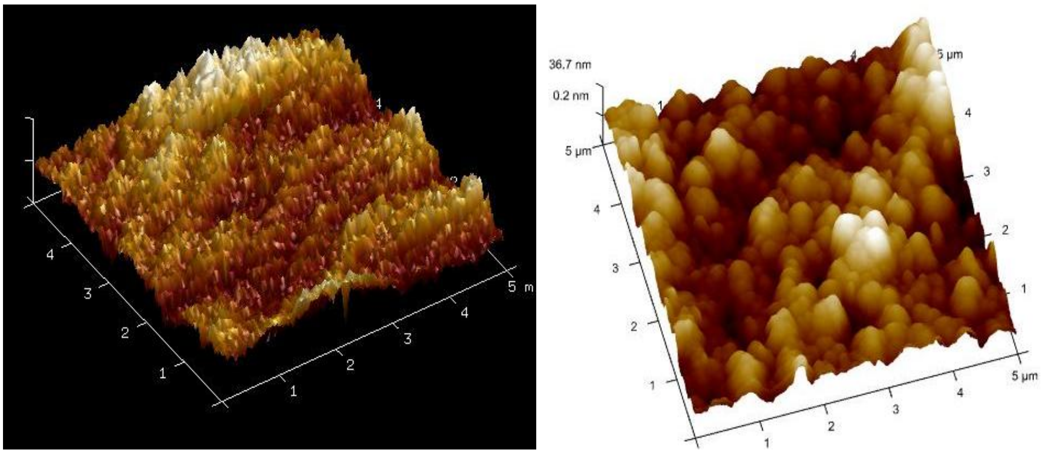

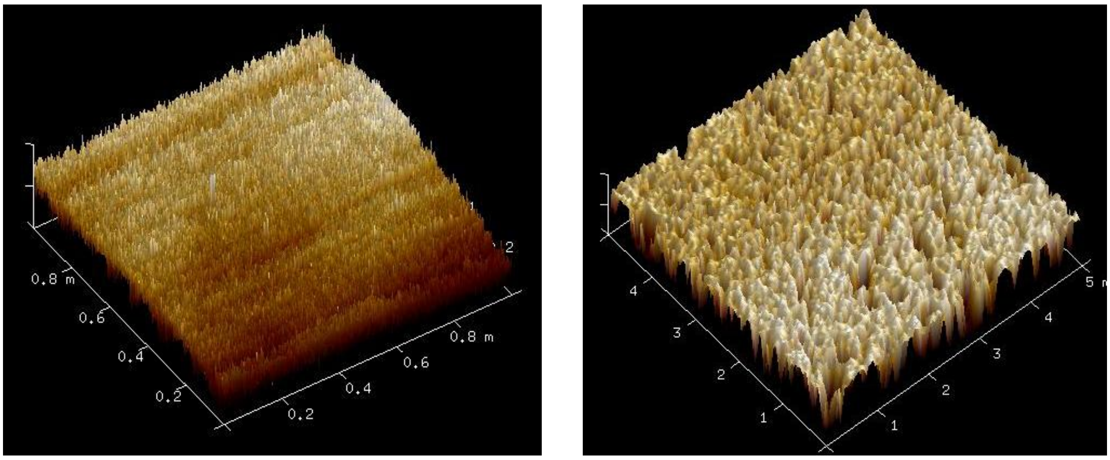

Figure 48. AFM topographical images (3D) of sputter deposited thin films.

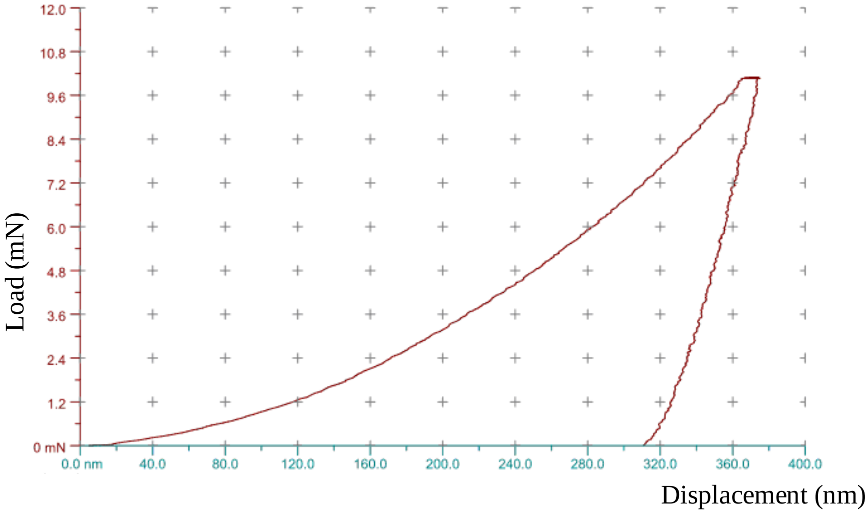

Figure 49. Load – displacement curve for Ti – Al thin film deposited on silicon substrate.

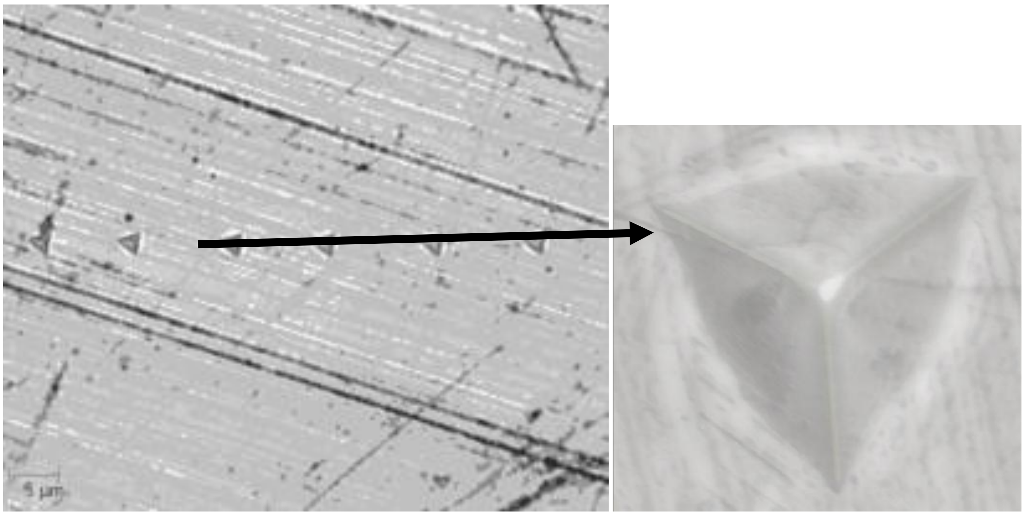

Figure 50. Image of 5 Berkovich indentations made on Ti – Al thin film deposited on silicon substrate for hardness measurement.

Table 7. Surface morphology parameters of thin films as determined from AFM measurements.

R_q (Total Roughness)	113 ±2 nm
R_{sk}	6.1 ±0.5 nm
R_{ku}	34.9 ±0.5 nm

5.6 Heat Treatment

5.6.1 Oxidation measurement

The oxidation behaviour of the specimens was determined by oxidation measurements. On exposure to hot air, which consists of oxygen, carbon dioxide, nitrogen, carbon monoxide, nitrogen monoxide, and some trace gases, it reacts with coatings to form oxide of respective elements. The interface between the substrate and the coated material particles and the top surface of the coatings are the high energy regions which are more prone for oxidation. The quantity of the oxide layer formed is analyzed in terms of the weight gain of the specimens per unit area exposed against oxidation time. Figure 51 represents the weight gain in each specimen (in g/cm^2) against time (in minutes) for coatings exposed to temperatures 600, 700, 800, 900, 1000 and 1100˚C respectively. The corresponding weight gain data with respect to time and temperature are mentioned in Table 8. after the oxidation of coatings.

The topography of the samples with Ti – Al coating after oxidation experiments were analyzed using JEOL JSM-6380LA scanning electron microscope. EDAX analysis was carried out in order to determine the alumina and titania weight percentage quantitatively which in turn explained the oxidation behaviour of the heat treated coatings. X- Ray analysis (figure 52) of the specimens was done using X-Ray Diffraction. The diffracting angles were set to 20^o to 80^o with a scanning speed of 1^o /min and scanning was done in continuous mode. The observed results show that the oxidation was pronounced after 900˚C compared to other lower temperature regimes of specimens.

5.6.2 Effect of exposure time and oxidation temperature

The effect of exposure time at a particular temperature on the oxidation behaviour of the coating at different temperatures is clearly visible in Figure 51. The common trend observed is that the weight-gain of the specimens per unit area at temperatures 600, 700, 800, 900, 1000 and 1100˚C increase with exposure time. The rise in weight-gain per unit area with time was severe during 25 to 30 min. Then after 30 min. of exposure time, the weight gain per unit area followed almost a linear increase due to attaining equilibrium condition. The oxidation rate was more pronounced for the specimens heated above 800 ºC compared to other specimens heated below this temperature.

It was observed that the crystallite size decreased as the annealing temperature was increased along with the increase in the lattice strain (Figure 53). This was due to the growth of titania and alumina phases at the time of heat treatment. Coatings show greater oxidation with respect to increase in exposure time. It is also observed that the coating with more aluminum has better oxidation resistance with respect to increase in exposure time, since the alumina forms prior to the titania formation. Also the formed alumina starts to cover the titanium in the coating. This is clearly visible by analyzing the oxidized coating by SEM (Figure 54 a, b, c) and EDS analysis.

By comparing the results as listed in the Table 8, it was observed that there was an increment in the weight gain of the specimens per unit area with increasing temperature. At higher temperatures, there is more energy available for the oxidation process. When temperature was raised from 600 to 700 ºC, the weight gain was not rigorous, but as the temperature was increased beyond 800 ºC, there was a observable enhancement in the weight gain for each sample. This indicates that above this temperature of about 800 ºC the oxidation process was rigorous. An increase in temperature from 800 to 900 ºC causes the weight gain almost to double. This is clearly visible from the Table 8. Weight gain was more above 900 ºC due to the formation of alumina and titania combined phases with respect to temperatures lower than 900 ºC where alumina phase dominates compared to the titania phases in the coatings. After 1100 ºC specimens show greater oxidation with rise in temperature and they form the alumina rich compounds over the coated regions. In comparison, the effect of temperature was pronounced in the oxidation process of the coatings even after 900 ºC. Hence the aluminum present in the coating effectively affects the oxidation rate at high temperatures.

Table 8. Oxidation characteristics of the coatings at specified temperatures.

Time (min)	Weight-gain per unit area (g/cm^2) Temperature in degree Celsius					
	600	700	800	900	1000	1100
5	0.0017	0.0023	0.0058	0.0085	0.0112	0.0129
10	0.0038	0.0049	0.0069	0.0096	0.0126	0.0156
15	0.0061	0.0078	0.0094	0.0119	0.0139	0.0193
20	0.0095	0.0116	0.0133	0.0149	0.0189	0.0221
25	0.0181	0.0199	0.0265	0.0299	0.0317	0.0356
30	0.0235	0.0243	0.0296	0.0325	0.0345	0.0412
40	0.0285	0.0279	0.0349	0.0395	0.0424	0.0569
50	0.0345	0.0361	0.0397	0.0417	0.0476	0.0658
60	0.0422	0.0482	0.0512	0.0534	0.0569	0.0756
120	0.0567	0.0596	0.0618	0.0654	0.0689	0.0891
180	0.0702	0.0722	0.0825	0.0876	0.0918	0.1653
240	0.0973	0.1305	0.1509	0.1821	0.2231	0.2854
300	0.1201	0.1537	0.1839	0.2983	0.3352	0.3861

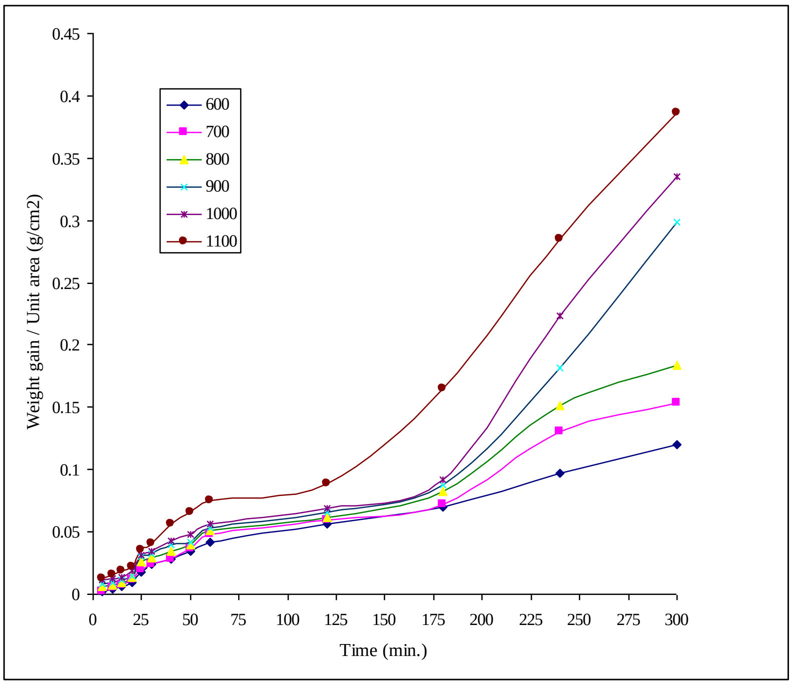

Figure 51. Oxidation profile in temperature range of 600 to 1100 ºC in 100 ºC intervals.

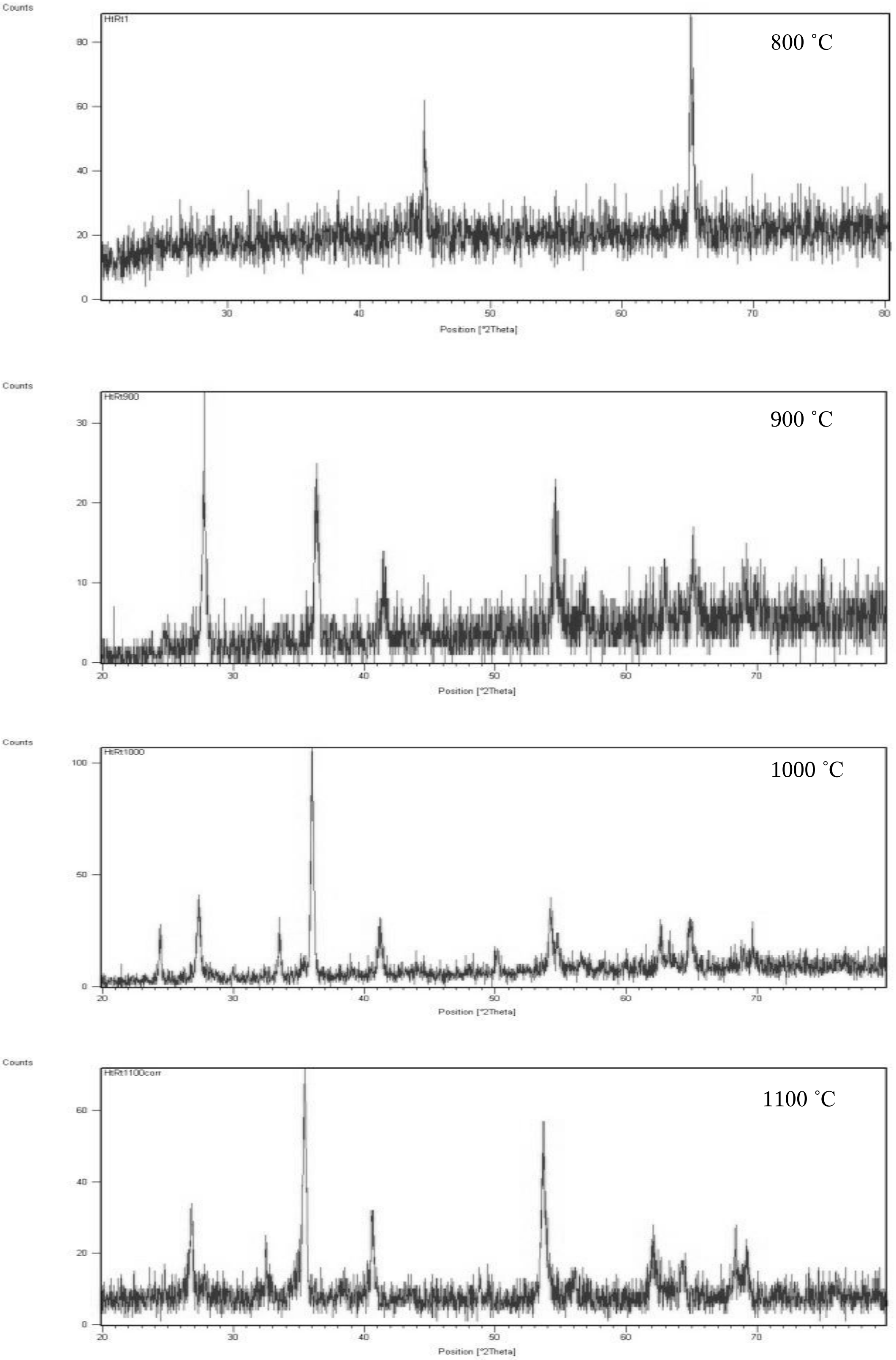

Figure 52. XRD pattern of heat treated film at 800, 900, 1000 and 1100 ˚C respectively.

Table 9. XRD data showing the aluminum and titanium oxide peak positions.

Temperature (°C)	2Theta (deg.)	d - Spacing (Å)	Intensity (I)	(h k l)	Texture Coefficient (T)	Phases Developed
600	38.2608	2.372	21.94	1 1 1	0.1593	$Al_{1+x}Ti_{1-x}$
	45.0108	2.014	100	2 0 0	0.7262	$Al_{1+x}Ti_{1-x}$
	65.5011	1.428	15.75	2 0 2	0.1143	$Al_{1+x}Ti_{1-x}$
700	44.9571	2.016	100	2 0 0	0.8324	$Al_{1+x}Ti_{1-x}$
	65.5149	1.424	9.5	2 0 2	0.0790	$Al_{1+x}Ti_{1-x}$
	78.7039	1.215	10.63	1 1 3	0.0884	$Al_{1+x}Ti_{1-x}$
800	44.9811	2.015	43.74	2 0 0	0.3042	$Al_{1+x}Ti_{1-x}$
	65.2245	1.430	100	2 0 2	0.6957	$Al_{1+x}Ti_{1-x}$
900	27.7525	3.214	100	1 0 6	0.3324	$Al_{1.67}O_4$(M)
	36.3698	2.470	86.55	1 0 1	0.2877	TiO_2 (T)
	41.5055	2.175	33.58	1 2 3	0.1116	Al_2O_3 (O)
	54.6128	1.680	58.55	6 0 1	0.1946	Al_2O_3 (M)
	65.2834	1.429	22.12	3 1 0	0.0735	TiO_2 (T)
1000	24.413	3.646	18.02	1 1 1	0.0720	Al_2O_3 (O)
	33.5342	2.672	17.17	0 3 1	0.0686	Al_2O_3 (O)
	36.0038	2.494	100	1 0 1	0.3998	TiO_2 (T)
	41.2196	2.190	18.99	1 2 3	0.0759	Al_2O_3 (O)
	54.2123	1.691	25.22	6 0 1	0.1008	Al_2O_3 (M)
	62.6095	1.483	14.04	2 0 4	0.0561	TiO_2 (T)
	64.8578	1.437	20.15	1 3 5	0.0805	Al_2O_3 (O)
1100	26.7928	3.327	37.28	0 0 7	0.1254	$Al_{1.67}O_4$(T)
	32.5061	2.754	9.93	1 1 2	0.0334	Al_2O_3 (T)
	35.4725	2.530	100	1 1 0	0.3365	Al_2O_3 (R)
	53.6453	1.708	61	2 2 3	0.2052	Al_2O_3 (O)
	62.0661	1.495	21.54	2 1 3	0.0724	TiO_2 (T)
	64.331	1.448	15.78	0 1 4	0.0531	$Al_{1.67}O_4$(T)

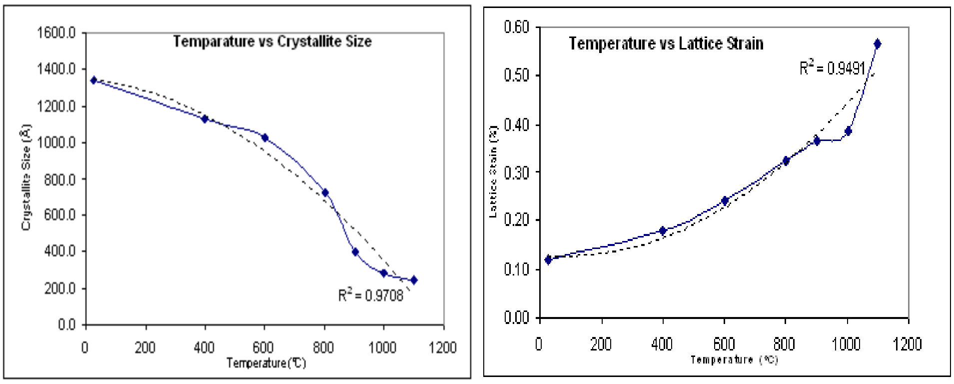

Figure 53. Variation of crystallite size and lattice microstrain with heat treatment temperature obtained by using XRD pattern of heat treated films.

5.6.3 Effect of aging

The variation in the hardness of the coatings with temperature can be associated with the development of oxide phase taking place at the time of heat treatment given to the coatings. This depends on aging kinetics which is a function of temperature and time. Uniform precipitation of oxide layer leads to more of uniform oxide layer regions in the coating. The oxidation initiated at the boundary and interfacial regions of the coatings where macro particles were present. The presence of big sputtered particles and the precipitates of phases or elements contribute to interfacial regions in the coating material. The aggregates of aluminum are more prone sites to oxidation. Hence it can be stated that the specimen with more amount of aluminum (≥ 51 at.%) shows maximum oxidation compared to specimen with less amount of aluminum (< 51 at.%). Figure 54b and Figure 54c give the SEM pictures of the heat treated coating after the oxidation measurements at selected temperature of 1000°C and 1100°C. Also the EDAX spectrum of the same was justifying the formation of oxides of titanium and aluminum.

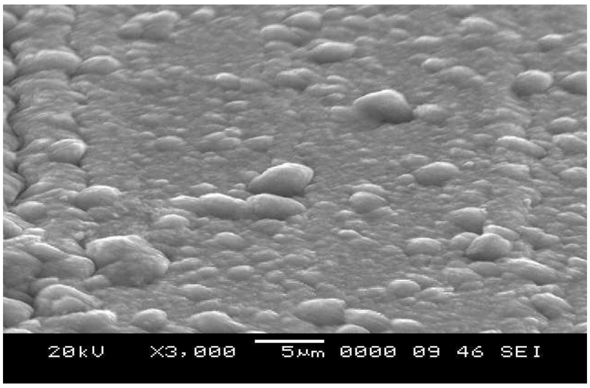

Figure 54a. SEM picture of as deposited coating before oxidation measurements.

5.6.4 Effect of annealing

Annealing conditions changed the elemental concentration in the films significantly. Depth profiles were carried after annealing in atmosphere and it was observed that annealing generates only a thin aluminum and titanium oxide film of some nm in thickness at the surface. The XRD data in Table 9., which was measured to verify EDS results, showed characteristic of the aluminum and the titanium oxide phases.

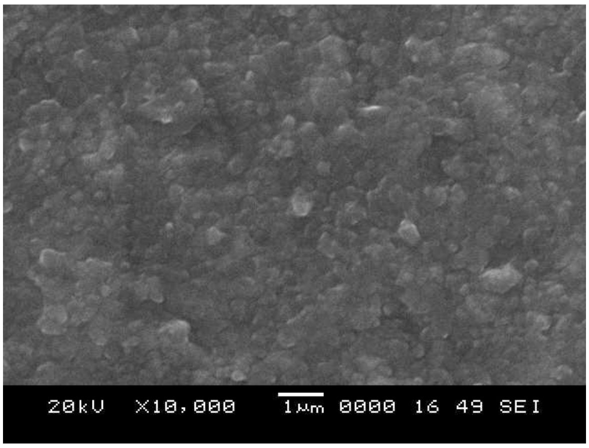

Figure 54b. SEM picture of the 1000°C heat treated coating.

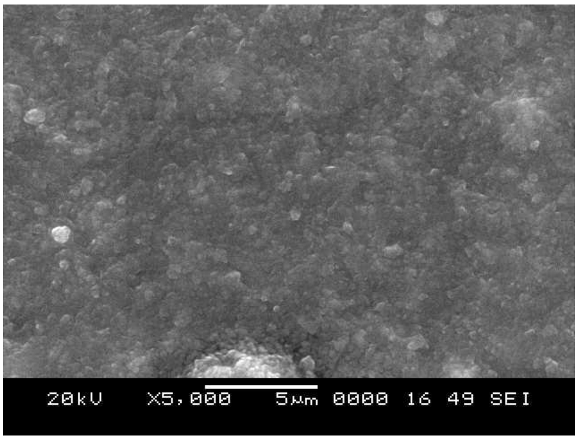

Figure 54c. SEM picture of the 1100°C heat treated coating.

Annealing in air at 800˚C or higher temperature values for more than 2 h resulted in increased thickness of the generated oxide layers. Samples, which were annealed for 2 h in air, showed an alumina layer at the film surface in thickness of some 150 nm. By annealing at 1000˚C under atmospheric condition the Ti content did not change significantly, whereas the Al concentration increased compared to the initial state. Annealing in air at 700 ˚Cresults in increase of the O and the Al content at the film surface with decrease in the ratio of Ti to Al. Only small content of oxidized Ti was found after annealing at 900 ˚C. The plots show the peak positions of the Al_2O_3 and the TiO_2. Annealing at 1100˚C generates film damage, as shown in Figure 55. In principle, surface areas are visible which were damaged by cracking, and delamination process effects. Samples annealed at 1100˚C in air not only showed a closed alumina and titania layer, but also damaged coating layer. In those regions characteristic peaks of substrate are also visible. Consequently, the uncoated hard metal surface can be seen. Oxidation process begins for annealing time of 1 h at a temperature value of about 700 ˚C, but the chemical decomposition of the Ti - Al phase was detected at a temperature of about 1000˚C in some of the samples. Generated thermal stresses cause cracking or local delamination of Ti – Al film regions resulting in oxidation of the uncovered metal surface.

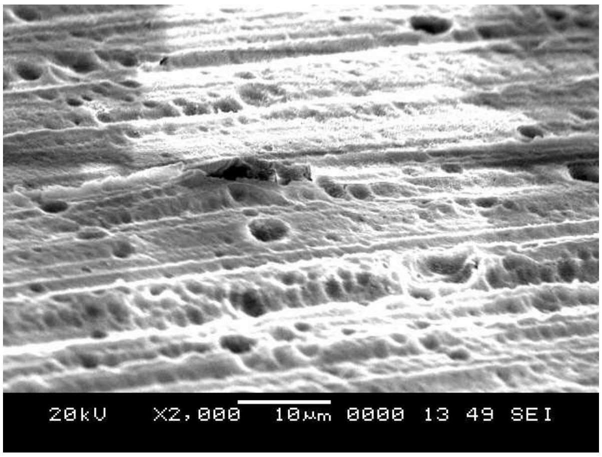

Figure 55. SEM showing film damage when annealed at 1100 ˚C.

5.7 Microhardness

The hardness of the thin film coated with thickness of a few microns is determined by measuring the microhardness of the surface. Coating thickness must be known to assess accuracy of these measurements. Microhardness testing is a method for measuring the hardness of a material on a microscopic scale. A Vickers indenter is impressed into the material at loads of a few grams (1, 2, 3, 5 and 10 g). The impression length was measured microscopically, and the test loads were used to calculate the hardness value. The hardness values obtained are useful indicators of a material's properties. Conversions from microindentation hardness values to tensile strength and other hardness scales (e.g., Rockwell) are carried out for coatings.

Microhardness tests differentiate the relative hardness of different compositions of intermetallic TiAl. But, it is not valid to compare the hardness of intermetallic TiAl entirely on the basis of single type of test, since elastic recovery is accompanied along with hardness. The microhardness values are listed in the Table 10. The substrates are affecting the microhardness values largely.

Table 10. Microhardness of the developed TiAl films on different substrate and of different thicknesses at a load of 5g.

Sl. No.	Substrate	Thickness (µm)	Microhardness (HV)	Microhardness (GPa)
1	Copper	0.9861	1837	18.02
2	Alumina	1.1245	1915	18.72
3	Mild Steel	1.1034	1858	18.22

A detailed investigation was carried out on the alumina substrates coated with thin film of TiAl. The alumina substrate was dissolved in 10% NaOH solution and dried. Then the free standing film was subjected to the XRD (Figure 57) and EDS on both sides. It was observed that there was growth of nano particles of TiAl compound on the substrate side. The SEM (Figure 56)carried on this region showed the finger like structures which are non uniform in size. The non-uniformity was attributed to variation in pore diameter (120 – 180 nm) of the alumina substrate. Also it may be due to the variation in pore filling and growth of the nano particles in the pores. The growth of the nano particles was observed only in the samples which are heated to a temperature of 450^{0}C at 25–30 ml/min. argon flow rate in standardized sputtering conditions. The AFM images also showed the growth of nano structures on it.

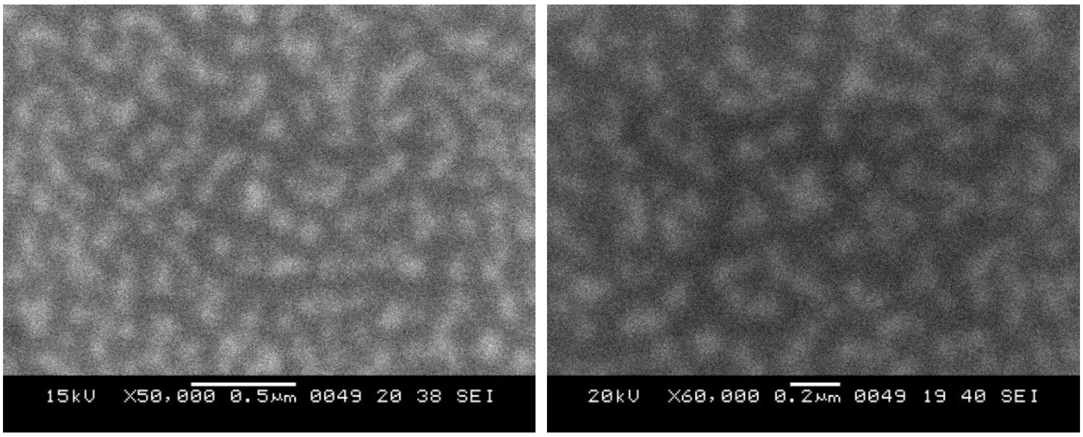

Figure 56. Image of nanometric TiAl particles grown on the alumina substrates

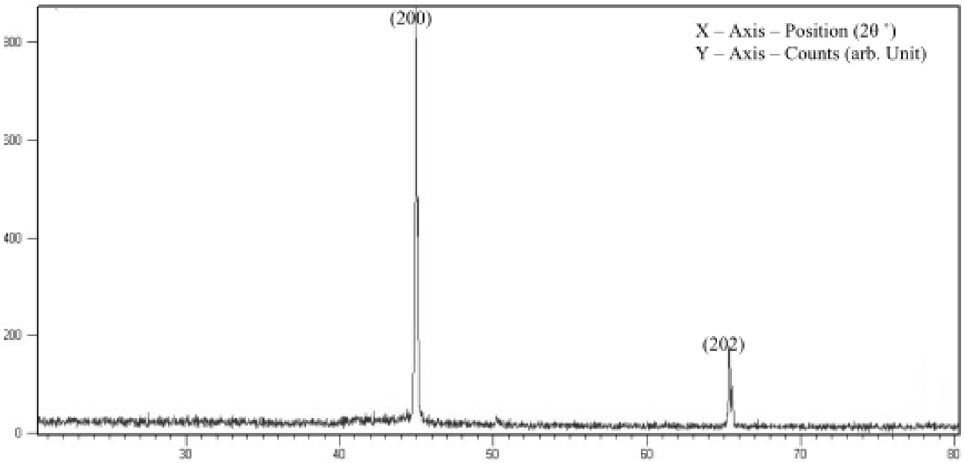

Figure 57. XRD of nanometric TiAl particles grown on the alumina substrates.

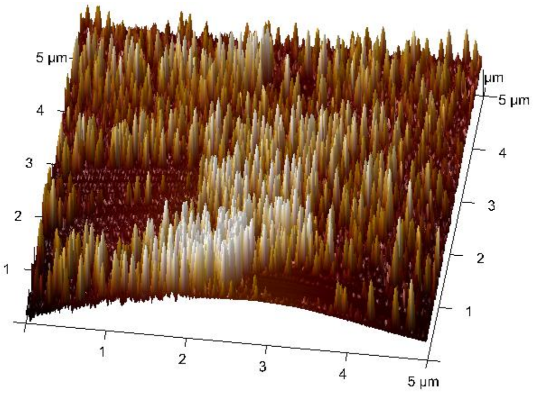

Figure 58. AFM topographical images (3D) of sputter-deposited thin films nanometric TiAl particles grown on the alumina substrates.

CHAPTER 6

CONCLUSIONS AND SCOPE FOR FUTURE WORK

1 CONCLUSIONS

The Ti – Al films were developed using co-deposition of individual titanium and aluminum in unbalanced dc magnetron sputtering on various substrates. The process parameters for the sputtering to obtain high quality uniform films were optimized. The optimized experimental values and parameters were used to obtain a good quality uniform Ti – Al films.

- The deposition rate was approximately 40 to 80 nm/min. for pure aluminum and titanium targets.
- The experiments carried out yielded the growth of intermetallic $Ti_{1-x}Al_{1+x}$ films which was confirmed by EDS and XRD analysis.
- The grown $Ti_{1-x}Al_{1+x}$ films were found to be in gamma region of Ti – Al phase diagram.
- The crystal structure of the grown film was found to be orthorhombic. The XRD analysis revealed the crystallite size of 123.7Å and lattice strain was found to be 0.1352.
- There were continuous columnar growths of the film on the substrate with good adherence.
- The coating has a granular structure which was extremely dense with no visible structure defects.
- Also EDS showed that the coating was containing 49 at. % of titanium and 51 at. % of aluminum.
- It was observed that there was a columnar growth perpendicular to the substrate in the optimized conditions in UBMS method in resemblance with the zone 2 structure as explained elsewhere.
- Heat treatment study of the coated films was carried out in the temperature regions of 400°C to 1200°C.

- Results from the study of oxidation of intermetallic Ti-Al thin films were presented. The oxidation behaviour of Ti - Al was found to be predominantly complex depending on temperature and atmosphere composition.
- Protective scales of alumina were formed in high oxygen environment up to a critical temperature and above that temperature mixed $TiO_2/A1_2O_3$ scale formed and grew at rates faster than that of alumina.
- Continuous alumina scales were not observed, even at temperatures below 1100˚C. Also it was observed that at this temperature cracking in the film and the film delamination which led to the substrate oxidization.
- A decrease in crystallite size with increase in the lattice strain was observed. This was due to the formation of TiO_2 and Al_2O_3 in the film at the time of heat treatment procedure.
- The microhardness studies of the deposited films were carried out and the average value (18.22 GPa) obtained was found to be in accordance with the literature.
- The AFM with nanoindentation revealed the uniformity of the film and nanohardness of the film.
- The SEM imaging carried on films of alumina substrates showed the growth of nanoparticles of Ti-Al and was confirmed by XRD.

2 SCOPES FOR THE FUTURE WORK

The equipment can be incorporated with the online monitoring of the process and the compound formation analysis equipments. Also a third target may be incorporated for the production of some more combinations of compound. The experiments may be continued for the synthesis of Ti_3Al and $TiAl_3$. Alumina anodiscs with nanometer pore diameter may be used as substrates for the production of nano rods of corresponding compounds. This can be further used for strengthening of the metals by dispersing them as reinforcements. The multi layers of the same combinations of same metals may be prepared and a comparative study can be done with the co-sputtered coatings.

REFERENCES

Adjaottor, A. A., Meletis, E. I., Logothetidis, S., Alexandrou, I. and Kokkou, S. (1995). "Effect of substrate bias on sputter-deposited TiC_x, TiN_y and TiC_xN_y Thin films." *Surf. Coat. Tech.*, 76-77, 142-148.

Ahn, S.H., Yoo, J.H., Kim, J.G. and Han, J.G. (2003). "On the corrosion behaviour of multilayered WC-TiAlN coatings on AISI D2 steel." *Surf. Coat. Tech.*, 163 - 164, 611 -619.

Bresolin, C., and Pirotta, S., (2002). "$TiAl_3$ formation kinetics in sputtered Ti/$AlCu_{0.5\%}$ Thin films." *Microelectron Engg.*, 64, 125-130.

Camille Jones, Y., William Luecke, E., and Evan Copland, (2006). "Neutron diffraction study of oxygen dissolution in α_2-Ti_3Al." *Intermetallics.*, 14, 54-60.

Chakraborty, A., and Earthman, J.C., (1998), "The Numerical Analysis of Creep Deformation and Cavitation in TiAl Intermetallic Alloys." *e – JOM.*, (vol. 50, no. 8).

Chen, Li., Du, Yong., Xiong, Xiang., Chang, Ke, K., Wu, J, Ming., (2011). "Improved properties of Ti-Al-N coating by multilayer structure." Int. Journal of Refractory Metals and Hard Materials, 29, 681–685.

Chen, Li., Paulitsch, Jörg., Du, Yong., Mayrhofer, Paul., (2012). "Thermal stability and oxidation resistance of Ti–Al–N coatings." Surf. Coat. Tech. 206, 2954–2960.

Chinmulgund, M., Inturi, R.B. and Barnard, J.A., (1995) "Effect of Ar gas pressure on growth, structure, and mechanical properties of sputtered Ti, Al, TiAl, and Ti_3Al films." *Thin Solid Films.*, 270, 260-263.

Chu, M.S. and Wu, S.K., (2004). "Improvement in the oxidation resistance of α_2-Ti_3Al by sputtering Al film and subsequent interdiffusion treatment." *Surf. Coat. Tech.*, 179, 257-264.

Deng, H., Chen, J., Inturi, R.B., and Barnard, J.A., (1995). “Structure, mechanical and tribological properties of d.c. magnetron sputtered TiB_2 and $TiB_2(N)$ Thin films.” *Surf. Coat. Tech.*, 76-77, 609-614.

Emilia Illekova., Jean-Claude Gachon., Alex Rogachev., Hamazasp Grigoryan., Julius Clemens Schuster., Anton Nosyrev., and Petr Tsygankov., (2008). “Kinetics of intermetallic phase formation in the Ti/Al multilayers.” *Thermochim Acta.*, 469, 77-80.

Hampshire, J., Kelly, P.J., and Teer, D.G., (2004). “The structure of co-deposited aluminum-titanium alloy coatings.” *Thin Solid Films.*, 418-424, 447-448.

Holubar, P.U., Jilek, M., and Sima, M., (2000). “Present and possible future applications of superhard nanocomposite coatings.” *Surf. Coat. Tech.*, 133 -134, 145 -151.

Hu, D., Huang, A., Jiang, H., Mota-Solis, N., and Xinhua, Wu., (2006) “Pre-yielding and pre-yield cracking in TiAl-based alloys.” *Intermetallics.*, 14, 82–90

Ipaz, L., Caicedo, J. C., Esteve, J., Espinoza-Beltran, F. J., and Zambrano, G., (2012). “Improvement of mechanical and tribological properties in steel surfaces by using titanium-aluminum/titanium-aluminum nitride multilayered system.” *Appl Surf Sci.*, Volume 258, Issue 8, 3805-3814.

Iriarte, G., F., Rodriguez, J., G., Calle, F., (2011). “Effect of substrate–target distance and sputtering pressure in the synthesis of AlN thin films.” Microsyst. Technol., 17, 381–386.

Jarms, C., Stock, H. R., and Mayr, P., (1998). “Mechanical properties, structure and oxidation behaviour of $Ti_{1-x}\ Al_x$ N-hard coatings deposited by pulsed d.c. plasma-assisted chemical vapour deposition (PACVD).” *Surf. Coat. Tech.*, 108–109, 206–210.

Kale, A., Seal, S., Sobczak, N., Morgiel, J. and Sundaram, K.B., (2001). "Effect of deposition temperature on the morphology, structure, surface chemistry and mechanical properties of magnetron sputtered Ti70-Al30 thin films on steel substrate." *Surf. Coat. Tech.*, 141, 252-261.

Karabacak, T., Singh, J. P., Ye, D.-X., Liu D.-L., Picu, C., Lu, T.-M., and Wang, G.-C., (2004), "Physical properties of nanostructures grown by oblique angle deposition." *J. Vac. Sci. Technol.* B 22, 2114 – 2121.

Kutschej, K., Mayrhofer, P. H., Kathrein, M., Polcik, P., Tessadri, R. and Mitterer, C., (2005). "Structure, mechanical and tribological properties of sputtered $Ti_{1-x}Al_xN$ coatings with $0.5<x<0.75$." *Surf. Coat. Tech.*, 200, 2358-2365.

Ling Pan, and David Luzzi, E., (2006). "A study on diffusion couples of Ti and polysynthetically twinned (PST) Ti–Al: I. Interdiffusion results." *Intermetallics.*, 14, 61–67.

Ling Pan, and David Luzzi, E., (2006). "A study on diffusion couples of Ti and polysynthetically twinned (PST) Ti–Al: II. Interdiffusion results." *Intermetallics.*, 14, 68–74.

Liu, S. G., Jin-Ming Wu., Sheng-Cai Zhang., Shu-Jie Rong., and Zhi-Zhang Li (2007). "High temperature erosion properties of arc-sprayed coatings using various cored wires containing Ti-Al intermetallics." *Wear.*, 262, 555-561.

Liu, Z., and Wang, G., (2005). "Improvement of oxidation resistance of 7-TiAl at 800 and 900 ^{0}C in air by $TiAl_2$ coatings." *Mater. Sci. Eng.*, A, 397, 50-57.

Maria Brogren., Geoffrey, L., Harding, Richard Karmhag, Carl, G., Ribbing, Gunnar, A., Niklasson, and Lars Stenmark., (2000). "Titanium – aluminum – nitride coatings for satellite temperature control." *Thin Solid Films.*, 370, 268 – 277.

Moskalewicz,T., Wendler, B., Smeacetto, F., Salvo, M., Manescu, A., Czyrska-Filemonowicz, A., (2008). "Microstructure, mechanical properties and oxidation behavior of the TiAl(Si,Ag) coating on near-α titanium alloy." Surf. Coat. Tech., 202, 5876–5881.

Nicolas Martin, and Christophe Rousselot, (1999). "Modelling of reactive sputtering processes involving two separated metallic targets." *Surf. Coat. Tech.*, 114, 235 – 249.

Oliveira, J.C., Manaia, A., and Cavaleiro, A., (2008). "Hard amorphous Ti-Al-N coatings deposited by sputtering." *Thin Solid Films.*, 516, 5032 – 5038.

Padmaprabhu, C., Kuppusami, P., Terrance, A.L.E., Mohandas, E., Raghunathan, V.S., Sangam Banerjee., and Milan, K. Sanyal., (2000). "Microstructural characterisation of TiAl thin films grown by DC magnetron co-sputtering technique." *Mater Lett.*, 43, 106–113.

Paksunchai, C., Denchitcharoen, S., Chaiyakun, S., Limsuwan, P., (2012). "Effect of Sputtering Current on Structure and Morphology of $(Ti_{1-x} Cr_x)N$ thin Films Deposited by Reactive Unbalanced Magnetron Co-sputtering." Procedia Engineering 32, 875 – 881.

Pal Dey, S., Deevi, S.C., and Alford, T.L., (2004). "Cathodic arc deposited thin film coatings based on TiAl intermetallics." *Intermetallics.*, 12, 985-991.

Park, K.H., Yoon, C.H., Lee, J.J., (2001). "Structure and properties of $(TiCr_x)N$ coatings produced by the ion-plating method." *Thin Solid Films.*, 385, 167-173.

Quesada, F., Marino, A. and Restrepo, E., (2006). "TiAlN coatings deposited by r.f. magnetron sputtering on previously treated ASTM A36 steel." *Surf. Coat. Tech.*, 201, 2925 – 2929.

Rafaja, D., Sima, M., Klemm, V., Schreiber G., Heger, D., Havela, L., and Kuzel, R., (2004). “X-ray diffraction on nanocrystalline $Ti_{1-x}Al_xN$ thin films.” *J Alloy Compd.*, 378, 107-111.

Ramos, A.S., Calinas, R., and Vieira, M.T., (2006). “The formation of γ-TiAl from Ti/Al multilayers with different periods.” *Surf. Coat. Tech.*, 200, 6196 – 6200.

Rigney, D.V., Viguie, R., Wortman, D.J., and Skelly, D.W., (1997). “PVD Thermal Barrier Coating Applications and Process Development for Aircraft Engines.” *J Therm Spray Techn.*, Volume 6(2), 167 – 175.

Rocha, Augusto, Luis., Ariza, Edith., Costa, Angela, Maria., Oliveira, Filipe, José., Silva, Ferreira, Rui., (2003). “Electrochemical behavior of Ti/Al_2O_3 interfaces produced by diffusion bonding.” Mat. Res. 6 , 439 – 444.

Romankov, S.E., Suleeva, S., Volkova, T.V., and Ermakov, E., (2002). “Influence of thermal treatment on the structure of Ti-Al films.” *Crystal Engineering.*, 5, 255-263.

Se-Hyun Ko, Bong-Gyu Park, Hitoshi Hashimoto and Toshihiko Abe (2002). “Effect of MA on microstructure and synthesis path of in-situ TiC reinforced Fe-28at.% Al intermetallic composites.” *Mater Sci Eng.*, A329-331, 78-83.

Shetty, A., R., Karimi, A., Cantoni, M., (2011). “Effect of deposition angle on the structure and properties of pulsed-DC magnetron sputtered TiAlN thin films.” Thin Solid Films, 519, 4262–4270.

Shiro Shimada and Motoki Yoshimatsu (2000), “Preparation of ($Ti_{12x}Al_x$)N from mixed alkoxide solutions by plasma CVD.” *Thin Solid Films.*, 370, 146 -150.

Shum, P.W., Li, K.Y., Zhou. Z.F., and Shen, Y.G., (2004), “Structural and mechanical properties of titanium-aluminum-nitride films deposited by reactive close-field unbalanced magnetron sputtering.” *Surf. Coat. Tech.*, 185, 245-253.

Smentkowski and Vincent, S., (2000), "Trends in sputtering – Review Article." *Progress in Surface Science*, Volume 64, Issues 1–2, Pages 1-58.

Tongbo Wei, Fengyuan Yan and Jun Tian (2005), "Characterization and wear- and corrosion-resistance of micro arc oxidation ceramic coatings on aluminum alloy." *J Alloy Compd.*, 389, 169–176.

Tonshoff, H. K., Karpuschewski, B., Mohlfeld, A., and Seegers, H., (1999), "Influence of subsurface properties on the adhesion strength of sputtered hard coatings." *Surf. Coat. Tech.*, 116–119, 524–529.

Toshimitsu Tetsui and Yoshimitsu Miura (2002), "Heat-resistant Cast TiAl Alloy for Passenger Vehicle Turbochargers." *Mitsubishi Heavy Industries, Ltd. Technical Review.*, Vol.39, 1 – 5.

Toshinari Yamazaki, Yoshio Okumura, Kenjiro Desaki, Toshio Kikuta, Hiroshi Anada and Noriyuki Nakatani (2009). "Application of TiAl laminate to a sputtering target for TiAlN films." *Vacuum.*, 83, 479-482.

Tuilier, M. H., Pa,c M. J., Covarel, G., Rousselot, C. and Khouchaf, L., (2007). "Structural investigation of thin films of $Ti_{1-x}Al_xN$ ternary nitrides using Ti K-edge X-ray absorption fine structure." *Surf. Coat. Tech.*, 201, 4536 – 4541.

Vieira, M.T., Trindade, B., Ramos, A.S., Fernandes, J.V. and Vieira, M.F., (2002). "Mechanical characterisation of γ-TiAl thin films obtained by two different sputtering routes." *Mater Sci Eng.*, A329-331, 147-152.

Wang, S.Z., Shao, G., Tsakiropoulos, P., and Wang, F., (2002). "Phase selection in magnetron sputter-deposited TiAl alloy." *Mater Sci Eng.*, A329-331, 141-146.

Xinhua Wu, H., Jiang, A. Huang, Hu D., Mota-Solis, N., and Loretto, M.H., (2006). "Microstructural study of pre-yielding and pre-yield cracking in TiAl-based alloys." *Intermetallics.*, 14, 91–101.

Yankov, R., A., Kolitsch, A., Borany von, J., Mücklich, A., Munnik, F., Donchev, A., Schütz M., (2012). “Surface protection of titanium and titanium–aluminum alloys against environmental degradation at elevated temperatures.” Surf. Coat. Tech. 206, 3595–3600.

Zhang, H., Peng, X., Wang, F., (2012). “Fabrication of an oxidation-resistant β-NiAl coating on γ-TiAl.” Surf. Coat. Tech. 206, 2454–2458.

Zhao, Y., H., Hu, L., Lin, G., Q., Xiao, J., Q., Dong, C., Yu, B., H., (2012). “Deposition, microstructure and hardness of TiN/(Ti,Al)N multilayer films.” Int. Journal of Refractory Metals and Hard Materials 32, 27–32.

Zywitzki, O., Klostermann, H., Fietzke, F. and Mode,s T., (2006). “Structure of superhard nanocrystalline (Ti,Al)N layers deposited by reactive pulsed magnetron sputtering.” *Surf. Coat. Tech.*, 200, 6522 – 6526.

LIST OF PAPERS PUBLISHED IN JOURNALS

Sudheendra, P., Surendranathan, A. O., Udayashankar, N. K., (2012). "Titanium – Aluminum Intermetallic Thin films Preparation by DC Sputtering & Their Characterization." International Journal of Mechanical Engineering, Vol. 2 Issue 3, 12 – 17.

Sudheendra, P., Surendranathan, A. O., Udayashankar, N. K., (2012). "Titanium – Aluminum Thin films Preparation By Oblique Angle Sputtering And Their Characterization." International Journal of Engineering Research & Technology, Vol. 1 Issue 8, 1 – 5.

Sudheendra, P., Surendranathan, A. O., Udayashankar, N. K., (2014). "Deposition of Ti-Al Intermetallic composite by Reactive Thermal Evaporation." Procedia Materials Science, 5, 962 – 968.

LIST OF CONFERENCE PAPERS PRESENTED

National Conferences:

Sudheendra, P., Surendranathan, A. O., Udayashankar, N. K., (2011). "Effect of Heat Treatment on the Sputter Deposited Titanium Aluminide thin films." Proceedings of National Conference in Physics CAPSRAA, OP - 29, Govindadasa First Grade College, Surathkal.

Sudheendra, P., Surendranathan, A. O., Udayashankar, N. K., (2010). "Growth of Ti – Al on the surface of Porous Alumina by Magnetron Sputtering." National Conference on Recent Trends in Chemical and Biological Sciences NCRTCBS, OP 18, Kuvempu University, Shankargatta.

Sudheendra, P., Surendranathan, A. O., Udayashankar, N. K., (2010). "Microstructural and Tribological Characterization of TiN coated Aluminum Alloy Al6061." Proceeding of National Conference on Multifunctional Nanomaterials and Nanocomposites NCMNN, 71, Bharathiar University, Coimbatore.

International Conferences:

Sudheendra, P., Surendranathan, A. O., Udayashankar, N. K., (2012). “Intermetallic titanium – aluminum thin films preparation by oblique angle unbalanced magnetron sputtering.” Proceedings of 3rd Asian Symposium on Materials and Processing 2012 ASMP, 79 – 80, IIT Madras, Chennai, Tamil Nadu.

Sudheendra, P., Surendranathan, A. O., Udayashankar, N. K., (2012). “Titanium – Aluminum Intermetallic thin films Preparation by Dc Sputtering And Their Characterization.” Proceedings of International Conference on thin films & Applications ICTFA, 119,School of Electrical & Electronics Engineering, SASTRA University, Thanjavur – 613 401, Tamil Nadu.

Sudheendra, P., Surendranathan, A. O., Udayashankar, N. K., (2012). “Titanium – Aluminum intermetallic thin films preparation by DC sputtering and their characterization.” Proceeding of International Conference on Advanced Materials ICAM, 256 – 257, PSG – IT Coimbatore, Tamil Nadu.

Sudheendra, P., Surendranathan, A. O., Udayashankar, N. K., (2010). “Microstructural and Tribological Characterization of Ti-Al coating developed by Reactive DC Magnetron Sputtering.” Proceeding of International Conference on Advancement of Nanoscience and Nanotechnology ICOANN, 155, Alagappa University, Karaikudi.

PUBLICATION DETAILS:

1. International Journal of Mechanical Engineering, ISSN: 2277-7059, Volume 1, Issue 1, Microstructural And Tribological Characterization Of Tin Coated Aluminum Alloy (Al6061). Anil Kumar H C[1], N.K. Udayashankar[2], Sudheendra P[3], H.S. Hebbar[4] .

2. Proceedings of International Conference on Advanced Materials – 2012 (ICAM – 2012 Macmillan Publishers India Ltd. (2012), Titanium – Aluminum intermetallic thin films preparation by DC sputtering and their characterization Sudheendra P[1]., A. O. Surendranathan[1], N. K. Udayashankar[2], K. S. Choudhari[2].

3. Journal of Porous Materials, (2012) DOI. 10.1007/s10934-012-9568-z, Publication date 02-08-2012. Fabrication and high-temperature structural characterization study of porous anodic alumina membranes. K. S. Choudhari[1], P. Sudheendra[2], N. K. Udayashankar[1].

4. International Journal of Mechanical Engineering, ISSN: 2277-7059 Volume 2 Issue 3 (March 2012), Titanium – Aluminum Intermetallic thin Films Preparation By Dc Sputtering And Their Characterization. Sudheendra P[1]., A. O. Surendranathan[1], N. K. Udayashankar[2], K. S. Choudhari[2].

5. Proceedings of 3rd Asian Symposium on Materials and Processing 2012 (ASMP-2012), Intermetallic titanium – aluminum thin films preparation by oblique angle unbalanced magnetron sputtering. Sudheendra P[1]., A. O. Surendranathan[1], N. K. Udayashankar[2].

6. Procedia Materials Science, (2014) DOI: 10.1016/j.mspro.2014.07.384, 5, 962-968. Deposition of Ti-Al Intermetallic composite by Reactive Thermal Evaporation. Sudheendra P[a]., A. O. Surendranathan[a], N. K. Udayashankar[b].

CURRICULAM VITAE

Sudheendra P, M.Sc, M.Tech.

Ph: +919448984038

sudheendrahebbar@gmail.com

EDUCATIONAL QUALIFICATION:

Examination Passed	Board / University	Class Obtained	Year
S.S.L.C	K.S.E.E.B, Bangalore	First	1996
PUC (P C M B)	Pre University Board	Second	1998
B.Sc. (P C M)	Mangalore University	First	2001
M. Sc (Materials Engineering)	Mangalore University	Second	2003
M. Tech. (Materials Engineering)	N I T K – Surathkal.	First	2006

PROFESSIONAL EXPERIENCE: Teaching

Name of the Institution	Period	
	From	To
Dept. of Mechanical Engg. Srinivas School of Engineering, Mukka – Surathkal.	22-08-2013	Till Date
Dept. of Met. Mat. Engg. National Institute of Technology Karnataka – Surathkal.	15-07-2012	30-05-2013
Moodlakatte Institute of Technology, Kundapura.	01-09-2007	10-07-2008
The New English PU College, Bhatkal.	03-06-2006	31-08-2007
S. M. S, PU College, Brahmavar .	01-06-2003	30-07-2004
St. Mary's PU College, Kundapura.	01-07-2003	30-04-2004